SECOND ANNUAL REPORT

SYNTHESIS AND EVALUATION OF POLYMERIC MATERIALS

GC-TR-93-2303

Prepared for
Naval Research Laboratory
4555 Overlook Avenue, SW
Washington, D.C. 20375-5000

As Required By
Contract Number
N00014-90-C-2269

Prepared by
GEO-CENTERS, INC.
7 Wells Avenue
Newton Centre, MA 02159

JULY 1993

SECOND ANNUAL REPORT

SYNTHESIS AND EVALUATION OF POLYMERIC MATERIALS

GC-TR-93-2303

Prepared for
Naval Research Laboratory
4555 Overlook Avenue, SW
Washington, D.C. 20375-5000

As Required By
Contract Number
N00014-90-C-2269

Prepared by
GEO-CENTERS, INC.
7 Wells Avenue
Newton Centre, MA 02159

JULY 1993

GEO-CENTERS, INC.

REPORT DOCUMENTATION PAGE

Form Approved
OMB No. 0704-0188

1. AGENCY USE ONLY (Leave blank)	2. REPORT DATE	3. REPORT TYPE AND DATES COVERED
	31 July 1993	Interim, 1 Mar 92 - 31 July 93

4. TITLE AND SUBTITLE
Synthesis and Evaluation of Polymeric Materials
Second Annual Report

5. FUNDING NUMBERS
C N00014-90-C-2269

6. AUTHOR(S)
E. Greenawald, J. Nagode, H. Hu, L. Levenberry,
R. Newbegin, H. Schrader, K. Groot, S. Kate

7. PERFORMING ORGANIZATION NAME(S) AND ADDRESS(ES)
GEO-CENTERS, INC.
7 Wells Avenue
Newton Centre, MA 02159

8. PERFORMING ORGANIZATION REPORT NUMBER
GC-TR-93-2303

9. SPONSORING/MONITORING AGENCY NAME(S) AND ADDRESS(ES)
Naval Research Laboratory
Code 6120
4555 Overlook Avenue, S.W.
Washington, D.C. 20375-5000

10. SPONSORING/MONITORING AGENCY REPORT NUMBER

11. SUPPLEMENTARY NOTES

12a. DISTRIBUTION/AVAILABILITY STATEMENT
Approved for public release
Distribution unlimited

12b. DISTRIBUTION CODE

13. ABSTRACT *(Maximum 200 words)*

GEO-CENTERS, INC. has been supporting the research efforts at the Naval Research Laboratory including novel fluoropolymers, conductive polymers, epoxies, and modified nylons. Major efforts were conducted in radiographic analysis development and use in evaluation of Sonar Rubber Domes (SRD) and Sonar Dome Rubber Windows (SDRW). This report is a summary of accomplishments for Year Two of the contract period of performance.

14. SUBJECT TERMS
Polymer, Sonar dome, radiograph, synthesis, SDRW, SRD, nondestructive evaluation, fluoropolymer, conductive polymer.

15. NUMBER OF PAGES
193

16. PRICE CODE

17. SECURITY CLASSIFICATION OF REPORT	18. SECURITY CLASSIFICATION OF THIS PAGE	19. SECURITY CLASSIFICATION OF ABSTRACT	20. LIMITATION OF ABSTRACT
Unclassified	Unclassified	Unclassified	UL

DISCLAIMER NOTICE

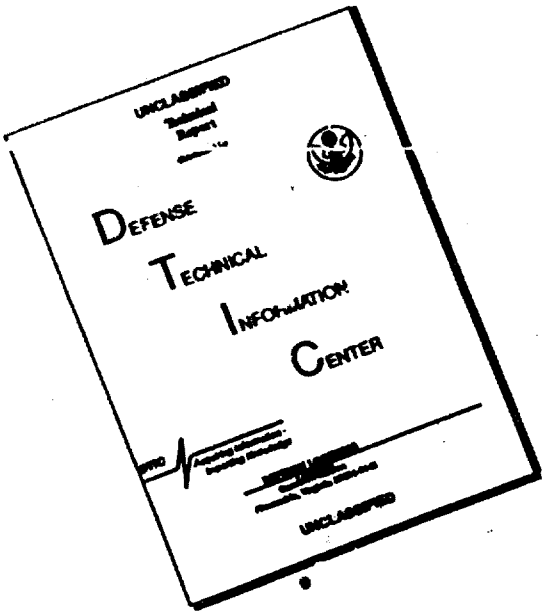

THIS DOCUMENT IS BEST QUALITY AVAILABLE. THE COPY FURNISHED TO DTIC CONTAINED A SIGNIFICANT NUMBER OF PAGES WHICH DO NOT REPRODUCE LEGIBLY.

TABLE OF CONTENTS

INTRODUCTION 1

TECHNICAL REPORT 2
1.0 EVALUATION OF SONAR DOME DAMAGE 2
1.1 Background 2
1.2 Radiographic Inspection 3
1.2.1 Inspection Results 3
1.3 Improved Nondestructive Evaluation (NDE) Methods 3
1.3.1 X-ray Backscatter Tomography (XBT) 3
1.3.2 Other Methods 4
1.3.3 Neural Networks 4
1.4 Database Management 4
1.5 Failure Analysis 5
1.6 Cord Load Measurement of the Monolithic SDRW - 1A 6
1.6.1 Background 6
1.6.2 Load Cell Measurements 6
1.6.3 Future Efforts 7
1.7 SRD Acoustic Deflection Project 7
1.8 SDRW Technical Package for NWSC 7
2.0 POLYMER SYNTHESIS AND EVALUATION 8
2.1 Fluorinated Polymers 8
2.2 L-Proline Modified Nylons 8
2.3 Blend Characterization 9
2.4 Biodegradable Materials 9
3.0 MISCELLANEOUS TECHNICAL SUPPORT 10
4.0 DOCUMENTATION 10

GEO-CENTERS, INC.

APPENDICES

Appendix A	Sonar dome rubber window (SDRW) and sonar rubber dome (SRD) radiographic inspection reports (March 1992 - April 1993)
Appendix B	Nondestructive Testing of Sonar Domes - project technical review
Appendix C	Sonar Dome NDE Program Summary
Appendix D	Operating Procedure for X-Ray Backscatter Tomography of Sonar Domes
Appendix E	One-Sided NDE of Sonar Rubber Domes
Appendix F	Quantitative Radioscopic Profile Analysis via Neurai Networks
Appendix G	Review of Recommendation to Place SDRW N113 in Monitor Status
Appendix H	Failure Analysis Report for SRD S/N:B017
Appendix I	Failure Analysis Report for SRD S/N:B022
Appendix J	Processable Fluoropolymers with Low Dielectric Constants: Preparation and Structure-Property Relationships of Polyacrylates and Polymethacrylates
Appendix K	Processable Fluoropolymers with Low Dielectric Constants: Preparation and Structure-Property Relationships of Polyacrylates and Polymethacrylates
Appendix L	L-Proline modified nylons
Appendix M	Phase Transitions in Polymer Blends via ^{129}Xe NMR Spectroscopy
Appendix N	Biodegradable Packaging Materials

INTRODUCTION

This report is a summary of GEO-CENTERS' research efforts for the Naval Research Laboratory (NRL) under contract number N00014-90-C-2269, entitled "Synthesis and Evaluation of Polymeric Materials". The period of performance was from May 1992 through July 1993 (contract year two). The majority of the work was carried out at NRL and NRL's Chesapeake Bay Detachment (CBD) using Chemistry Division, Acoustics Division, Materials Science & Technology Division, and NRL-CBD Support facilities, and in collaboration with NRL staff scientists. Additional work was carried out at the U.S. Army RD&E Center in Natick, M..

The work has resulted in several publications in scientific journals, and presentations at various scientific meetings. Copies of the publications are appended to this report. The various research projects in which GEO-CENTERS has been involved under this contract are divisible into two main groups, as follows:

- Evaluation of sonar dome damage
- Polymer synthesis and evaluation

The sonar dome projects have involved fleet support functions as well as research. GEO-CENTERS, INC. has provided the interpretation and analysis of radiographic inspection data in support of a routine fleet sonar dome inspection program. We have also conducted failure analyses of individual domes. Research projects have focused upon nondestructive evaluation methods. In addition, engineering support for NRL's research efforts and database management support for the sonar dome effort have been provided.

In the area of synthesis and evaluation, GEO-CENTERS, INC. has conducted research on the synthesis of novel polymers, such as fluoropolymers, epoxies, and modified nylons. An effort has been initiated to develop new biodegradable packaging materials. The task has also involved the characterization and evaluation of these materials with respect to their mechanical, rheological, chemical, and electrical properties. In addition, the characterization methods have been investigated and improved upon where applicable. Detailed discussions of these accomplishments are provided in the following paragraphs, and in the appendices.

TECHNICAL REPORT

1.0 EVALUATION OF SONAR DOME DAMAGE

1.1 Background

Sonar Dome Rubber Windows (SDRW) and Sonar Rubber Domes (SRD) are installed on Navy surface combatants to provide a protective window for the transmission of sonar signals. These structures provide a hydrodynamic fairing around the sonar transducer arrays for the purpose of eliminating turbulence and system self-noise. They also protect the sonar system from the actions of the sea and collisions with debris.

Sonar domes are fabricated from a steel cord reinforced rubber composite material. The SDRW is a large, bow-mounted structure which is fitted to ten classes of cruisers, destroyers, and frigates. The SRDs consist of two types, which are directly associated to a specific sonar system--AN/SQS-56 and AN/SQQ-23. The AN/SQS-56 SRD is a 273-inch-long keel-mounted dome installed on *Perry* class frigates, while the AN-SQQ-23 SRD is a 400-inch-long keel dome installed on four classes of cruisers and frigates which are currently being phased out of service. The larger of the keel domes is installed on some ships in pairs. In the following the summary, we will refer to all of the structures as "sonar domes". SDRW or SRD will be used when specifically applicable.

Sonar domes have a history of rupturing during service. Studies performed by NRL have demonstrated that the SDRW failures are due to corrosion fatigue failure of the steel reinforcement cords in the splice region of the composite structure. The SRD failures are not as well understood. Both corrosion fatigue and other mechanisms have been identified during SRD failure analyses.

X-ray radiography has been used to detect incipient corrosion fatigue damage. An inspection program has been set up with the goal of maintaining an up-to-date evaluation of the entire anti-submarine warfare fleet's sonar domes. Since replacement domes are also subject to the same problems, the need to inspect, monitor, and repair or replace them still remains. Radiographic inspection has been routinely used as a basis for determining these options. In addition, the accumulated radiographic data have contributed to the failure analysis effort by revealing patterns of damage distribution and have been correlated with other data. The inspection and analysis methods developed in response to the SDRW failure problem have since become applicable for use on similar problems with the smaller keel domes.

GEO-CENTERS' support of the sonar dome corrective action program (CAP) has been in the areas of radiographic inspection, database management, failure analysis, materials development, and improved methods for nondestructive evaluation. The following paragraphs synopsize these efforts.

1.2 Radiographic Inspection

GEO-CENTERS' role in the radiographic inspection program has involved the interpretation of radiographs provided by the Navy's inspection contractors, development and maintenance of standards for the radiographic data, and of the criteria for determining the action to be taken.

As the sonar dome radiographs arrive, they are processed immediately. Any damage or pertinent features are located, measured, and diagrammed either as a hand sketch or as a computer generated image. The appropriate recommendation for action to be taken is based on the standardized criteria devised at NRL. The results are communicated verbally to the NRL task manager and/or others designated by NRL (typically NAVSEA 06U1B). The data are also entered into the appropriate database, and a report is generated for distribution.

1.2.1 Inspection Results

During the period of performance, GEO-CENTERS has evaluated 61 radiographic sonar dome inspections--27 SDRWs in service, 9 newly manufactured SDRWs, 8 SRDs in service, and 17 new SRDs. For each inspection a report was written detailing our findings, including illustrations of the inspection area and damage locations. The recommended action is determined by a set of well defined and established criteria. The inspection reports are initially transmitted to NAVSEA via modem for immediate use in determining the action to be taken. Accumulations of these reports are provided as appendices in a summary memorandum to NRL. These memoranda are then distributed to NAVSEA as NRL letter reports. Four such letter reports have been generated during the period of performance. The summary pages from each letter report have been compiled and included as Appendix A.

1.3 Improved Nondestructive Evaluation (NDE) Methods

1.3.1 X-ray Backscatter Tomography (XBT)

XBT is being investigated as a pierside inspection method for AN/SQS-56 sonar rubber domes (SRD). This project has now developed into a major effort. NRL has obtained NAVSEA support to lease a commercially available x-ray scanner (Philips Comscan), and additional support is being provided by ONR under their Logistics Technology Exploratory Development Program, resulting in a three year research effort. Progress on this program has been presented at an ONR technical review held at NIST on April 9, 1993. Copies of the presentation's viewgraphs have been included as Appendix B.

A narrative description of the program with summaries of completed and planned work has also been provided to ONR for inclusion in their Technology Program Plan (Appendix C).

A written operating procedure for the XBT system (Appendix D) has been approved by NRL's Health Physics Section and the Navy's Radiological Affairs Support Office (RASO).

1.3.2 Other Methods

Based on a technical evaluation of NDE performance issues, we have placed our emphasis and resources on the development of XBT. Other NDE methods have been proposed as candidates for one-sided inspections of SRDs. In comparison to XBT, these other methods promise to be less expensive and easier to implement, although their resolutions have proven to be lower than that of XBT. These methods may be utilized as inexpensive, preliminary screening techniques for identifying the most seriously damaged SRDs. Based on the results from the preliminary screening, a more detailed evaluation using XBT may be scheduled. A paper summarizing this concept has been written in collaboration with NRL and was presented to the 41st Defense Working Group on NDE in Tucson, Arizona (November 1992). A copy of this paper has been included as Appendix E.

1.3.3 Neural Networks

Artificial neural networks have been used for pattern classification applications in a variety of fields, including NDE. In the first year annual report, we discussed the application of neural networks in sonar dome cord profile analysis. Current efforts have demonstrated the applicability of neural nets in the quantitative measurement of object features from radioscopic data. Using a computer simulation of the x-ray transmission data, we have generated network training and testing data sets for a variety of flaw measurement problems. It has been shown that the neural network's tolerance to variation in object location or orientation makes this technique ideal for automated inspection applications, which would otherwise require accurate data registration. A feed-forward back-propagation network configuration and various representations of the profile data have been used. These results were presented at the Review of Progress in Quantitative Nondestructive Evaluation (La Jolla, California) in July 1992 and have been published in the proceedings of that meeting. A copy of the manuscript has been enclosed as Appendix F.

1.4 Database Management

Developing and maintaining databases are important to many aspects of the sonar dome program. Under previous contracts, GEO-CENTERS developed databases for SDRW and SRD tasks. Currently, records are maintained on every SDRW/SRD installed or newly manufactured. Complete histories of each SDRW/SRD (installation, radiographic inspections, repairs, removal) are available. An inventory of spare SDRW/SRD is also maintained.

These databases have provided a library of information for statistical analysis. In turn, the statistical programs have allowed the development of inspection interval and recommendation damage criteria for SDRWs in service. A recommended inspection schedule has been created based on this data, varying with the type of sonar dome and pre-determined condition. By adhering to this schedule, the fleet can minimize the risk of sonar dome failures at-sea. Further, the ability to reasonably predict a SDRW's life expectancy under varying conditions now exits, and should assist NAVSEA in projecting annual budgets for SDRW purchases and maintaining fleet readiness.

Occasionally the need arises to review the criteria in which SDRW-action recommendations are based. Statistical analysis regarding damage site lengths and growth rates enabled the Navy to make a cost effective decision about the fate of a particular SDRW, when the established criteria has been questionable. An NRL letter report to NAVSEA pertaining to this topic has been included as Appendix G.

During this reporting period, GEO-CENTERS has continued to maintain all previously created databases and to develop new database applications for SDRW and SRD as required by the needs of the sonar dome program. The SRD database has been divided into two separate databases: one for AN/SQQ-23 and one for AN/SQS-56 keel domes. Although all the databases continually undergo program editing and overhaul, application development has centered about the needs of the AN/SQS-56 SRD program. Progress has been made towards automating the inspection data entry procedure, and in the development of a new system to electronically transfer the SRD damage findings into a formal graphics format. This was previously done with the SDRW database. A brief synopsis of the SRD database code has been provided to the COTR as a separate document, and has not been included with this report.

1.5 Failure Analysis

Sonar domes fail when the amount of sustained structural damage severely compromises the load carrying capability of the dome. At that point, the dome is likely to rupture, allowing seawater to come in contact with the sonar array. This is known as a failure at sea. If a sonar dome is inspected prior to rupture, and the damage is beyond what the criteria allows for a dome in service, it is removed. This is regarded as a failure by inspection (X-ray). To be assured that the best pre-conditions exist for laboratory analysis, only the failure-by-inspection sonar domes are analyzed. During this period of performance, failure analysis reports on two SRDs were completed. These reports have been included as Appendix H and Appendix I.

1.6 Cord Load Measurement of the Monolithic SDRW - 1A

1.6.1 Background

The acquisition of the cord load data must be completed for every newly designed sonar dome prototype produced. The manufacturer installed numerous load-cell gauges during the fabrication of the first spliceless or "monolithic" SDRW. GEO-CENTERS has provided logistical and technical support to this task. This has involved gauge placement and calibration, cabling, and data processing.

The first six-ply monolithic SDRW was fabricated as layup 252, bearing the serial number 1A. During construction of the 1A, load cells were placed within the structural plies to measure loads in critical areas. Prior to the actual sea trial, acoustic deflection measuring devices will also be installed to measure surface movements at the load cell locations.

The first phase of this project involved the calibration of all the load cells and instruments prior to curing. Initial calibration was performed by the manufacturer under GEO-CENTERS and NRL observation. After the calibration, a load (pressurization) test was performed, where all the cells were taken to an operational status. The second phase involved testing the cured dome at various pressures and checking the equipment setup and computer algorithms.

Soldered and crimped spade lugs were used to terminate all wire ends, except for the load cell ends that were soldered in place. No specific protection has been provided to the spaded lug ends since they are replaceable.

The manufacturer has installed 85 calibrated load cells on SDRW-1A. These load cells consist of a 36x2x2 mm brass billet with four active gages in a full bridge configuration. Two of the active gages were mounted for maximum strain; the other two were mounted for poisson strain. Each load cell was supplied with a factory assigned serial number, gage factor, offset value, and an initial load calibration.

1.6.2 Load Cell Measurements

Pre-cure base line readings were taken at 75°F after SDRW layout completion. The excitation voltage (Vex) was 4 VDC. Three readings were taken per cell for verification. All 85 cells were tested by measuring the resistance between the cell's strain gages (a properly functioning strain gage should read approximately 350 ohms). The cells were tested before and after installation into the plies. Three cells failed after an induced voltage was applied, and were replaced. Due to production time constraints, pre-cure loads were not taken. Analysis of the data revealed that the cells were linear within the expected load range. Baseline readings were then taken for all the load cells.

The second phase of the project involved pressurizing the SDRW and using a prototype equipment setup. Readings were taken at 0 psig with the dome empty, and at 16.5 psig, 35.6 psig, and 56.0 psig with the dome full of water.

1.6.3 Future Efforts

Measurements taken from the load cells on the SDRW-1A are to be compared with values obtained from load cells on earlier prototypes. In addition, these data will be combined with acoustic deflection data to construct a finite element model.

1.7 SRD Acoustic Deflection Project

SRD inner surface deflection data has been gathered to assist in the development of a finite element model, and ultimately provide a substantial basis for future structural modification, and new sonar dome design. It is also the hope that these data will assist with understanding the failure mechanism for SRD.

Data were gathered with the help of two computers working synchronously, controlling a series of acoustic sensors attached to the inner surface of the dome. Data were collected on board the *USS Kauffman* at various speeds, sea states, and during various ship maneuvers under actual service conditions. Data processing has included the following: the arrangement of original data into a spreadsheet format and applying correction factors; the conversion of the original x-y-z data into surface normal vectors; and the calculation of the deflection range, minimum, and maximum surface normal deflections. A fair amount of data processing still remains before a report can be released.

1.8 SDRW Technical Package for NWSC

As part of the task to maintain SDRW/SRD engineering data, we have provided technical assistance to the Naval Weapons Support Center (NWSC) in Crane, Indiana. NWSC is in the process of documenting various manufacturing processes, procedures, and material requirements associated with U.S. Navy weapons and defense systems, including sonar domes. Our knowledge of sonar dome construction requirements and procedures has enabled us to review, evaluate, and make the necessary changes to the engineering documentation. To date, this work has consisted of converting these documents into current ASTM, SAE, and MIL standards. All documents have been made to conform with applicable MIL-S. Due to the proprietary nature of the material, no further discussion will follow.

2.0 POLYMER SYNTHESIS AND EVALUATION

The Materials Chemistry Branch is responsible for the development and characterization of new polymeric materials for Navy applications. GEO-CENTERS' support of the branch's efforts has been broad based involving the synthesis and characterization of many varied materials. The main focus has been in developing synthetic polymers that emulate the elastic linkages found in natural polypeptides and polymers that yield enhanced dielectric properties. Characterization has involved several diagnostic methods including different types of thermal analyses, scanning electron microscopy (SEM), transmission electron microscopy (TEM), nuclear magnetic resonance (NMR), electron spin resonance (ESR) and infrared and ultraviolet spectroscopic analyses. The methods and techniques of characterization have been investigated to meet the increasing requirements for better precision in the polymeric research. In addition, we have used mechanical, rheologic, and dielectric tests when appropriate. The specific project areas are discussed in the summaries which follow.

2.1 Fluorinated Polymers

The highly polar nature of the carbon-fluorine bond has been used to provide improved properties as compared to the hydrogen-containing or other halogen-containing analogs. Fluorine-containing epoxies or acrylics generally exhibit resistance to water penetration, chemical reaction, and environmental degradation; they also show differing degrees of surface tension, friction coefficient, optical clarity, refractive index, vapor transmission rate, and electromagnetic radiation resistance.

Previously, this task has included efforts to design and synthesize the heavily fluorinated epoxy and acrylic resins to produce compounds with dielectric constants among the lowest recorded in the literature. This has resulted in a new class of processable heavily fluorinated acrylic resins that exhibit very low dielectric constants. During this period of performance, we have further investigated the structure-property relationships of these polymers. This work is discussed fully in the publication included as Appendix J. An abstract of a manuscript in preparation has also been included as Appendix K.

2.2 L-Proline Modified Nylons

The conformational constraints that L-proline imposes upon natural polypeptides has been recognized as the most significant factor in the occurrence of ß bends and pleats. The amino group of this most unusual natural α-amino acid is secondary and contained in a five-membered ring structure. One explanation is that the peptide linkage formed with the amine group lacks an available hydrogen atom for hydrogen bonding. The implications on the material properties, as opposed to the biological properties, of natural and synthetic polyamides containing L-proline are most interesting. Thus an effort has been initiated to define the minimal structure of synthetic polymer for which L-proline will control the elastic properties.

An abstract of a paper in preparation, outlining current efforts, has been included as Appendix L.

2.3 Blend Characterization

The polymer blend research efforts have shifted towards developing currently available materials, rather than the discovery and development of new blends to suit a given purpose. Thus, the focus has been in gaining a better understanding of the thermodynamics and the dynamic behavior of potentially useful polymer blends. This is being accomplished in part by characterizing the blends' thermal transitions to better understand the phase behavior.

Standard thermal analysis techniques, such as calorimetry, are somewhat insensitive to specific morphologies which can produce minute changes in the slope of the thermal response of a compound. In addition, blend components exhibiting proximal glass transition temperatures may be unresolvable using conventional analytical methods. Through the use of ^{129}Xe nuclear magnetic resonance (NMR), it has been possible to gain a resolution advantage over conventional methods. In addition, xenon is soluble in many polymers, with the atoms residing in the free volume. Since the chemical shift of ^{129}Xe is proportional to the density of its environment, it provides a measure of the free volume in the polymer. Below the glass transition temperature, segmental motion of the polymer chains is suppressed, so that Xe atoms are trapped in different sites. The distribution in the local free volume produces variations in the chemical shift, resulting in an inhomogeneously broadened ^{129}Xe NMR line. Rapid diffusion of the polymeric components collapses the inhomogeneously broadened resonance into a narrow line; the observed chemical shift is an average over the inhomogeneously broadened line. GEO-CENTERS participated in the characterization and subsequent evaluation of the blends for this work, and co-authored a publication currently in press (Appendix M).

2.4 Biodegradable Materials

The Biodegradable Materials Program involves a joint effort between various science and engineering directorates--U.S. Army's Natick Research Center, NRL and GEO-CENTERS, INC.--for the development of biodegradable packaging materials. The U.S. Navy's interest in these materials has become heightened, since constraints will be placed on at-sea disposal by international treaties in the coming year. Packaging materials constitute a large portion of such waste. The main goal of this program is to utilize the current polymer blend technology in developing biodegradable materials that are suitable for packaging. An interim progress report has been included as Appendix N.

3.0 MISCELLANEOUS TECHNICAL SUPPORT

GEO-CENTERS frequently gives technical support to the Materials Chemistry Branch pertaining to test equipment maintenance, computer hardware and software support, training, materials testing, and test preparation. The following is a list of some of the tasks that have been accomplished during this period of performance:

Equipment Maintenance/Personnel Training--We have performed routine maintenance on various test devices and analytical equipment. This has involved routine assessment of the equipment's performance, system calibration, installation of options and upgrades, and system refits. New users are regularly trained and supervised on these systems.

Computer Hardware/Software Upgrades--In the Materials Chemistry Branch, GEO-CENTERS has performed numerous computer hardware installations, upgrades, and repairs. Software upgrades have been installed, and new database programs were written to allow effective communication between various locations at NRL. In addition, we have organized a branch wide effort to connect all PC users to the NRL Wide-Area-Network, and thus to *Internet*. This effort should take place during the next report period.

Materials Testing/Sample Preparation--GEO-CENTERS has been involved with short-term testing for various projects within the Materials Chemistry Branch. During the first year, we completed both destructive and non-destructive testing and an evaluation of sonar dome contract samples for NAVSEA. During this period of performance, we have prepared polymer samples for testing by another naval facility. Since laser surface oblation experiments were to be carried out on these samples, a preparation technique was developed to ensure that a class "A" quality surface resulted. Several different sizes of low and high density polyethylenes with varying melt indexes were prepared.

4.0 DOCUMENTATION

During the period of performance, GEO-CENTERS' research efforts have led to several presentations and publications. The following is a listing of these citations, and their location in the appendices:

C.F. Poranski and E.C. Greenawald, "One-Sided NDE of Sonar Rubber Domes," presented to the 41st Defense Working Group on NDE, Tucson, Arizona, November 1992. (Appendix E)

E.C. Greenawald and C.F. Poranski, "Quantitative Radioscopic Profile Analysis via Neural Networks," presented to the Review of Progress in Quantitative Nondestructive Evaluation at La Jolla, California, July 1992. (Appendix F)

H.S.-W. Hu and J.R. Griffith, "Processable Fluoropolymers with Low Dielectric Constants: Preparation and Structure-Property Relationships of Polyacrylates and Polymethacrylates," Polym. Prepr., 34(1), 401-402. (Appendix J)

H.S.-W. Hu and J.R. Griffith, "Processable Fluoropolymers with Low Dielectric Constants: Preparation and Structure-Property Relationships of Polyacrylates and Polymethacrylates," presented to the 1993 meeting of the American Chemical Society, Denver, Colorado, March-April 1993. (Abstract) (Appendix K)

H.S.-W. Hu, J.R. Campbell, and J.R. Griffith, "L-Proline-Modified-Nylons: The Formation of Molecular Turns from Intramolecular Hydrogen Bonding in a Copolyamideurea," Polym. Prepr., manuscript in preparation. (Appendix L)

J.H. Walton, J.B. Miller, C.M. Roland, and J.B. Nagode, "Phase Transitions in Polymer Blends via ^{129}Xe NMR Spectroscopy," Macromolecules, in press. (Appendix M)

APPENDIX A

SONAR DOME RUBBER WINDOW (SDRW) AND SONAR RUBBER DOME (SRD) RADIOGRAPHIC INSPECTION REPORTS (MARCH 1992 - APRIL 1993)

GEO-CENTERS, INC.

DEPARTMENT OF THE NAVY
NAVAL RESEARCH LABORATORY
WASHINGTON, D.C. 20375-5000

IN REPLY REFER TO

9165/Prob 61-1549
6120-201
JUN 15 1992

From: Commanding Officer, Naval Research Laboratory
To: Commander, Naval Sea Systems Command (Code 06U1D, S. Silverstein)

Subj: SONAR DOME RUBBER WINDOW (SDRW) AND SONAR RUBBER DOME (SRD) RADIOGRAPHIC INSPECTION REPORTS (MARCH-MAY 1992)

Encl: (1) Two copies of subject report

1. Enclosure (1) is forwarded for your information and retention.

S. FOX
By direction

Blind Copy to: (w/1 cy encl (1)
NRL, Code 6120, C. Poranski
NRL, Code 6120, J. Nagode

MEMORANDUM

June 2, 1992

From: James B. Nagode
To: Chester F. Poranski, Jr.

Subj: SONAR DOME RUBBER WINDOW (SDRW) AND SONAR RUBBER DOME (SRD) RADIOGRAPHIC INSPECTION REPORTS (MARCH - MAY 1992)

1. USS HEWITT (SDRW): No corrosion fatigue damage is apparent from the radiographs. Routine inspection schedule is recommended. See Appendix A.

2. USS ARLEIGH BURKE (SDRW): No corrosion fatigue damage is apparent from the radiographs. Routine inspection schedule is recommended. See Appendix B.

3. USS CHANCELLORSVILLE (SDRW): No structural damage is apparent from the radiographs. Routine inspection schedule is recommended. See Appendix C.

4. USS COMTE DE GRASSE (SDRW): No structural damage is apparent from the radiographs. Routine inspection schedule is recommended. See Appendix D.

5. USS BIDDLE (SDRW): Previously reported damage has grown. The continued monitoring of this SDRW is recommended. See Appendix E.

6. USS HUE CITY (SDRW): No structural damage is apparent from the radiographs. Routine inspection schedule is recommended. See Appendix F.

7. USS LONGBEACH (SRD-23): Four damage sites are apparent from the radiographs, one involving two plies. See Appendix G.

8. USS DAVIS (SRD-56): Five damage sites are apparent from the radiographs, one involving two plies. See Appendix H.

9. EX-USS SAMPLE (Brazilian Navy CT PARANA SDRW): Previously reported damage has grown. The continued monitoring of this SDRW is recommended. See Appendix I.

10. USS LAKE CHAMPLAIN (SDRW): No structural damage is apparent from the radiographs. Routine inspection schedule is recommended. See appendix J.

11. USS ELLIOT (SDRW): One damage site is apparent from the radiographs. We recommend that this SDRW be monitored. See Appendix K.

12. BF GOODRICH SRD-56 LAYUPS 118, 119, and 120 (S/N 21, 22, and 23): No structural damage is apparent from the radiographs. See Appendixes L, M, and N, respectively.

13. BF GOODRICH SDRW-SL LAYUP 250, and SDRW-2 LAYUP 35: No structural damage is apparent from the radiographs. See Appendixes O, and P, respectively.

DEPARTMENT OF THE NAVY
NAVAL RESEARCH LABORATORY
WASHINGTON, D.C. 20375-5320

IN REPLY REFER TO

9165/Prob 61-1549
Ser 6120/304

From: Commanding Officer, Naval Research Laboratory
To: Commander, Naval Sea Systems Command (Code 06U1D, S. Silverstein)

Subj: SONAR DOME RUBBER WINDOW (SDRW) AND SONAR RUBBER DOME (SRD) RADIOGRAPHIC INSPECTION REPORTS (MAY - AUGUST 1992)

Encl: (1) Two copies of subject Report

1. Enclosure (1) is forwarded for your information and retention.

MEMORANDUM

September 9, 1992

From: James B. Nagode
To: Chester F. Poranski, Jr.

Subj: SONAR DOME RUBBER WINDOW (SDRW) AND SONAR RUBBER DOME (SRD) RADIOGRAPHIC INSPECTION REPORTS (MAY - AUGUST 1992)

1. USS HEWES (SDRW): No corrosion fatigue damage is apparent from the radiographs. Routine inspection schedule is recommended. See Appendix A.

2. USS FAHRION (SRD-56): Four damage sites are apparent from the radiographs, one of which involves two plies. See Appendix B.

3. USS FITCH (SRD-56): Three damage sites are apparent from the radiographs. See Appendix C.

4. USS UNDERWOOD (SRD-56): No structural damage is apparent from the radiographs. See Appendix D.

5. USS O'BANNON (patched SDRW): No new damage is apparent from the radiographs. The continued monitoring of this SDRW is recommended. See Appendix E.

6. USS KIDD (SDRW): Two previously reported damage sites are unchanged since the last inspection. The continued monitoring of this SDRW is recommended. See Appendix F.

7. USS YORKTOWN (SDRW): Previously reported damage is unchanged since the last inspection. The continued monitoring of this SDRW is recommended. See Appendix G.

8. USS CARON (SDRW): Previously reported damage has grown since the last inspection. The continued monitoring of this SDRW is recommended. See Appendix H.

9. BFGOODRICHSDRW-SL LAYUPS 251, 252 (monolithic), 253, and 254: No structural damage is apparent from the radiographs. See Appendixes I, J, K, and L, respectively.

10. BFGOODRICHSRD-56 LAYUPS 121, 122, and 123: No structural damage is apparent from the radiographs. See Appendixes M, N, and O, respectively.

GEO-CENTERS, INC.

DEPARTMENT OF THE NAVY
NAVAL RESEARCH LABORATORY
WASHINGTON, D.C. 20375-5320

IN REPLY REFER TO

9165/Prob 61-1549
Ser 6120/418

DEC 09 1992

From: Commanding Officer, Naval Research Laboratory
To: Commander, Naval Sea Systems Command (Code 06U1D, S. Silverstein)

Subj: SONAR DOME RUBBER WINDOW (SDRW) AND SONAR RUBBER DOME (SRD) RADIOGRAPHIC INSPECTION REPORTS (AUGUST - NOVEMBER 1992)

Encl: (1) Two copies of subject report

1. Enclosure (1) is forwarded for your information and retention.

W. B. FOX
By direction

Blind Copies to:
Code 6126, C. F. Poranski, Jr.
Code 6126, J. Nagode

MEMORANDUM

From: James B. Nagode
To: Chester F. Porar ,ki, Jr

Subj: SONAR DOME RUBBER WINDOW (SDRW) AND SONAR RUBBER DOME (SRD) RADIOGRAPHIC INSPECTION REPORTS (AUGUST -NOVEMBER 1992)

1. USS BOONE (FFG28) SRD-56: Nine damage sites are reported, one of which involves two structural plies. See Appendix A.

2. USS THORN (DD988) SDRW: One damage site is apparent from the radiographs. We recommend that this SDRW be monitored. See Appendix B.

3. USS REUBEN JAMES (FFG57) SRD-56: Four damage sites are apparent from the radiographs, one of which involves two structural plies. See Appendix C.

4. USS BEARY (FF1085) SDRW: No damage is apparent from the radiographs. Routine inspection schedule is recommended. See Appendix D.

5. USS BREWTON (FF1086) SDRW: Previously reported damage has grown. The continued monitoring of this SDRW is recommended. See Appendix E.

6. USS TEXAS (CGN39) SDRW: Previously reported damage is unchanged. The continued monitoring of this SDRW is recommended. See Appendix F.

7. USS TICONDEROGA (CG47) SDRW: The first damage site is reported. We recommend that this SDRW be monitored. See Appendix G.

8. USS MERRILL (DD976) SDRW: The first damage is reported. We recommend that this SDRW be monitored. See Appendix H.

9. USS SCOTT (DDG995) SDRW: The first damage site is reported. We recommend that this SDRW be monitored. See Appendix I.

10. USS CARR (FFG52) SRD-56: Four damage sites are reported, two of which involve two structural plies. See Appendix J.

GEO-CENTERS, INC.

11. USS AINSWORTH (FF1090) SDRW: No damage is apparent from the radiographs. Routine inspection schedule is recommended. See Appendix K.

12. BFGOODRICH SDRW-SL LAYUPS 255, 256, and 257: No structural damage is apparent from the radiographs. See Appendixes L, M, and N, respectively.

13. BFGOODRICH SRD-56 LAYUPS 124, 125, 126, and 127: No structural damage is apparent from the radiographs. See Appendixes O, P, Q, and R, respectively.

GEO-CENTERS, INC.

DEPARTMENT OF THE NAVY
NAVAL RESEARCH LABORATORY
WASHINGTON, D.C. 20375-5320

IN REPLY REFER TO

9165/61-1549
Ser 6120-115

APR 27 1993

From: Commanding Officer, Naval Research Laboratory
To: Commander, Naval Sea Systems Command (Code 06U1D, S. Silverstein)

Subj: SONAR DOME RUBBER WINDOW (SDRW) AND SONAR RUBBER DOME (SRD) RADIOGRAPHIC INSPECTION REPORTS (NOVEMBER 1992 - APRIL 1993)

Encl: (1) Two copies of subject report

1. Enclosure (1) is forwarded for your information and retention.

W. B. FOX
By direction

Blind Copy to:
Code 6120, C. F. Poranski, Jr.
Code 6120, J. B. Nagode

MEMORANDUM

April 14, 1993

From: James B. Nagode
To: Chester F. Poranski, Jr.

Subj: SONAR DOME RUBBER WINDOW (SDRW) AND SONAR RUBBER DOME (SRD) RADIOGRAPHIC INSPECTION REPORTS (NOVEMBER 1992 - APRIL 1993)

1. EX-USS ROBERT E. PEARY (FF1073) SDRW: No damage is apparent from the radiographs. Routine inspection schedule is recommended. See Appendix A.

2. USS VINCENNES (CG49) SDRW: Previously reported damage has grown since the last inspection. The continued monitoring of this SDRW is recommended. See Appendix B.

3. USS ANZIO (CG68) SDRW: No damage is apparent from the radiographs. Routine inspection schedule is recommended. See Appendix C.

4. USS INGERSOLL (DD990) SDRW: One damage site is apparent from the radiographs. We recommend that this SDRW be monitored. See Appendix D.

5. USS SHILOH (CG67) SDRW: No damage is apparent from the radiographs. Routine inspection schedule is recommended. See Appendix E.

6. USS DAVID R. RAY (DD971) SDRW: No damage is apparent from the radiographs. Routine inspection schedule is recommended. See Appendix F.

7. USS GROVES (FFG29) SRD-56: No structural damage is apparent from the radiographs. See Appendix G.

8. USS JOHN YOUNG (DD973) SDRW: No damage is apparent from the radiographs. Routine inspection schedule is recommended. See Appendix H.

9. USS KIDD (DDG993) SDRW: Previously reported damage is unchanged since the last inspection. The continued monitoring of this SDRW is recommended. See Appendix I.

GEO-CENTERS, INC.

10. USS GATES (CG51) SDRW: Previously reported damage has grown since the last inspection. New damage is also apparent. We recommend that this SDRW be repaired or replaced. See Appendix J.

11. BFGOODRICH SDRW-SL LAYUPS 258 and 259: No structural damage is apparent from the radiographs. See Appendixes K, and L, respectively.

12. BFGOODRICH SRD-56 LAYUPS 128, 129, 130, 131, 132, 133, 134, 135, and 136: No structural damage is apparent from the radiographs. See Appendixes M, N, O, P, Q, R, S, T, and U, respectively.

GEO-CENTERS, INC.

APPENDIX B

NONDESTRUCTIVE TESTING OF SONAR DOMES - PROJECT TECHNICAL REVIEW

GEO-CENTERS, INC.

ADVANCED TEST EQUIPMENT AND METROLOGY

PROJECT TECHNICAL REVIEW 9 APRIL 1993

NONDESTRUCTIVE TESTING OF SONAR DOMES

Chet Poranski
Materials Chemistry Branch
Naval Research Laboratory

Ed Greenawald
Materials R&D Department
Geo-Centers, Inc

ADVANCED TEST EQUIPMENT AND METROLOGY

PROJECT TECHNICAL REVIEW 9 APRIL 1993

NONDESTRUCTIVE TESTING OF SONAR DOMES

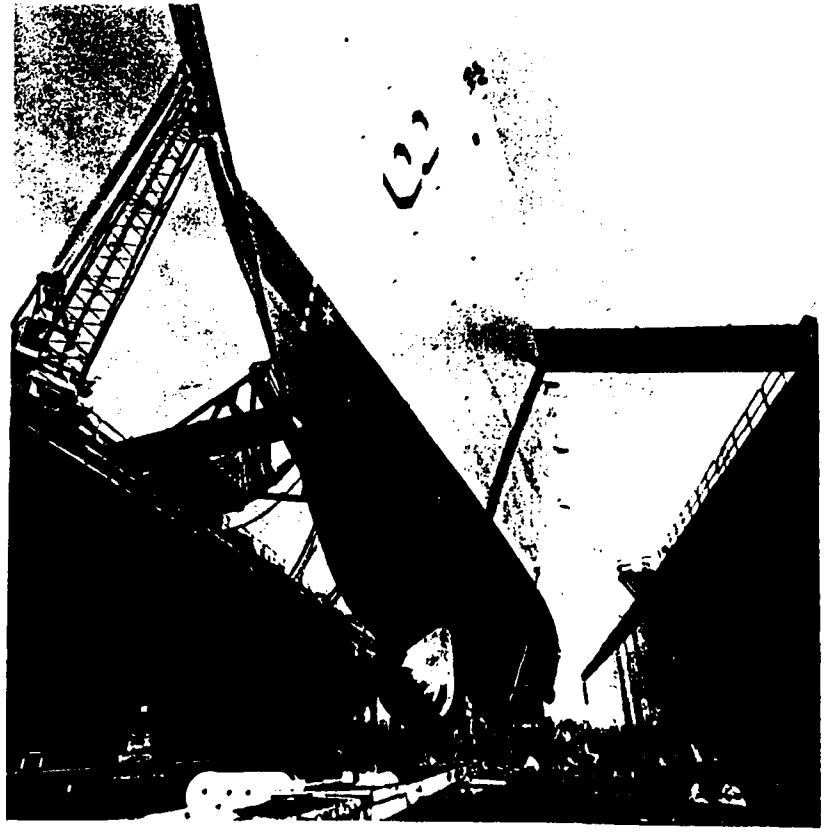

AN/SQS-56 TYPICAL DOME INSTALLATION

ADVANCED TEST EQUIPMENT AND METROLOGY

PROJECT TECHNICAL REVIEW 9 APRIL 1993

NONDESTRUCTIVE TESTING OF SONAR DOMES

NEED

- Composite sonar domes subject to failure at sea
- X-ray radiography effective to detect and monitor damage
- Keel dome radiography (FFG-7 Class)
    - requires costly drydocking and dome removal
    - too infrequent for effective damage monitoring
- Needed: One sided NDT method applicable underwater
- NAVY transition partner: NAVSEA Surface Ship ASW Group (O6U1)

ADVANCED TEST EQUIPMENT AND METROLOGY

PROJECT TECHNICAL REVIEW 9 APRIL 1993

NONDESTRUCTIVE TESTING OF SONAR DOMES

AN/SQS-56 REPLACEMENTS

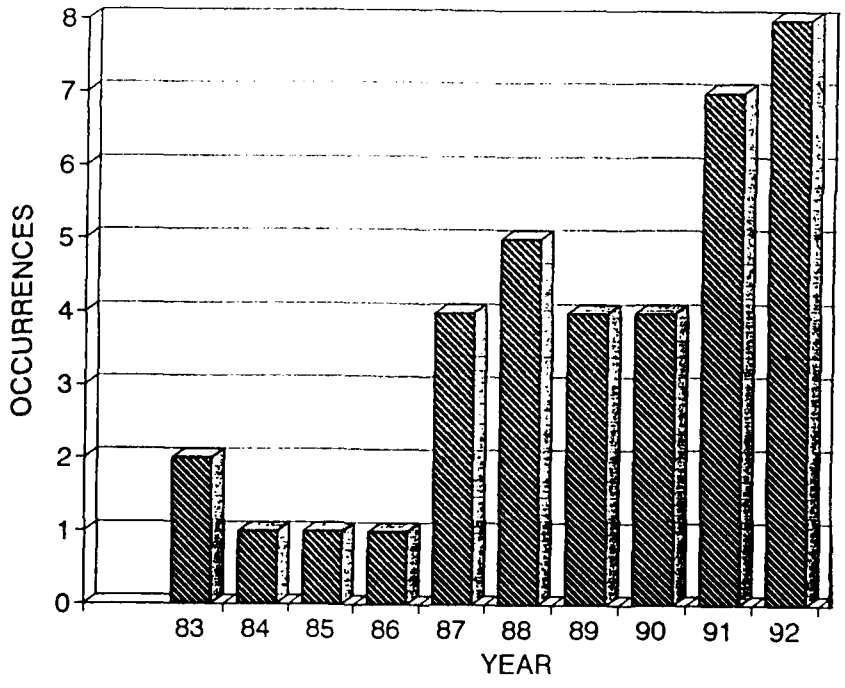

ADVANCED TEST EQUIPMENT AND METROLOGY

PROJECT TECHNICAL REVIEW 9 APRIL 1993

NONDESTRUCTIVE TESTING OF SONAR DOMES

SONAR RUBBER DOME CORRECTIVE ACTION PROGRAM (AN/SQS-56)

INTERDISCIPLINARY PROGRAM -- COORDINATION BY NRL

- Inspection (NRL)
  - Interpretation of Radiographs
  - Damage Monitoring, historical data base
  - New Methods
- Repair Procedures (BF Goodrich)
- Failure Analysis (NRL)
- SRD Dynamics at Sea (NRL)
  - Modeling - FEM (APL, U. Washington)

ADVANCED TEST EQUIPMENT AND METROLOGY

PROJECT TECHNICAL REVIEW 9 APRIL 1993

NONDESTRUCTIVE TESTING OF SONAR DOMES

STATE-OF-THE-ART

- Radiographic inspection of sonar domes is well developed (10 year program)
- Successful inspection program for bow-mounted domes (SDRW)
- Keel-mounted domes (SRD) inaccessible - Removal requuired
- A one-sided SRD inspection method is needed

ADVANCED TEST EQUIPMENT AND METROLOGY

PROJECT TECHNICAL REVIEW 9 APRIL 1993

NONDESTRUCTIVE TESTING OF SONAR DOMES

TECHNICAL OBJECTIVE

- Develop a prototype SRD inspection system
- Capabilities:
  - Transportable
  - Dome access: Exterior only
  - Inspection environment: Drydock and Pierside (underwater)
  - Identification of SRD ply sub-structures
  - Detection of broken steel cords and related damage

ADVANCED TEST EQUIPMENT AND METROLOGY

PROJECT TECHNICAL REVIEW 9 APRIL 1993

NONDESTRUCTIVE TESTING OF SONAR DOMES

TECHNICAL APPROACH

- One-sided NDT options: Shearography, MFL, Ultrasound, X-ray backscatter
- Trade-offs: Image quality (resolution, noise, quantitative vs. qualitative)
  Inspection time, complexity, cost
- Priorities: Image quality - Data interpretation - Fit with existing program
- X-ray backscatter promises best approximation to ideal (current) image quality
- Approach:
  - Develop x-ray backscatter tomography system for quantitative NDT
  - Base system on commercially available equipment to lower costs

ADVANCED TEST EQUIPMENT AND METROLOGY

PROJECT TECHNICAL REVIEW 9 APRIL 1993

NONDESTRUCTIVE TESTING OF SONAR DOMES

TECHNICAL PROBLEM

- Steel/rubber composite material - Hand lay-up - Complex, curved, layered structure
- Plan: Tomographic process - 3D data

- Limitations of x-ray backscatter technique
  - Severe superposition artifacts in non-homogeneous materials
  - Penetration limits - degradation of data with increasing depth
  - Resolution limits - require separation of broken cord ends
- Plan: Perform 3-d reconstruction using back propagation & a priori knowledge
  Pressurize dome to separate broken ends

- Inspection environment
- Plan: Containerize system for transport/climate control - enclose scanner

ADVANCED TEST EQUIPMENT AND METROLOGY

PROJECT TECHNICAL REVIEW 9 APRIL 1993

NONDESTRUCTIVE TESTING OF SONAR DOMES

WORK PROGRESS DESCRIPTION

- Background
- System description
- X-ray system acquisition
- Safety Requirements
- System containerization
- Scanner manipulator
- Preliminary scans of removed damaged sonar domes
- Data analysis

ADVANCED TEST EQUIPMENT AND METROLOGY

PROJECT TECHNICAL REVIEW 9 APRIL 1993

NONDESTRUCTIVE TESTING OF SONAR DOMES

SRD COMPOSITE MATERIAL

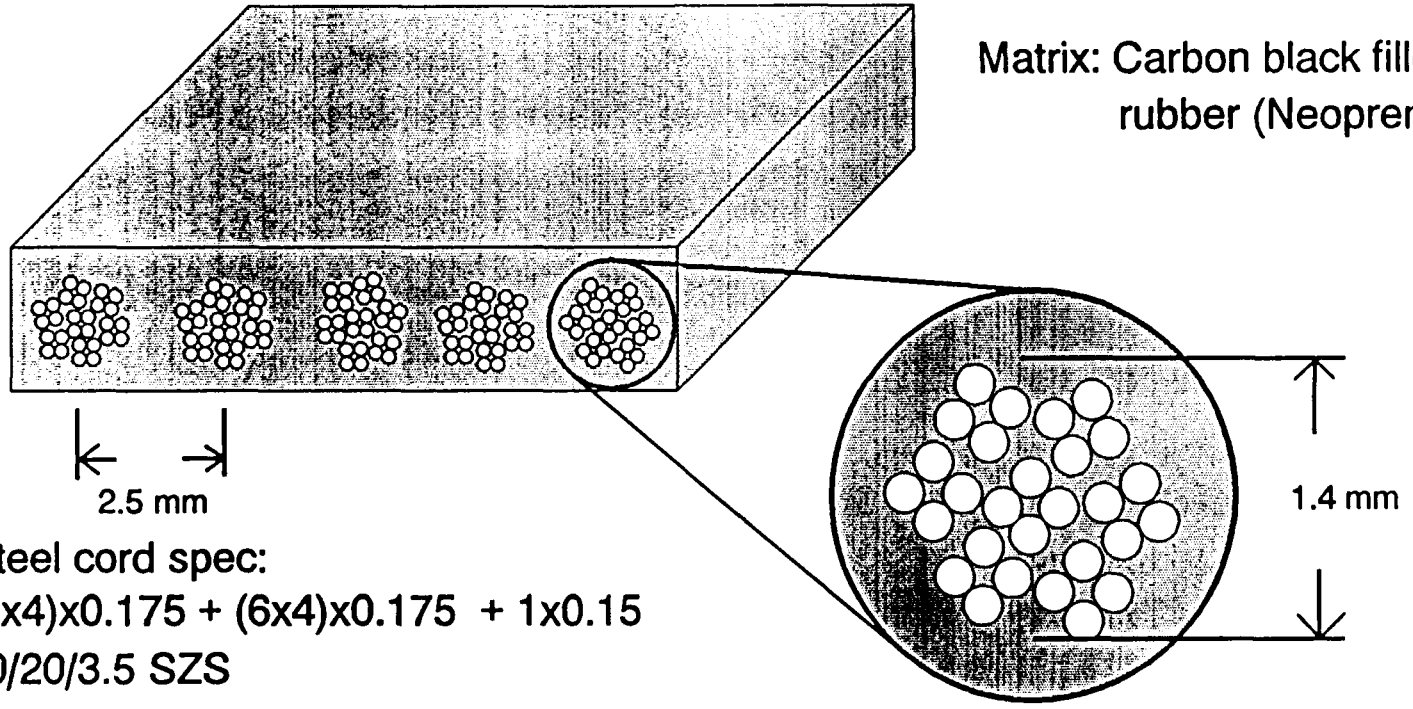

Matrix: Carbon black filled rubber (Neoprene)

Steel cord spec:
(1x4)x0.175 + (6x4)x0.175 + 1x0.15
10/20/3.5 SZS

ADVANCED TEST EQUIPMENT AND METROLOGY

PROJECT TECHNICAL REVIEW 9 APRIL 1993

NONDESTRUCTIVE TESTING OF SONAR DOMES

AN/SQS-56 SRD CONSTRUCTION FEATURES

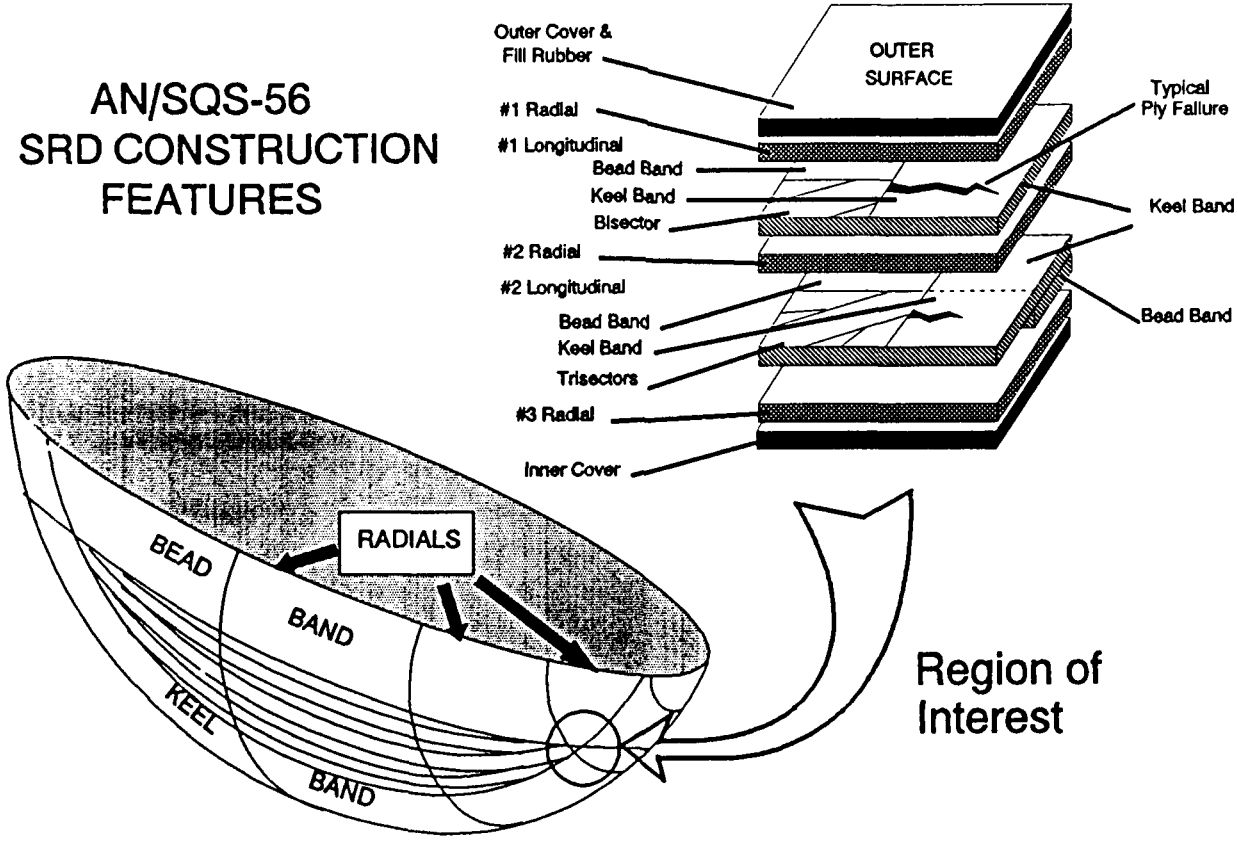

ADVANCED TEST EQUIPMENT AND METROLOGY

PROJECT TECHNICAL REVIEW 9 APRIL 1993

NONDESTRUCTIVE TESTING OF SONAR DOMES

SRD CONSTRUCTION DETAILS IN REGION OF INTEREST

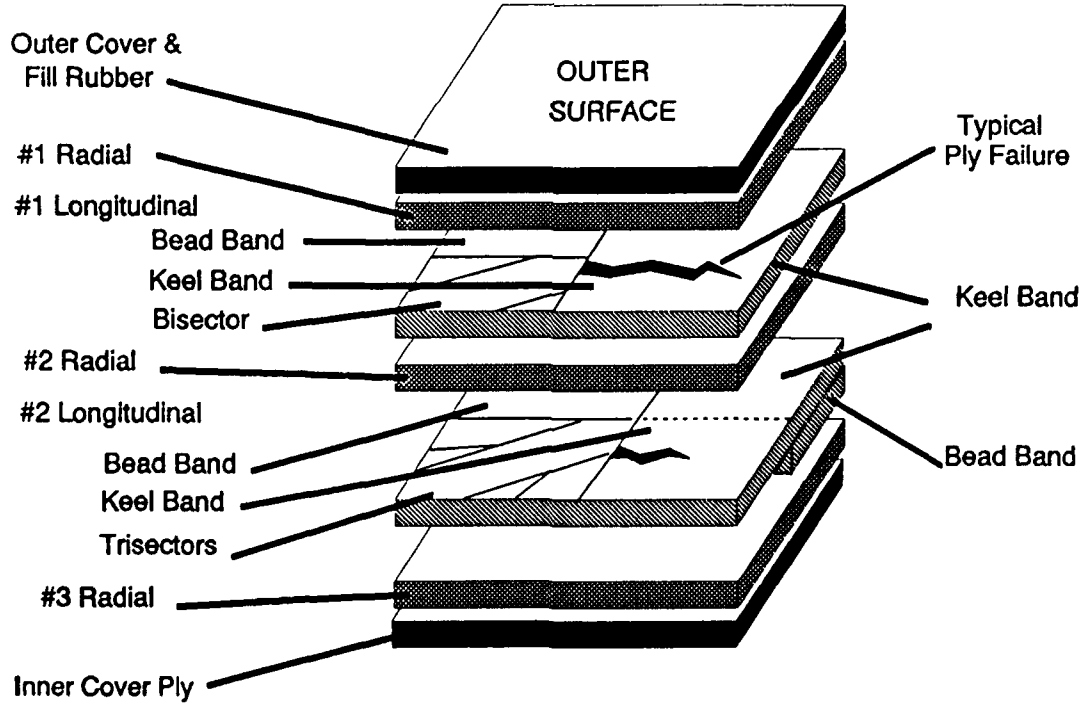

ADVANCED TEST EQUIPMENT AND METROLOGY

PROJECT TECHNICAL REVIEW 9 APRIL 1993

NONDESTRUCTIVE TESTING OF SONAR DOMES

X-RAY INSPECTION METHODS

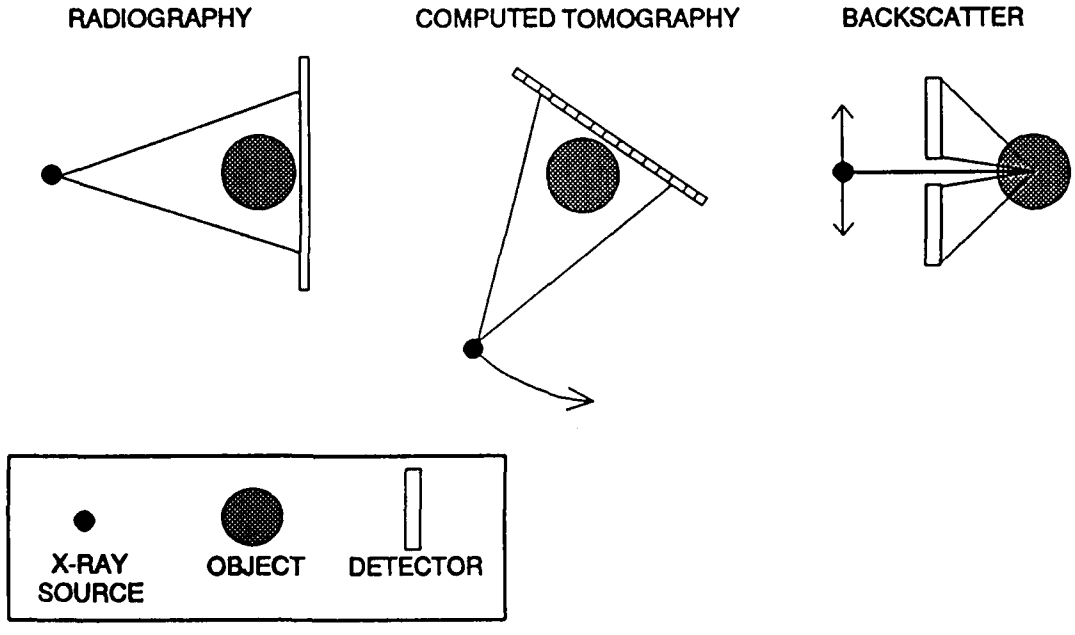

ADVANCED TEST EQUIPMENT AND METROLOGY

PROJECT TECHNICAL REVIEW 9 APRIL 1993

NONDESTRUCTIVE TESTING OF SONAR DOMES

THEORETICAL BASIS FOR XBT

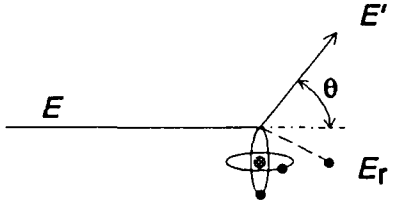

COMPTON SCATTER INTERACTION

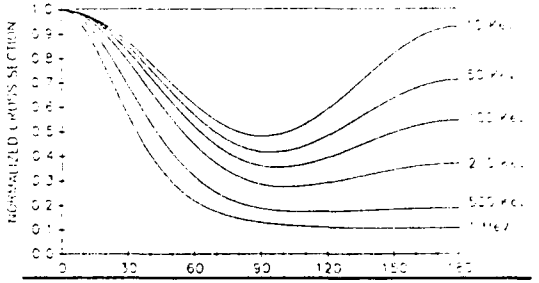

NORMALIZED SCATTER CROSS SECTION
AS FUNCTION OF SCATTER ANGLE

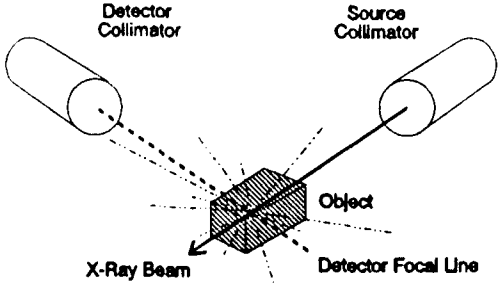

COLLIMATED SCATTER DETECTION

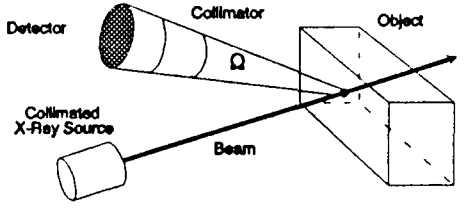

COMPTON SCATTER DETECTION
OVER A SOLID ANGLE

ADVANCED TEST EQUIPMENT AND METROLOGY

PROJECT TECHNICAL REVIEW 9 APRIL 1993

NONDESTRUCTIVE TESTING OF SONAR DOMES

HIGHLIGHTS OF XBT DEVELOPMENT HISTORY

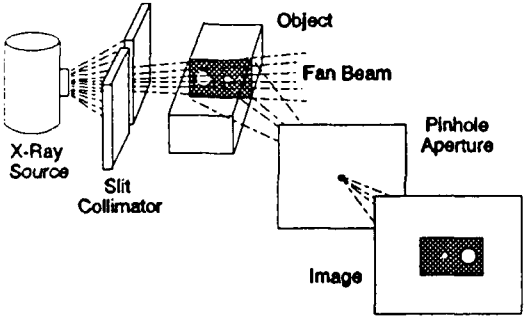

SCATTER TOMOGRAPHY PINHOLE CAMERA
Strecker, 1982

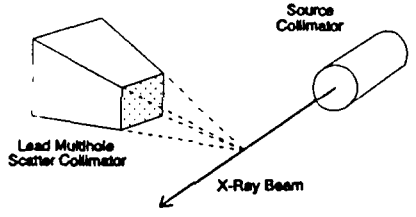

IRT FOCUSING COLLIMATOR
Costello, et al, 1983

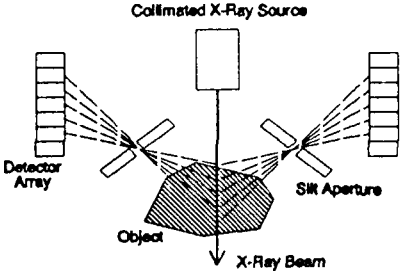

LINE SCATTER IMAGING
Harding, 1985

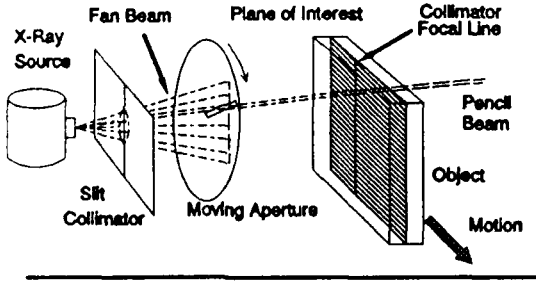

SCANNING BEAM TOMOGRAPHY
Annis & Bjorkholm, 1987

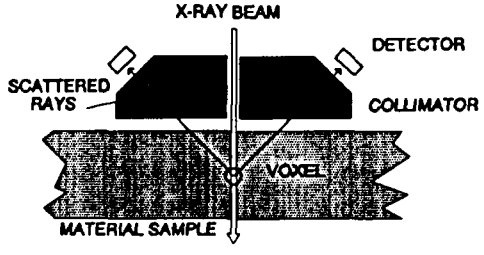

ARACOR BIT SCANNER, 1990

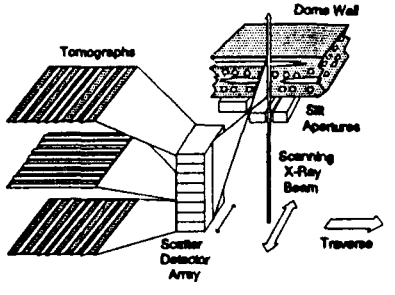

PHILIPS COMSCAN, 1992

ADVANCED TEST EQUIPMENT AND METROLOGY

PROJECT TECHNICAL REVIEW 9 APRIL 1993

NONDESTRUCTIVE TESTING OF SONAR DOMES

X-RAY BACKSCATTER TOMOGRAPHY OF SONAR DOMES
CONCEPTUAL DIAGRAM

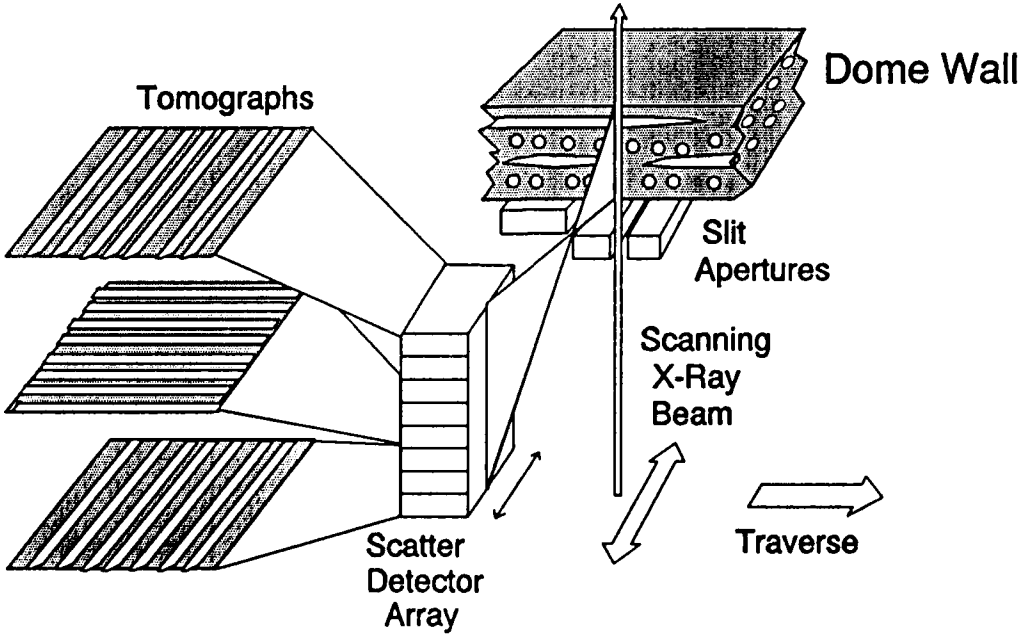

ADVANCED TEST EQUIPMENT AND METROLOGY

PROJECT TECHNICAL REVIEW 9 APRIL 1993

NONDESTRUCTIVE TESTING OF SONAR DOMES

PHILIPS COMSCAN X-RAY SCANNER

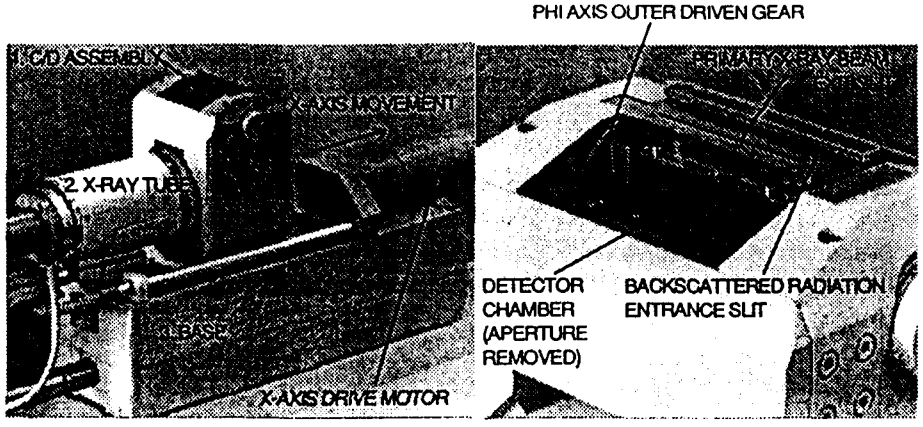

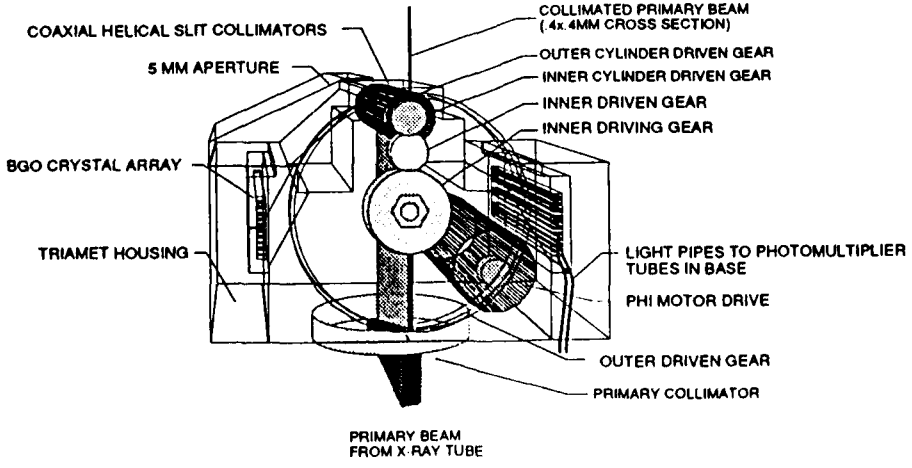

ADVANCED TEST EQUIPMENT AND METROLOGY

PROJECT TECHNICAL REVIEW 9 APRIL 1993

NONDESTRUCTIVE TESTING OF SONAR DOMES

XBT SYSTEM DIAGRAM

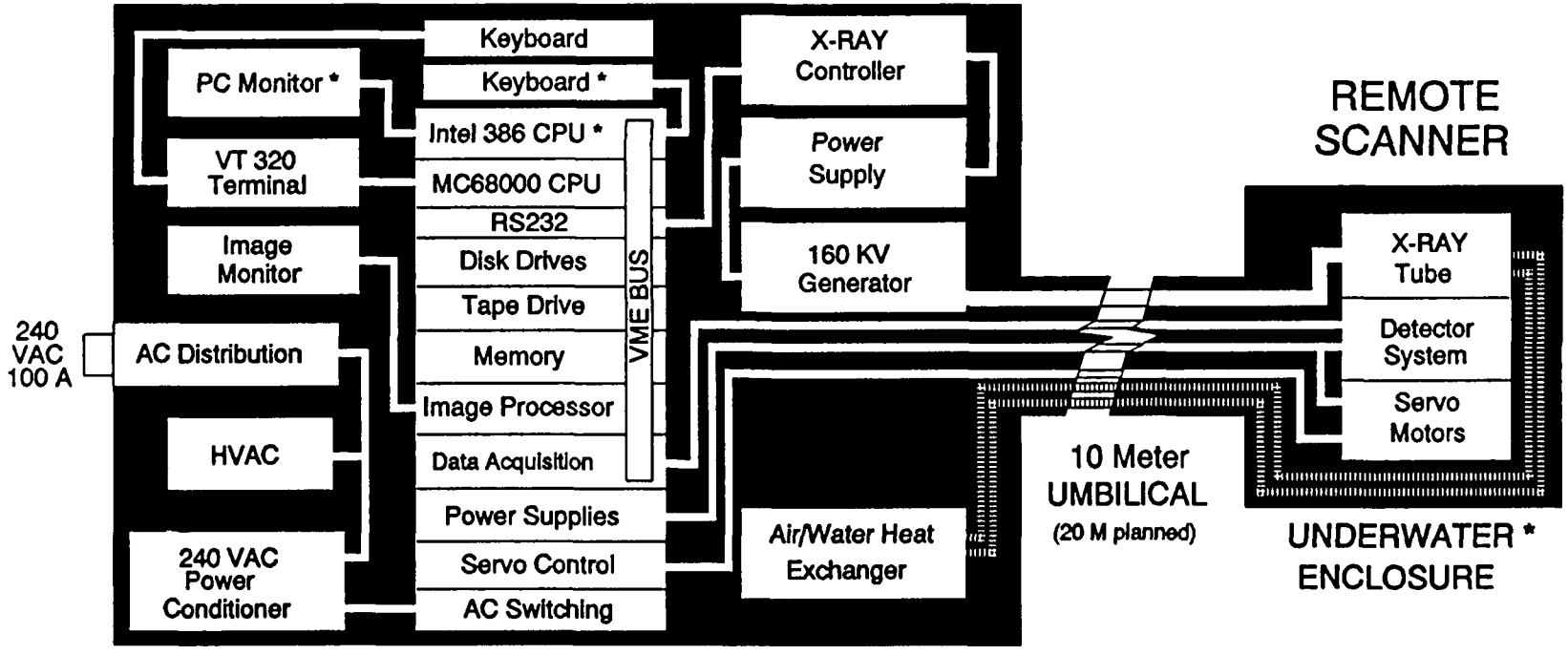

* planned options

ADVANCED TEST EQUIPMENT AND METROLOGY

PROJECT TECHNICAL REVIEW 9 APRIL 1993

NONDESTRUCTIVE TESTING OF SONAR DOMES

SYSTEM CONTAINER AND SCANNER MANIPULATOR

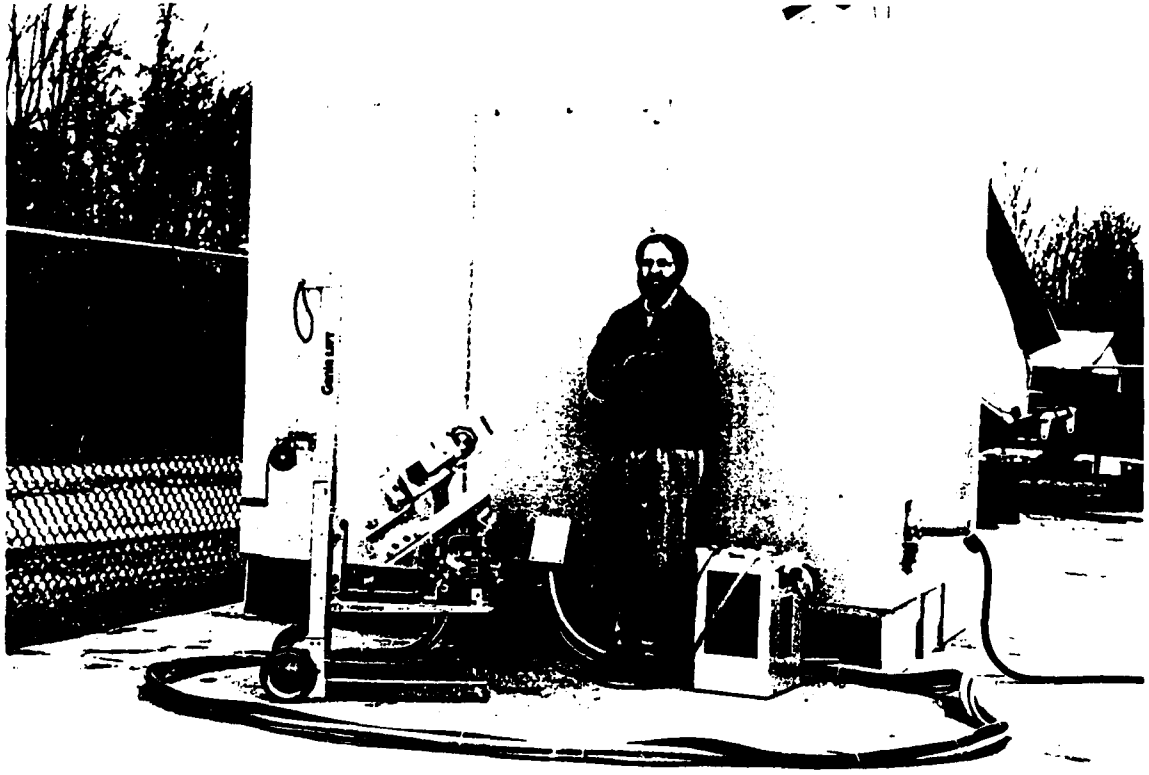

ADVANCED TEST EQUIPMENT AND METROLOGY

PROJECT TECHNICAL REVIEW 9 APRIL 1993

NONDESTRUCTIVE TESTING OF SONAR DOMES

SYSTEM CONTAINER - OPERATOR AREA

ADVANCED TEST EQUIPMENT AND METROLOGY

PROJECT TECHNICAL REVIEW 9 APRIL 1993

NONDESTRUCTIVE TESTING OF SONAR DOMES

SCANNER MANIPULATOR

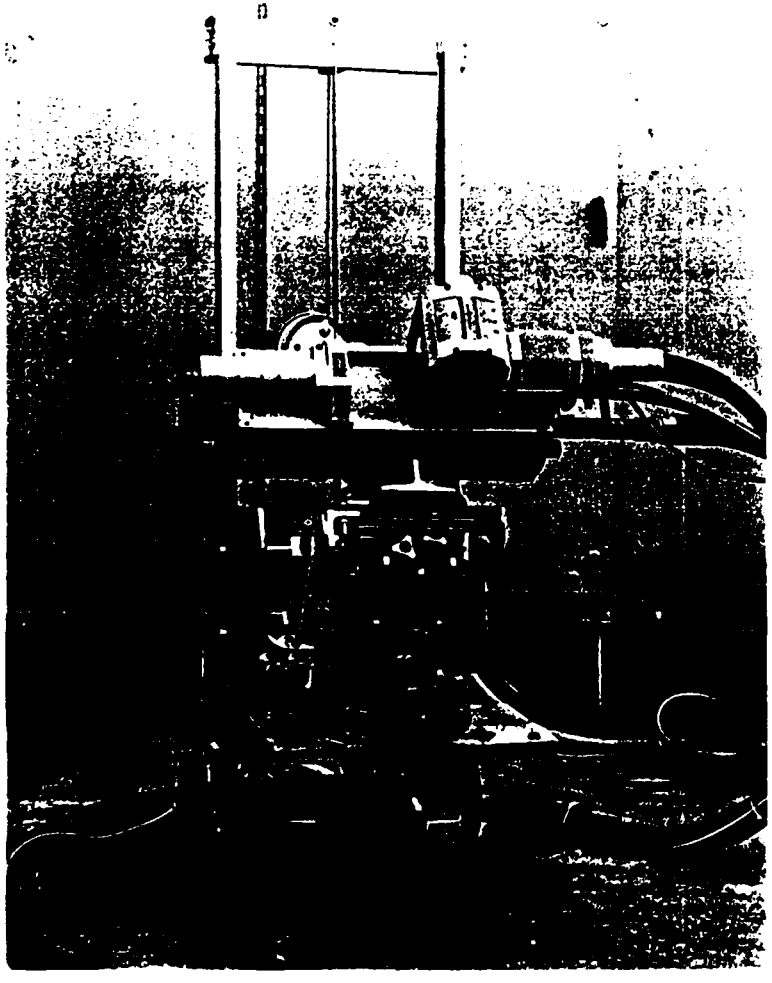

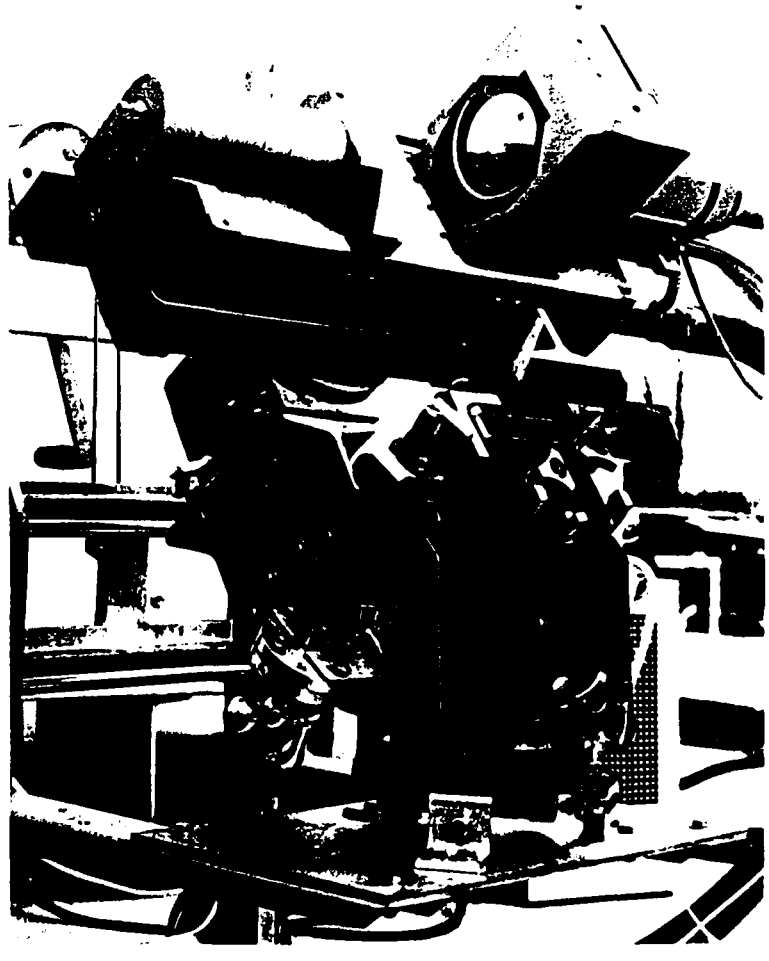

ADVANCED TEST EQUIPMENT AND METROLOGY

PROJECT TECHNICAL REVIEW 9 APRIL 1993

NONDESTRUCTIVE TESTING OF SONAR DOMES

INSPECTION OF REMOVED SRDS

USS CLARK

USS FAHRION

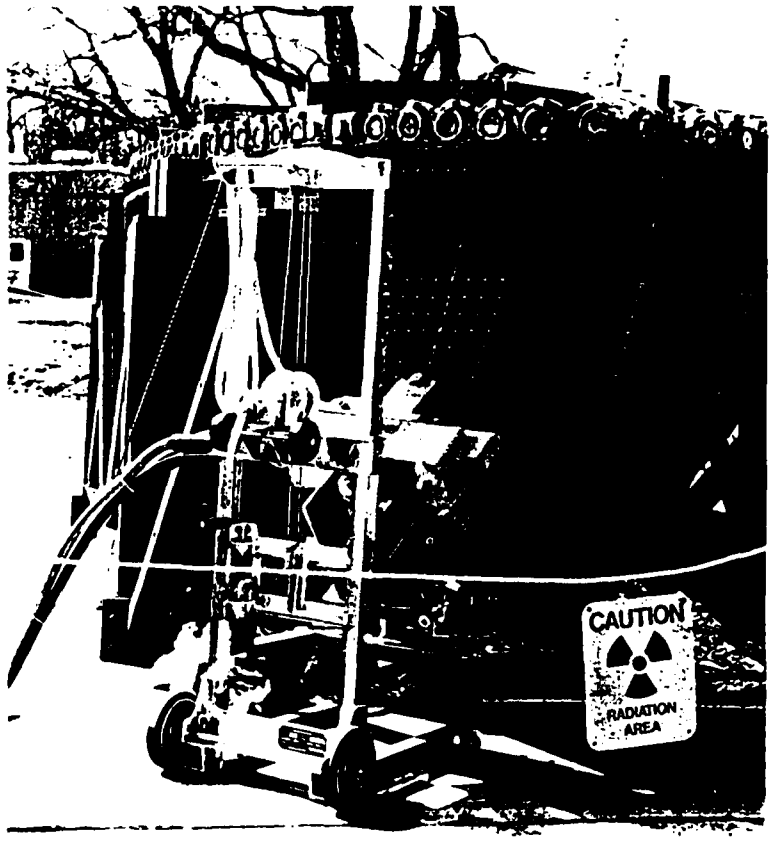

ADVANCED TEST EQUIPMENT AND METROLOGY

PROJECT TECHNICAL REVIEW 9 APRIL 1993

NONDESTRUCTIVE TESTING OF SONAR DOMES

SAFETY REQUIREMENTS COMPLETED

- TRAINING
  - Equipment Operation
  - Radiation Safety
- PROCEDURES
  - Personnel Dosimetry & Survey Instruments
  - Health Physics Survey of Site and Equipment
  - Written Inspection Procedure Approved by NAVSEA RASO

ADVANCED TEST EQUIPMENT AND METROLOGY

PROJECT TECHNICAL REVIEW 9 APRIL 1993

NONDESTRUCTIVE TESTING OF SONAR DOMES

XBT EVALUATION OF USS CLARK (FFG-11) SRD S/N A8

- SRD removed from ship for radiography - damage found
- XBT inspection conducted at NRL CBD site
  - Port side #1 & #2 keel band damage detected
  - SRD structural ply features detected - difficult w/increasing depth
- Bow Section of SRD cut out for radiography, dissection, analysis

ADVANCED TEST EQUIPMENT AND METROLOGY

PROJECT TECHNICAL REVIEW 9 APRIL 1993

NONDESTRUCTIVE TESTING OF SONAR DOMES

TOMOGRAPHS OF SRD KEEL BAND DAMAGE - USS CLARK (FFG-11) S/N A8

Layer 2

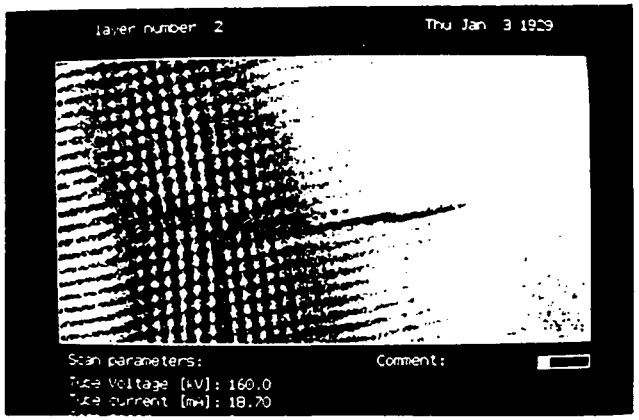

Layer 6

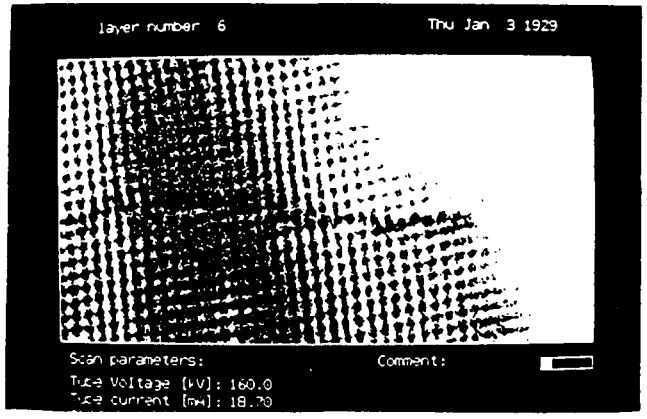

Layer 4

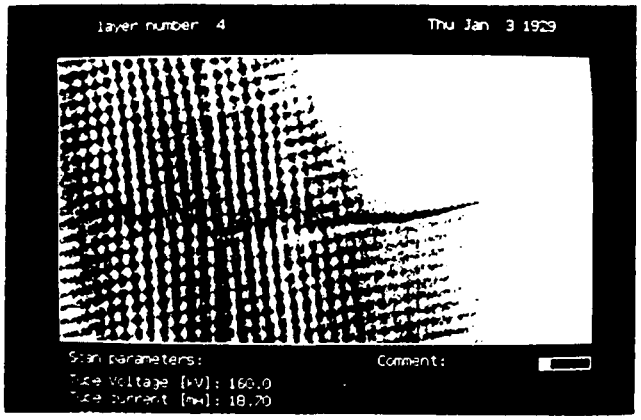

Layer 8

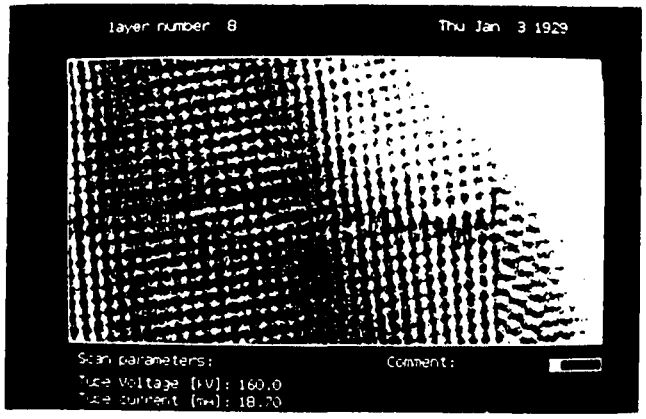

ADVANCED TEST EQUIPMENT AND METROLOGY

PROJECT TECHNICAL REVIEW 9 APRIL 1993

NONDESTRUCTIVE TESTING OF SONAR DOMES

XBT EVALUATION OF USS FAHRION (FFG-22) SRD S/N A11

- SRD removed from ship for radiography - damage found
- XBT inspection conducted at NRL CBD site
  - Starboard keel band damage not detected while SRD relaxed
  - Keel band loaded (water) - starboard damage detected
- Bow Section of SRD to be cut out for radiography, dissection, analysis

ADVANCED TEST EQUIPMENT AND METROLOGY

PROJECT TECHNICAL REVIEW 9 APRIL 1993

NONDESTRUCTIVE TESTING OF SONAR DOMES

TOMOGRAPHS OF SRD KEEL BAND DAMAGE - USS FAHRION (FFG-22) S/N A11

RELAXED

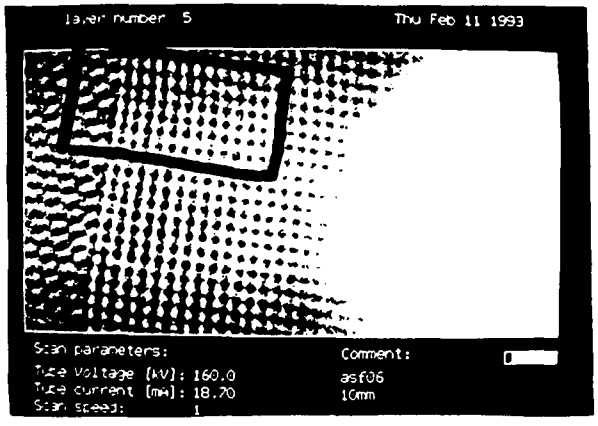

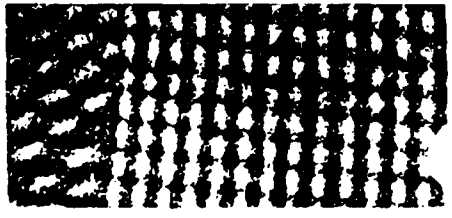

LOADED (WATER)

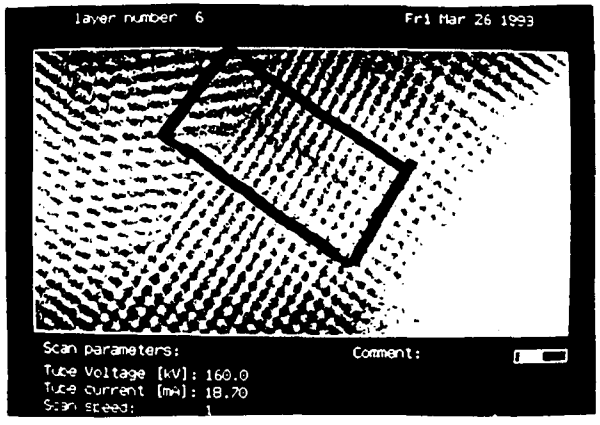

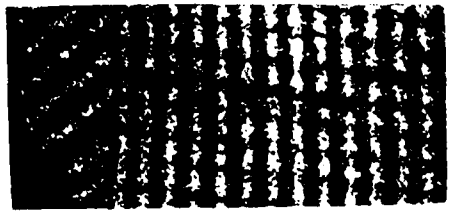

ADVANCED TEST EQUIPMENT AND METROLOGY

PROJECT TECHNICAL REVIEW 9 APRIL 1993

NONDESTRUCTIVE TESTING OF SONAR DOMES

ARTIFACTS OF SONAR DOME XBT

CORD SHADOW ARTIFACT

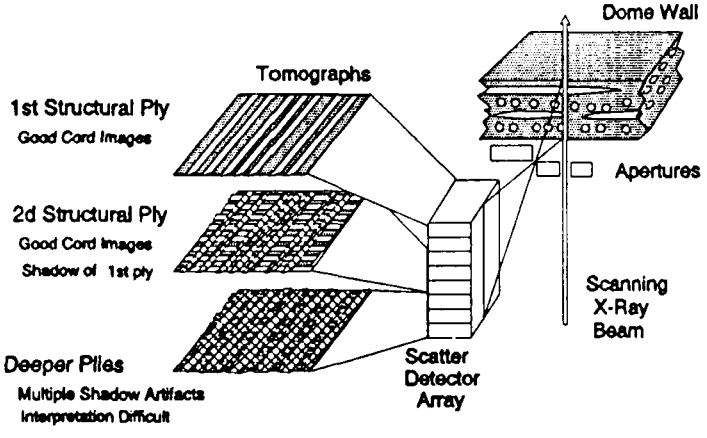

DOME CURVATURE ARTIFACT

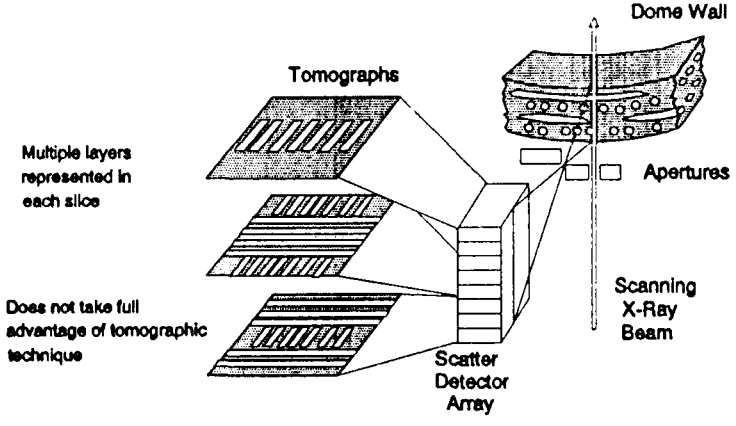

ADVANCED TEST EQUIPMENT AND METROLOGY

PROJECT TECHNICAL REVIEW 9 APRIL 1993

NONDESTRUCTIVE TESTING OF SONAR DOMES

ACCOMPLISHMENTS

- All milestones on schedule
  - System containerization completed
  - Scanner manipulator completed
  - Data from 2 damaged domes (removed from FFG-7 Class)
- Preliminary results
  - Successful detection of #1 & #2 keel band damage
  - No detection of #2 bead band damage

NONDESTRUCTIVE TESTING OF SONAR DOMES

PROJECTED OUT-YEAR ACCOMPLISHMENTS

FY 93
- Complete prototype hull attachment fixture
- Conduct removed dome and drydock inspections *
- Begin image processing and reconstruction work

FY 94
- Complete final hull attachment fixture and underwater enclosure
- Continue drydock inspections - Demonstrate underwater inspection *
- Complete image processing and reconstruction methods

FY 95
- Conduct drydock and pierside SRD inspections *
- Develop data compression/transmission methods
- Final report

FY 96
- Transition

* (subject to ship availability)

ADVANCED TEST EQUIPMENT AND METROLOGY

PROJECT TECHNICAL REVIEW 9 APRIL 1993

NONDESTRUCTIVE TESTING OF SONAR DOMES

TRANSITION

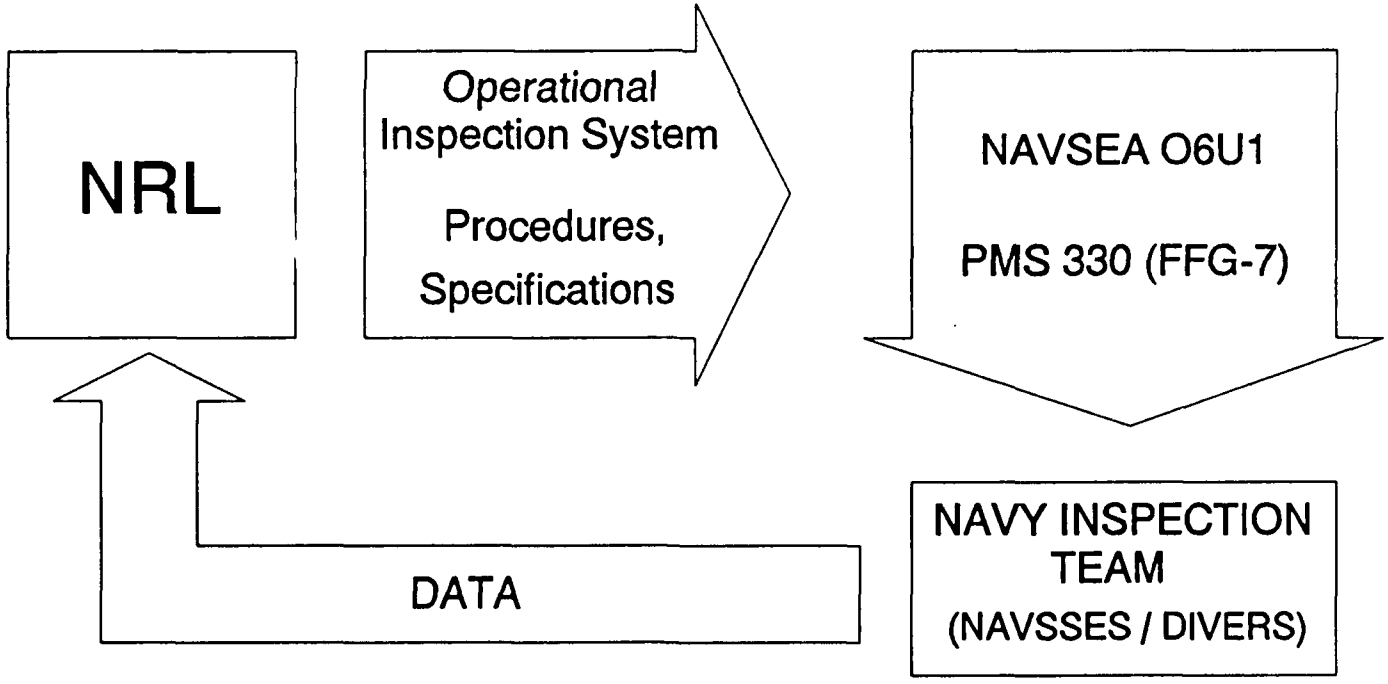

ADVANCED TEST EQUIPMENT AND METROLOGY
PROJECT TECHNICAL REVIEW 9 APRIL 1993

NONDESTRUCTIVE TESTING OF SONAR DOMES

APPENDIX: RESEARCH TASKS

- Prototype SRD Inspection System Development
  - Optimum Scanning sequence, Geometry
  - Indexing Mechanism
  - Underwater Adaptation
- DataAcquisition
  - Scan Removed SRDs
  - Scan In Service SRDs (Drydock)
  - Scan In Service SRDs (Pierside)
- Data Analysis & Interpretation
  - Compare with Transmission Radiography
  - Image Processing
    - Artifact Removal
    - Image Enhancement
    - 3-D Reconstruction
    - Feature Recognition
    - Data Compression

APPENDIX: XBT SYSTEM SPECIFICATIONS

- X-ray parameters: 160 kV 19 mA metal-ceramic x-ray tube w/ 1 mm Be window

- Scan parameters:

  X-ray beam cross-section: 0.4 mm x 0.4 mm
  Scan area: 50 mm x 100 mm
  Scan time: variable 75 - 375 seconds in 5 steps
  Depth range: aperture & material dependent 5-50 mm

- Data parameters:

  22 slices (e.g. 0.9 mm overlapping slices using 10 mm aperture)
  250 x 500 pixels per slice
  A/D accuracy: 16 bits (8 bits stored)
  Max resolution: 0.4 mm x 0.4 mm x 0.4 mm (5 mm aperture)
  Display: 1 or 2 slices on 512 x 512 video screen

APPENDIX C

SONAR DOME NDE PROGRAM SUMMARY

GEO-CENTERS, INC.

Task D-9. Nondestructive Testing of Sonar Domes. Develop new technology capabilities that will provide for underwater inspection of sonar rubber domes (SRDs) at pierside to locate and identify stress corrosion, corrosion fatigue, and tensile fatigue/failure. Develop transportable prototype SRD inspection system based on x-ray backscatter tomography (XBT). Develop all hardware and procedures for underwater use and develop image processing and computer reconstruction methods for display and interpretation of data. Demonstrate and validate system performance.

NONDESTRUCTIVE TESTING OF SONAR DOMES

Navy Problem/Deficiency

Keel mounted Sonar Rubber Domes (SRDs) on Navy surface combatants are subject to unexpected rupture at sea. The mechanisms of stress corrosion, corrosion fatigue, and tensile failure have been implicated. X-ray radiography is used to manage a similar failure problem with the larger bow mounted Sonar Dome Rubber Windows (SDRWs). Both drydock and pierside (underwater) techniques are used. But radiography requires access to the dome interior. Since keel domes have no airlock, access is limited to drydock availabilities. Furthermore, the AN/SQS-56 SRD, installed on FFG-7 class frigates, must be removed from the hull for inspection. Major benefits in operational readiness and significant cost savings would result from the development of a one-sided underwater inspection technique for SRDs.

Technical Objective/Expected Payoffs

Our objective is to develop a pierside SRD inspection capability which would considerably improve the effectiveness of the SRD inspection program. Payoffs are expected in the following areas:

(a) Costs per SRD inspection will be lowered, due to the elimination of drydocking ($1M per occurrence) and removal requirements.

(b) Inspections will be more frequent, with timing based upon technical considerations and pierside availability rather than drydock availability. This will allow the identification of high risk SRDs and monitoring of lesser damaged SRDs. The expected decrease in SRD failures-at-sea will result in increased operational readiness.

(c) Identification of the damaged SRD population will facilitate planning for procurement to maintain spare inventories.

(d) Inspection data will contribute to the ongoing SRD

failure analysis and corrective action effort.

Technical Background and Approach

Sonar Rubber Domes (SRD), also known as keel domes, rupture due to the failure of the steel cord elements of the steel/rubber composite dome wall. Preliminary failure analysis work suggests a failure mechanism similar to that seen in the larger bow mounted Sonar Dome Rubber Windows (SDRW). The failure scenario involves water intrusion via cracks, migration via voids or cord wicking, corrosion of cords exposed to the water, and fatigue of weakened cords during flexure of the dome wall.

The SDRW has been the subject of a successful Corrective Action Program (CAP) during which the failure mechanisms were characterized and a radiographic inspection program was implemented. Inspection methods were first developed for use in drydock. Then an underwater technique was developed for use at pierside. The entire fleet has been surveyed. High risk SDRWs were identified and repaired or replaced. A large population of damaged SDRWs with minor damage remain in service while monitored via annual inspection. Failures-at-sea, formerly increasing at an alarming rate, have been nearly eliminated. Planned replacements are occurring at a manageable rate. Operational disruptions have been reduced and considerable cost savings have resulted.

The same methods developed for SDRW inspection are currently also used to inspect SRDs. Using standard industrial radiography procedures, film is placed on the inside surface of the SRD and the area is irradiated from the outside to form an x-ray transmission image. This process requires access to both sides of the dome wall. SRD interiors, unlike those of the larger SDRWs, are accessible only in drydock. Further, the AN/SQS-56 SRD must be removed from the hull. This requirement has handicapped the inspection program.

In order to apply the lessons learned in the SDRW program to SRDs and to achieve similar success in managing this problem, it will be necessary to inspect all of the SRDs in service and to accumulate periodic inspection data. Our current capability is inadequate to achieve these goals. A pierside inspection methodology is needed. The technology must be sufficiently sensitive to detect internal SRD damage and be applicable from the exterior of the submerged dome.

X-ray backscatter tomography (XBT) is a new one-sided x-ray technology which provides image data representing the composition of a planar slice within the inspected object. The process is based upon the Compton scattering interaction between incident x-rays and electrons in the material. Each volume element, or voxel, in the slice is interrogated by a narrow x-ray beam and collimated scatter detectors. Both the location of the voxel and its scatter signal are acquired and used to form an image.

Multiple slices can be acquired to represent the whole volume to be inspected. Unlike the better known computed tomography (CT), XBT requires access only to the source side of the object.

Both resolution and required dwell time per voxel are determined by the x-ray beam and detector aperture sizes. Because of this trade-off, systems providing practical inspection times have lower resolution than provided by radiography. But, they have the advantage of three dimensional resolution. Since the beam and scatter signal are both modulated by material outside the voxel being measured, XBT has usually been applied to homogeneous materials which are either thin or of low density. Under these conditions, undesirable effects are minimized.

Numerous applications of XBT have been proposed in the literature and a few have been developed to the demonstration phase. However, this technology has never been widely implemented. This is due both to the above mentioned trade-offs and to the availability of the well developed CT technology. Some one- sided problems are amenable to other solutions such as ultrasound. Only recently has there been a suitable x-ray scanner on the market, obviating the need for costly development of a one-of-a-kind scanner.

There are also some drawbacks and trade-offs to consider in this sonar dome application. While XBT is expected to provide the benefits of one-sided inspection, resolution will be poorer than the current film based method. We will also be pushing this technology to new limits, with respect to depth penetration. Safety considerations will also be paramount in the development and use of equipment involving radiation, high voltage, and undersea work. The introduction of new highly specialized inspection methods to replace a proven standard technology will also require more skilled inspectors and more costly maintenance of inspection equipment. We believe these problem areas are outweighed by the payoffs described above.

Our approach will be to develop and field an XBT inspection system suitable for the in-situ inspection of AN/SQS-56 SRDs. It will be cost-effective to base the system on a commercially available x-ray backscatter scanner. The Philips Comscan System is currently the only such instrument available.

The criteria for successful inspection will be the detection of failed steel cords in the outer longitudinal ply and runs of broken cords greater than 1 inch in the second longitudinal ply. Attempts will also be made to resolve damage to the deeper overlapped longitudinal structures. XBT evaluations will be verified by comparison with radiographic inspection data and by physical dissection of the inspected SRDs.

There are four major sub-tasks in the developmental effort:

1. Mechanical Prototype. The proposed system consists of a

number of sub-systems: a power conditioner; power supplies; 160 KV high voltage generator; x-ray system controller; rack containing computers, data acquisition boards, and servo controls; a computer terminal and three CRT monitors; heat exchanger for x-ray tube coolant; and a remote x-ray scanner head with cables and coolant hoses. All of this equipment is to be installed in a transportable container. The container will have a shock mounted floor, watertight doors, and overhead trolley crane for deployment of the scanner. The container will also be insulated and have lighting, heating and air-conditioning, and sound absorbing panels. Hardware will be developed for attaching the scanner to the ship's hull and for indexing the scanner through a sequence of positions on the dome surface. An underwater scanner enclosure with 20 meter umbilical to the surface will be developed.

2. Methodology and data acquisition. This work will involve actual inspection of SRDs. First, we will inspect domes removed for cause and SRDs which become available in drydock. Inspection coverage requirements will be determined and scanner parameters will be optimized. Data will be compared with radiography results. Underwater inspections will ultimately be demonstrated. Data acquisition, storage and transmission sub-systems will be developed and modified as required.

3. Data Analysis. New computer reconstruction methods will be needed to meet inspection sensitivity objectives. This will require the characterization of system performance. The development of a computer model of the process is planned to aid in the evaluation of reconstruction strategies. Data visualization methods will be evaluated and implemented. Data compression and transmission methods will also be investigated.

4. Transition. (See Transition Plan, below.)

Summary of Current Year Work

FY 93 (New start)

Fabrication of the shipping/utilization container (SUC) was completed and the XBT system components were installed within for field operation. A light weight manipulator was designed and fabricated to provide 5-axis control of the scanner for sonar dome inspection trials. A trailer was fitted out to provide workshop and storage space at the Chesapeake Beach field site. The SUC has been located on an existing concrete pad. Space is provided on the pad to place removed sonar domes for inspection trials.

Design work was begun for the prototype hull attachment and scanning fixtures to be used in drydock inspection trials. We plan to complete and test this hardware by the end of FY 93.

Operating procedures were written and approved by the Navy

Radiation Affairs Safety Office. This was required before operation of the system was permitted. XBT inspections were conducted of damaged SRDs removed from the USS CLARK (FFG-11) and USS FAHRION (FFG-22). These domes had been radiographed and found to contain a number of typical damage sites. The known damaged areas were inspected using the XBT system with various scanning speeds, apertures, and orientations.
The data produced were compared with the transmission radiographs.

The results demonstrate the ability of XBT to detect keel band damage, but not the deeper bead band damage. Also, in one case keel band damage was undetected unless the dome was loaded with water. This indicates that broken cord ends must be separated a certain distance to be resolved. We propose to ensure separation by pressurizing the in-situ domes. This will be tried at the next drydock opportunity.

With regard to the problem resolving deeper structure, we have determined that data from a given depth contains artifacts of the XBT process. The most damaging artifact to interpretation is caused by attenuation of both primary and scattered x-rays by overlying steel cords. This superposition problem will be targeted in the reconstruction effort. We have begun the development of computer reconstruction and image processing methods to increase the effective depth of XBT inspection and improve interpretation. We are also developing software and evaluating commercially available programs for data visualization.

We plan to inspect 2 more removed SRDs as well as at least one in-service SRD by the end of FY 93.

Planned Work

FY 94

Hull attachment hardware, indexing fixtures, scanner enclosure, and an extended umbilical will be designed and built for underwater use. The chief problem is to maintain contact between the x-ray scanner window and the dome surface, while providing remote position indexing and corrective adjustments. The emphasis will be on developing simple designs for ease of use by inspection divers, low weight, low maintenance, and reliability. The field site trailer will be converted to a scanning laboratory for characterizing the XBT system performance characteristics and evaluating other applications.

Data acquisition work will be continued. The emphasis will be on providing data for the analysis tasks, trials of hardware systems, and planning with the dive team. If possible, we will conduct inspections in conjunction with planned SRD radiography in order to compare results.

A demonstration of underwater SRD inspection will be conducted.

A candidate has been identified for an ONR Post-Doctoral Fellowship and his proposal, entitled "Reconstruction Method for X-ray Backscatter Tomography," will be submitted to ASEE for review. The reconstruction development work will be completed by the end of FY 94.

FY 95

Drydock inspections will be continued, contingent on ship availability. Results will be compared with those of conventional inspections. We will also conduct underwater inspections of SRDs, subject to ship pierside availabilities. Equipment and procedures will be fine-tuned as required.

Data compression/transmission methods will be developed for the remote display and interpretation of data.

A final report will be prepared as well as an XBT inspection manual and system specifications.

FY 96

Transition to NAVSEA (See below).

Transition Plan

The prototype system will be sufficiently developed for direct transition to routine field use by FY 96. The system and its documentation will be transferred to the NAVSEA Surface Ship ASW Group (Stan Silverstein, 06U1D). NAVSEA will identify an appropriate Navy entity to conduct the inspections. Inspection data will be transmitted to NRL for interpretation.

The unique capabilities of the XBT system also have potential for application to other NDE problems within DOD, DOE and NASA, as well as the aircraft and nuclear industries. Informal contacts are being maintained with the NDE community and collaborative efforts are anticipated.

Relationship to Other Programs

This is part of the NAVSEA ASW Group's Sonar Rubber Dome Corrective Action Program. The current sonar dome inspection program is described under "Technical Background and Approach", above.

The Air Force is currently sponsoring programs to apply x-ray backscatter technology to rocket motor and advanced composite airframe NDE. Collaborations on two of these programs were instrumental in providing initial data from sonar dome samples for our XBT feasibility study.

Test XBT scans of composites are planned in collaboration with the Navy Center of Excellence for Composites.

APPENDIX A:

GLOSSARY OF TERMS

NDE — Nondestructive Evaluation (aka NDT, NDI). Non-invasive inspection methods such as x-ray and ultrasound.

SDRW — Sonar Dome Rubber Window. Bow mounted steel reinforced rubber sonar dome.

Sonar Dome — Dome providing a fairing for the sonar transducer system.

SRD — Sonar Rubber Dome. Keel mounted steel reinforced rubber sonar dome.

SUC — Shipping/Utilization Container. Transportable container for the x-ray backscatter system from which the system can be operated in the field.

Voxel — Volume element. 3-D version of the 2-D "pixel".

XBT — X-Ray Backscatter Tomography. One-sided NDE method based upon Compton scattering, an interaction between x-ray photons and electrons.

APPENDIX B: PUBLICATIONS AND PRESENTATIONS

1. C.F. Poranski and E.C. Greenawald, "One-Sided NDE for Sonar Rubber Domes," Proceedings, 41st Defense Working Group on Nondestructive Testing, Tucson, AZ, Nov. 1992, in press.

2. E.C. Greenawald and C.F. Poranski, "Artifacts in X-Ray Backscatter Tomography of Non-Homogeneous Objects," accepted for presentation to Review of Progress in Quantitative Nondestructive Evaluation, Bowdoin College, Brunswick, ME, Aug. 1993.

3. Y.S. Ham, E.C. Greenawald, and C.F. Poranski, "X-Ray Backscatter Tomography of Low Density, Low Atomic Number Materials," abstract submitted to ASNT for presentation to Radiologic NDT III: Advancements, Automation, and Imaging, Atlantic City, NJ, Aug. 1993.

4. E.C. Greenawald, Y.S. Ham, and C.F. Poranski, "Visualization of X-Ray Backscatter Data," abstract submitted to the ASNT for presentation at their Fall Conference, Long Beach CA, Nov. 1993.

APPENDIX D

OPERATING PROCEDURE FOR X-RAY BACKSCATTER TOMOGRAPHY OF SONAR DOMES

GEO-CENTERS, INC.

OPERATING PROCEDURE FOR X-RAY BACKSCATTER TOMOGRAPHY (XBT) OF SONAR DOMES

Revision 1, March 3, 1993

CONTENTS

1. SCOPE. 1

2. SAFETY. 1
   2.1. Regulations. 1
   2.2. Operator Qualifications. 1
   2.3. Radiation Survey. 2
   2.4. Restricted Areas. 2
   2.5. Safety and Warning Devices. 3
   2.6. Beam Direction. 4
   2.7. Impaired Safe Operation. 4
   2.8. Emergency Procedures. 4

3. OPERATION. 4
   3.1. Preparatory Procedures. 4
   3.2. Scanning Operations. 6
   3.3. Post-operational Procedures. 6
   3.4. Other Procedures. 7

1. SCOPE.

This document is intended to govern the use of a Philips Comscan XBT instrument during the development of nondestructive inspection procedures for sonar domes. The work will be accomplished at the Naval Research Laboratory's Chesapeake Bay Detachment and at Navy or private shipyards to be determined by ship availabilities.

2. SAFETY.

2.1. Regulations.

All work shall be governed by the regulations and procedures contained in NRLINST 5100.11E "Radiation Protection Manual" which apply to the use of x-ray generating equipment.

2.2. Operator Qualifications.

2.2.1. Operators are defined as personnel with authority to arm or energize the x-ray producing sub-system of the Comscan instrument. No one other than designated operators will be permitted to operate the system. A list of operators will be posted at the operator's console. Operators shall be responsible for safe operation of the XBT system in compliance with all applicable regulations.

2.2.2. Operators must complete a one week training course provided by the Comscan manufacturer which includes practical operating experience as well as radiation safety material.

2.2.3. Operators must complete a physical examination and submit the following forms to NRL Code 1240 with approval of the XBT instrument custodian and their division superintendent:

NDW-NRL 5101/12116 "User/Operator/Custodian Authorization"
NDW-NRL 5101-4001 "Application for Dosimeter"

Operators must complete any additional safety training required by NRL Code 1240.

2.2.4. Operators will be provided with the following documents:

NRLINST 5100.11E "Radiation Protection Manual."

10 CFR 19 "Notices, Instructions, and Reports to Workers;

Inspections."

10 CFR 20 "Standards for Protection Against Radiation."

NRC Form 3 "Notice to Employees."

NRC Regulatory Guide 8.29 "Instruction Concerning Risks from Occupational Radiation Exposure."

NRC Regulatory Guide 8.13 "Instruction Concerning Prenatal Radiation Exposure."

2.3. Radiation Survey.

Operators must request a radiation survey from Code 1244 when any significant change is made to equipment or procedures. This would include the installation of new equipment, changes in warning or alarm circuits, relocation or reconfiguration of major system components, or major repairs to the x-ray subsystem. Code 1244 approval must be obtained before operating under such circumstances.

2.4. Restricted Areas.

2.4.1. Shipping/Utilization Container (SUC).

The XBT system is operated from within the SUC. During scanning operations, this area is subject to radiation monitoring and personnel dosimetry requirements as determined by Code 1244. During x-ray system warm-up the SUC will be monitored to insure radiation levels below 0.5 mrem per hour. The SUC will be continuously monitored during operations via a survey meter provided by Code 1244. If required, lead foil shielding will be used around the scanner head to meet the 0.5 mrem requirement.

2.4.2. Radiation Area.

Prior to operating the XBT system, a perimeter will be established to limit access to the vicinity of the XBT scanner head. Access will be limited by means of physical barriers or ropes and all avenues of approach to the scanner will be marked by signs bearing the standard radiation symbol and the label "Caution - Radiation Area". The perimeter will be surveyed during x-ray system warm-up to insure radiation levels below 2 mrem per hour. The SUC must be outside the radiation area. Any major movement of the scanner to a new region of interest (e.g. from starboard to port or from forward to aft) will require a new survey of the radiation area perimeter. Operators will always have an operating survey meter with them when entering the radiation area as a protection against alarm system failure or

mis-communication. During scanning operations, the radiation area will be observed to insure that it remains clear of personnel.

2.4.3. High Radiation area.

During operations, the immediate vicinity of the scanner head will be treated as a high radiation area (defined as a calculated level of 100 mrem hour). Signs bearing the standard radiation symbol and the label "High Radiation Area" will be placed at the scanner head.

2.5. Safety and Warning Devices.

The following safety and warning devices will be used:

3-position main power key switch (Off, stand-by, and armed). The key cannot be removed in the armed position.

X-ray system controller panel warning lights.

An illuminated sign located inside the SUC, bearing the standard radiation symbol and the words "X-Ray On."

A red light located in the vicinity of the scanner.

A pre-warning alarm bell located in the vicinity of the scanner. This bell will be audible from outside the radiation area and from within the SUC.

2.5.1. When the x-ray system is armed, the red warning light on the controller, the red warning light located at the scanner, and the "x-ray on" sign in the SUC will be continuously illuminated.

2.5.2. When high voltage is switched on, a pre-warning will be provided for a period of five seconds prior to the generation of x-rays. During this pre-warning, the alarm bell will sound and the blue lamp on the controller will be on.

2.5.3. During the production of x-rays, the red lamps and red led mode display on the control panel will flash at a rate of 1 Hz., as will the "X-ray On" sign in the SUC and the red light at the scanner. An audible 1 Hz clicking sound will also be provided by the controller.

2.5.4. An afterradiation warning will be provided after the high voltage is turned off by continuous illumination of the warning lamps until residual high voltage is dissipated.

2.6. Beam Direction.

The scanner will be operated such that the scanning beam is directed normal to the sonar dome surface except for calibration purposes or for scanning other material samples, when it will be aimed straight up or down. Under no circumstances will the beam be directed horizontally without an intervening target material.

2.7. Impaired Safe Operation.

Whenever it is likely that safe operation is impaired the XBT system will be made inoperative and secured against operation. The appropriate servicing authority and Code 1244 must be informed.

2.8. Emergency Procedures.

When an operator becomes aware of a safety rule violation, personnel exposure, failure of warning devices or interlocks, or other accident or emergency situation, he will immediately switch off the x-ray system and main power switch and take such action as required to minimize adverse impact on personnel and property. He will request immediate assistance by calling the local emergency phone number, if appropriate (4040 at NRL CBD). He will report any radiological safety accident or violation to Code 1244 (202-767-2232). The system will remain inoperable subject to guidance from Code 1244.

3. OPERATION.

Operation of the XBT system will be conducted in accordance with the safety requirements described above and the procedures provided in the Philips Comscan User's Manual and the Philips MG-164 x-ray system documentation. Step by step instructions for sonar dome inspection are provided below.

3.1. Preparatory Procedures.

3.1.1. Remove the scanner and water cooler from the SUC. Mount the scanner on its tripod or other fixture and position it to scan the region of interest on the sonar dome.

3.1.2. Remove the warning lamp stanchion with alarm bell from the SUC and connect the two color coded power cords to the matching outlets provided in the SUC at the power supply. Position the stanchion near the scanner. Check that the "X-Ray On" sign in the SUC is plugged into its outlet.

3.1.3. Place the radiation area barriers and signs at a previously surveyed safe distance or at least 10 feet from the scanner.

3.1.4. Charge and read pocket dosimeters (2 per person) and enter readings into the dosimeter log. Ensure that all personnel are wearing their NRL issued dosimeter.

3.1.5. Switch on the 240 VAC main switch on the power conditioner.

3.1.6. Switch the x-ray controller key switch to "Standby" position. The white power lamp will light and the mode display will read "10-". Complete the warm-up mode entry to 101, 102, or 103 as appropriate (See the warm-up mode chart posted near the controller).

3.1.7. Verify that the radiation area is clear of all personnel.

3.1.8. Switch the x-ray controller key switch to "Armed" position. The green stand-by lamp will light indicating that all interlocks are closed and tube cooling is in operation. The warning lights should all be illuminated. Check that warning lamps are operational.

3.1.9. Press the black "H.V. on" switch on the controller. The blue pre-warning lamp will light. Verify that the audible pre-warning bell is operational. After the 5 second pre-warning, the x-ray tube will be energized at 80 KV and will ramp up to 160 KV according to the warm-up mode.

CAUTION: If it is necessary to stop x-ray generation for any reason, press the red "H.V. Off" switch on the controller. DO NOT USE THE KEY SWITCH TO TURN OFF HIGH VOLTAGE. This is harmful to the high voltage system.

3.1.10. During the warm up period complete the following: Survey the SUC interior to ensure that radiation levels are below 0.5 mrem per hour. Survey the radiation area perimeter to ensure levels below 2.0 mrem per hour. Verify that the warning devices are operational.

CAUTION: If the x-ray tube overheats or other fault occurs x-rays will be automatically shut off. In the case of automatic or manual shut off, it necessary to manually re-start x-rays as in paragraph 3.1.9. It is also important to re-establish that the radiation area is clear of personnel.

3.1.11. After completion of the warm-up procedure, switch the key to "Stand By" position and remove it.

3.1.12. Set the x-ray controller mode to 400.

3.1.13. Turn on the Comscan control rack main power switch.

3.1.13. Turn on the photomultiplier power supply and adjust voltage clockwise to 850 V. Lock the potentiometer.

3.1.14. Turn on the servo system.

3.2. Scanning Operations.

3.2.1. Position the scanner to inspect the region of interest.

CAUTION: During scanning operations, the operator should always approach the scanner with the x-ray system key in his possession and a survey meter in his hand. (The key is not removable from the armed position - only from stand-by or off.)

CAUTION: A major movement of the scanner, such as from the sonar dome starboard to port or forward to aft, will necessitate a re-survey of radiation area perimeters and of the SUC.

3.2.2. Verify that the radiation area is clear of personnel.

3.2.3. Arm the x-ray system by turning the key switch to "Armed" position and press the black "H.V. On" switch. X-rays will now be generated as required under Comscan program control.

3.2.4. Conduct the scanning operation from the console in accordance with the Philips User's Manual. X-rays will be produced under program control, but only after manual switching of the "H.V. On" button. If the green controller panel lamp goes out for any reason, it is necessary to manually reset the "H.V. On" button before continuing.

3.2.5. After completing a scan, switch the x-ray controller key to standby position and remove it.

3.2.6. Conduct additional scans as required by repeating the sequence described in paragraphs 3.2.1. - 3.2.5.

3.3. Post-operational Procedures.

3.3.1. After scanning operations are completed, switch

off the x-ray controller and remove the key. Verify with a survey meter that x-ray production has ceased.

CAUTION: Wait a minimum of three minutes cool-down time with the controller on standby to dissipate residual heat in the x-ray tube. Switching off the x-ray controller also turns off the water cooler.

3.3.2. Quit the Comscan program.

3.3.3. Turn down the photomultiplier voltage to 0 and turn off the power supply.

3.3.4. Turn off the Comscan rack main power switch.

3.3.5. Turn off the power conditioner.

3.3.6. Return the scanner and water cooler to the SUC.

3.3.7. Disconnect the safety light and bell, and return the stanchion to the SUC.

3.3.8. Read personnel pocket dosimeters and record readings in the dosimeter log.

3.3.9. Enter the session's activity in the Utilization Log, to include the date, operators, and x-ray parameters. Enter work accomplished into the lab book.

3.4. Other Procedures.

The scanning of calibration standards or other material samples will be conducted as described under paragraph 3.2. with the exception that the scanning beam will be aimed straight up or down into the target material. Samples will be mounted over or under the head for scanning.

APPENDIX E

ONE-SIDED NDE OF SONAR RUBBER DOMES

GEO CENTERS, INC

Presented to the 41st Defense Working Group on NDE, Tucson, Arizona, Nov. 1992.

ONE-SIDED NDE OF SONAR RUBBER DOMES

Chester F. Poranski
Materials Chemistry Branch
Naval Research Laboratory
Washington, DC 20375
Autovon 297-2488

Edward C. Greenawald
Geo-Centers, Inc.
10903 Indian Head Highway
Fort Washington, MD 20744

ABSTRACT

Sonar Rubber Domes (SRDs) protect the sonar transducers mounted on the keels of Navy surface anti-submarine vessels such as frigates (FFG) and destroyers (DDG). Ruptures of these domes usually occur due to a combination of stress corrosion and overload of the steel reinforcing cords. NDE by x-ray inspection identifies broken steel cord reinforcing elements, permitting risk assessment and planning for dome replacement. However, ships must be in drydock for x-ray inspection. This limits access for NDE to times when other maintenance requires drydocking. Also, one type of SRD requires removal from the ship for an x-ray inspection. The Naval Research Laboratory (NRL) is evaluating one-sided NDE techniques with the goal of inspecting SRDs at pierside. Preliminary results are presented for x-ray, acoustic, magnetic, mechanical and optical methods.

INTRODUCTION

The rubber sonar domes used on Navy ships to protect sonar transducers provide superior performance compared to their steel predecessors. They have a better impedance match with the sea water, leading to greater acoustic energy transmission through the dome. There are no internal support struts which can lead to internal acoustic reflections. And they are covered with an anti-fouling rubber which reduces maintenance and keeps the dome surface hydrodynamically smoother for longer times.

There are two types of rubber sonar domes in the fleet. The Sonar Dome Rubber Window (SDRW) is a bow mounted dome, and the Sonar Rubber Dome (SRD) is the keel mounted type. They are both made of layers of steel-cord-reinforced rubber fabric, arranged to provide the proper shape and strength.

Though they differ in installation location and shape, the two types of domes share one significant feature - they can rupture in service. Seawater enters the internal dome structure and finds its way to the steel cords, where corrosion may occur. In regions of high stress due to flexure, the weakened wires break and the rubber ruptures.

In the early 1980's, the Naval Sea Systems Command (NAVSEA) began a program of corrective actions for the SDRW. Two of NRL's tasks in the program were failure analysis and NDE development. NRL reported on the NDE work at this meeting in 1983[1]. The important results were procedures for x-ray inspection both in drydock and underwater at pierside. The underwater procedure is especially important because it eliminates the need for drydocking a ship for NDE of the SDRW. Currently, SDRWs are inspected on a regular schedule depending on their condition status. NAVSEA knows the condition of over 90% of the SDRWs in service and can manage that class of domes effectively.

The SRDs are another case altogether. There are x-ray inspection procedures for them. But because of inadequate access to their interiors, there is no way to inspect them unless the ships are in drydock. Inspection of the smaller of the two types of SRDs even requires removal of the dome from the ship. Drydocking ships is expensive and time consuming, and drydock availability is scarce. At present, NDE inspections of SRDs are done only when ships are in drydock for some other reason. Hence the condition of 43% of the SRD population is currently unknown. Figure 1 illustrates the high proportion of uninspected SRDs as well as the high proportion of those inspected which are damaged and therefore at risk of failure.

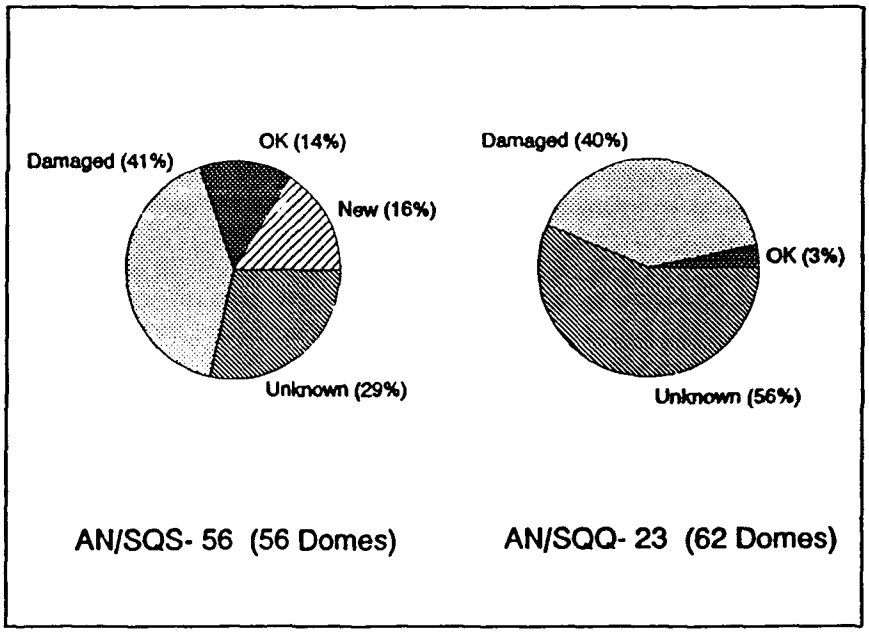

Figure 1. Condition of two types of SRDs currently in service. Domes are designated "New" if under two years in service, "OK" if NDE indicates no damage, "Damaged" if NDE so indicates, "Unknown" if never inspected and not "New".

Recurring unexpected failures of SRDs have raised concerns in the Fleet. NAVSEA has tasked NRL to investigate alternative NDE techniques. NRL had previously evaluated gamma ray backscatter techniques[2] and speckle-shearing interferometry (shearography) for SDRW void detection. While successful as laboratory demonstrations, the techniques were considered impractical for field use without major development efforts.

Because of recent advances in one-sided x-ray backscatter [3,4] and laser shearography, NRL proposed a new look at these technologies for detection of SRD wire cord damage. Two years ago we presented the results of our evaluation of x-ray backscatter, and our plan for continued development of this method[5]. In this paper, we will provide an update on this effort, as well as several other one-sided methods under consideration. Since the small AN/SQS-56 SRD presents the greatest access problem and the ship classes using AN/SQQ-23 SRDs are slated for retirement, we will focus our effort on the former. The term SRD in the following discussions will refer to the AN/SQS-56. The techniques discussed, however, are generally applicable to the larger domes.

SRD CONSTRUCTION

To understand the problems associated with the NDE of sonar domes, it is necessary to understand the SRD internal structure. A study of the SRD fabrication sequence makes sense of this complex structure. The composite SRD wall is made of carbon black filled synthetic rubber reinforced by steel cords, in a manner similar to tire construction. The basic building material for SRD fabrication is a "fabric" made by calendaring the steel cords between two sheets of rubber. This fabric is then manually cut and pieced into a concave mold to build up the wall thickness. The piecing pattern is precisely specified to provide 5 steel-reinforced structural layers. The cord direction is alternated orthogonally to provide three "radial" plies and two "longitudinal" plies.

Various named sub-structures exist within the design for each ply. Two important structures in the longitudinal plies are known as keel bands and bead bands. The keel bands are laid along either side of the keel line, or centerline. Bead bands are laid around the upper periphery of the dome. They are so named because the dome is anchored to the hull attachment hardware via a "bead" cable, similar to a tire's. The areas between the keel and bead bands are filled in starting from lines which bisect or trisect the angles between the bands. We refer to the resulting ply structures as bisectors and trisectors. Figure 2 illustrates this construction.

During the fabrication of the dome, each layer is cemented into the mold. First a layer of rubber treated with an antifoulant is placed against the mold to become the outer SRD surface. Then the alternating radial and longitudinal plies are laid in, beginning with the first, or outermost, radial. Finally a non-reinforced cover ply is put in which becomes the inner surface of the dome. The finished dome is vacuum bagged and cured under pressure in an autoclave.

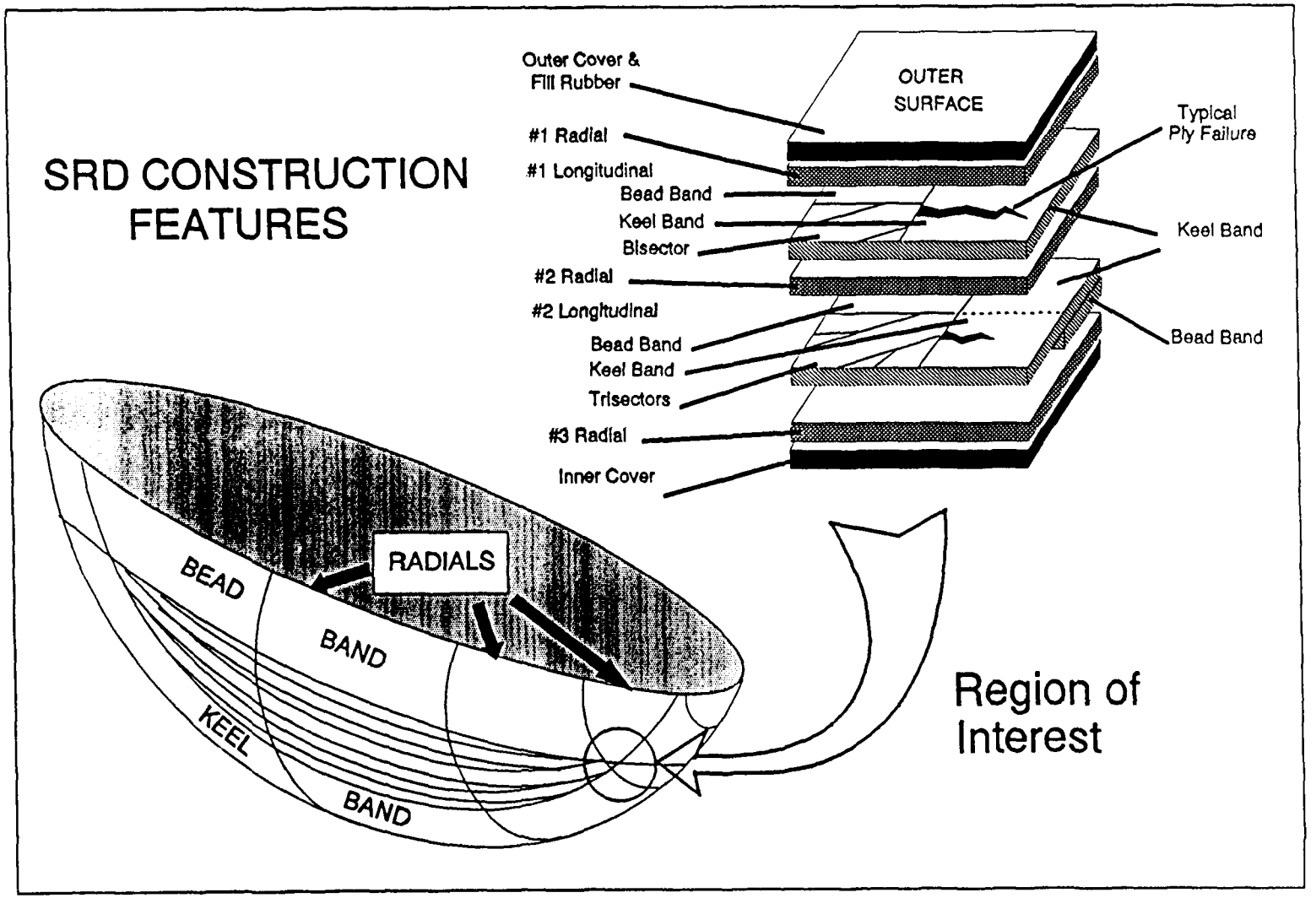

Figure 2. Diagram of SRD construction features. The section shown at upper right illustrates the complexity of the region of interest in the vicinity of the intersection of the bead and keel bands.

SRD FAILURE

A number of SRDs have failed at sea. In addition, a high proportion of SRDs exhibit damage when radiographed. NRL has been tasked to determine the cause of failure. This work is incomplete, but several conclusions may be drawn from the data available.

SRD ruptures typically occur in the forward end, along the radial ply direction, breaking across the longitudinal plies. Keel band cords break sequentially, in a "run" pattern. The radial plies have no reinforcement in the direction across the break, so the rubber splits, allowing loss of SRD pressure. Due to the curvature of the SRD, the alternating plies are less orthogonal at the forward and aft ends of the dome. The keel and bead bands, both nominally in the longitudinal "direction", intersect there. Keel and bead band damage seen on radiographs is invariably within inches of this intersection. Figure 3 shows the distribution of observed damage sites as a function of distance from the keel/bead band edge intersect.

As to the question of why the keel bands break, there is evidence of the existence of internal water pathways from the bead area which allow seawater to contact the steel cords. Water can then wick within the cords to a locus of flexure. Such loci are suspected in regions where a stiffness gradient exists due to changes in wall thickness and structure. Similar problems have been found to be responsible for failure of bow domes. It is also noteworthy that keel bands have been known to break in the larger AN/SQQ-23 dome while undergoing pressure testing before even seeing service. These breaks were also near the keel/bead band intersection. We suggest that the keel/bead band configuration concentrates cord loads near the intersect. We also suspect that the transfer of loads from the bisector and trisector plies which terminate at or near the intersection also contributes to the problem. Clearly the layup design is implicated in SRD failure, as well as possible water intrusion.

We are planning to dissect several damaged SRDs to conduct a detailed failure analysis. Finite element modeling of the SRD, being done at the University of Washington Applied Physics Laboratory, may also shed light on the design problem. Sea trials using an acoustic deflection measurement system are planned to provide data on the dynamic behavior of the SRD while underway in various sea and operating conditions.

INSPECTION CRITERIA

The short term, most immediate, purpose of SRD NDE is to determine if an SRD has sustained damage which places it at risk of failure and to characterize the damage in such a way as to determine the appropriate action to be taken. Action options include continuing the routine operation of the SRD, replacement or repair of a damaged SRD, or continuing to monitor damage until a critical level is reached.

The achievement of the purpose stated above, however, requires the development of meaningful criteria for the action decisions. This leads to

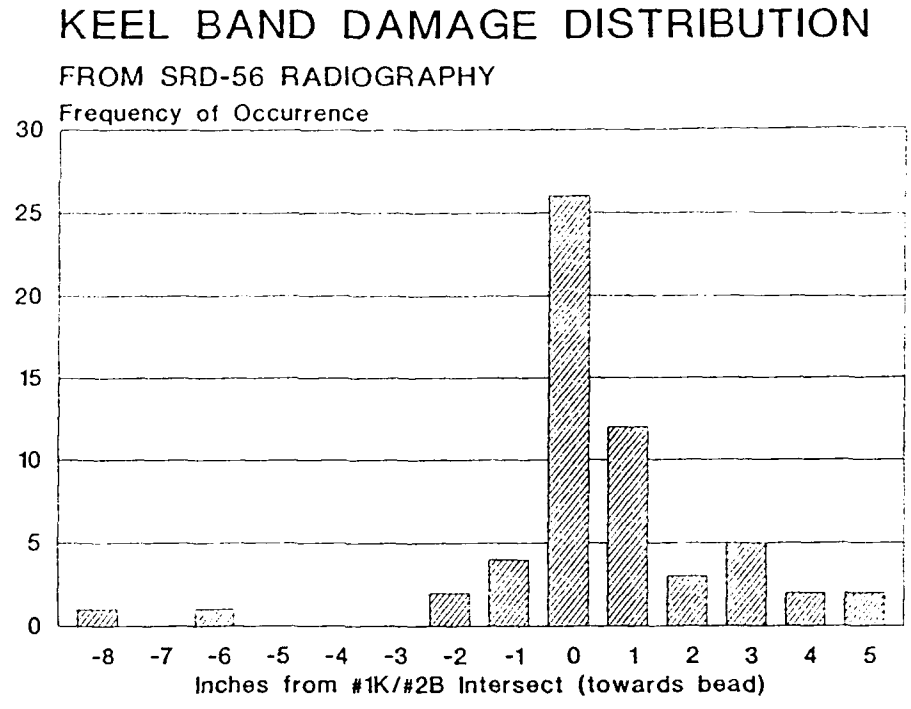

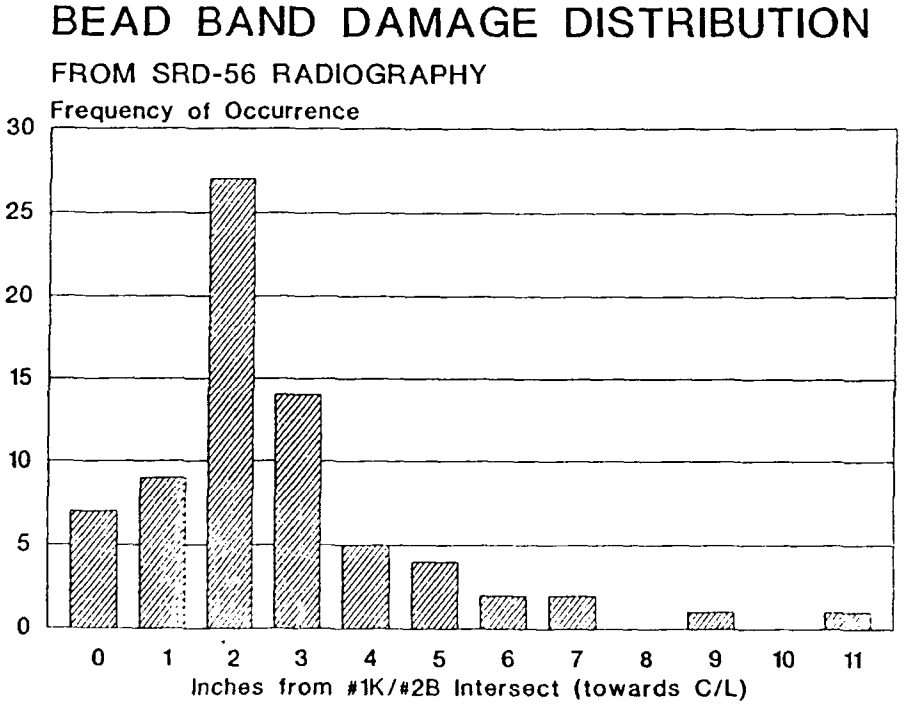

Figure 3. The distribution of damage sites, determined from radiographic inspections, shows a concentration of damage near the intersections of the bead and keel bands.

another, long term, purpose of NDE: to accumulate a base of data which will be useful in the failure analysis effort and will provide a basis for taking action.

A one-sided inspection method is sought which is applicable underwater. The method will replace or augment the currently used x ray radiography. The benefit of such a one-sided technique is the elimination of the current need to drydock the ship and remove its SRD.

Current Capability

NDE is currently accomplished by means of x ray radiography. This method is capable of resolving individual wire elements (.175 mm and .150 mm) of the steel cords. Broken cords (1.48 mm dia.) are readily identified as are frayed or partially damaged cords and cord ends which are normal SRD structural features. Ply images are superimposed on the film which can cause interpretive difficulties.

SRD damage typically appears as a continuous "run" of broken cords in one or more of the longitudinal ply sub-structures. Damage is characterized and reported in terms of the number of damage sites, the location of each site relative to known structural features, the extent of each run in inches to the nearest 0.5 inch, the number of plies broken at each site, and the identification of the ply sub-structures which are damaged (keel bands, bead bands, etc.)

The current x-ray inspection data base contains 164 inspections of new and in-service AN/SQQ-56 and AN/SQS-23 SRDs.

One-Sided Capability

The inspection regions of interest (ROI) will be the currently inspected four areas in the vicinity of the intersections of the keel bands and bead bands.

Ideally, the chosen method would provide information comparable to that currently obtained by radiography. This would enable us to benefit from our experience managing a similar problem with Sonar Dome Rubber Windows (SDRW). Furthermore, similarity of data would allow the addition of new results to the current base of data to be used for development of action criteria.

It is not expected that any one-sided techniques will provide the resolution obtained by radiography. Further, we expect most one-sided methods to exhibit a decrease in capability with increasing flaw depth. Our requirements will reflect this by specifying better resolution of damage in the #1 longitudinal ply. This ply is the second structural ply from the outer SRD surface and is usually the first to sustain damage. Detection of cord damage here is important for early detection of a damage site.

The following minimum requirements will determine the suitability of candidate techniques:

1. Detection of any broken cords in the #1 keel band.

2. Detection of any run of more than 5 broken cords in the #2 keel band.

3. Detection of any run of more than 10 broken cords in the #2 bead band.

4. Identification of broken ply sub-structures (#1 or #2 keel band or bead band.)

5. No false damage indications due to structural features such as ply edges and cut cord ends.

One-Sided Screening Evaluation

One sided NDE techniques which are unable to meet the above criteria for SRD inspection may be useful as a preliminary or screening type of evaluation. In particular, methods which are inexpensive and easily implemented are sought to identify SRDs most in need of a higher quality inspection. Any consistent sensitivity to high levels of damage may be of use for this purpose.

X-RAY BACKSCATTER TOMOGRAPHY

X-ray backscatter tomography (XBT), not to be confused with computed tomography (CT), is based upon the Compton scattering interaction. XBT systems create and detect scattered photons in such a way as to identify the location within the object where the interaction producing the scattered photons occurs. The simplest implementation of this concept requires a pinhole collimated x-ray source and a pinhole collimated detector with intersecting axes. When an object is irradiated by the narrow beam, the scattered rays emanating from the point of intersection within the object are detected. By moving the source, detector or object to interrogate each volume element (voxel) in a plane of interest, data can be acquired to represent the density as a function of position. This can be displayed as a "slice" through the material. Sophisticated XBT systems use a scanning x-ray beam, arrays of detectors, and computerized image acquisition to greatly speed the process. Our previous paper[5] provides a more detailed theoretical overview.

At this meeting two years ago, we presented our study of the feasibility of using XBT for NDE of sonar domes[5]. At that time, we had conducted test scans of a damaged AN/SQQ-23 SRD specimen at three laboratories using three very different instruments. We concluded that this technology was well suited for our application. We have since acquired (leased) an instrument of our own, and have begun to develop an inspection system.

Philips Comscan

We chose the Philips Comscan system for our project for several reasons: it is the only XBT system available "off the shelf"; its design is amenable to our plans for remote (underwater) implementation of the x-ray scanner; its performance with respect to depth penetration, resolution, scanning volume, and speed, meet our requirements.

The Comscan system contains a 160 KeV industrial x-ray subsystem with its controller, power supplies, x-ray tube, and cooler. The compact x-ray tube is cradled in the scanner which also contains the collimators, scanning beam mechanism, shielding, servo control mechanism, backscatter detectors, photomultipliers, and fiber optics data telemetry circuits. A control rack houses power supplies and a VME bus chassis with host computer, memory, storage, image processing, and servo control modules. A high voltage generator provides the 160 KV. The scanner is connected to the control rack, high voltage generator, and cooler via ten meter cables and hoses. A terminal is provided for the operator interface and a display is provided for viewing the scanned images. Additional options include an ethernet port, a PC compatible terminal, and various sets of apertures providing different depth ranges and resolutions.

During operation of the scanner, the x-ray tube output is collimated to a fan shaped beam. The intersection of this beam with a helical aperture in a rotating cylinder, produces a scanning .4 mm x .4 mm square beam. The beam is reciprocated to scan a 50 mm width. Servo controlled motion of the entire scanner head over a distance of 100 mm sweeps out an area 50 mm x 100 mm. Twenty two successive tomographs are produced in one pass. This is accomplished by projecting the backscattered rays onto an array of detectors via a slit aperture. Figure 4 illustrates the process. Each layer image is 250 by 500 pixels. Sixteen bits of scatter data are recorded for each pixel and eight of these provide a 256 grey level display. Five scanning speeds are selectable from 75 to 375 seconds. The depth and thickness of the volume scanned are determined by the geometry of changeable aperture sets. Standard apertures allow 5mm, 10mm, and 50mm working thickness with 5mm, 10mm, and 10mm of dead space, respectively.

Preliminary Results

We have temporarily installed the Comscan system in a trailer at NRL's Chesapeake Bay Detachment facility. Four SRDs have also been located there. These domes have been removed from service due to x-ray inspection findings. All are known to contain structural ply damage, but none have ruptured, and none appear to be damaged externally. During acceptance testing of the Comscan system, some preliminary scans were made of the SRD removed from the USS Clark. The radiographs indicated the presence of broken cords in the keel bands and bead bands near the forward intersections of their edges.

Our preliminary XBT scans have identified damaged cords in both keel bands of the Clark SRD. These are our first images of AN/SQS-56 damage. Figure 5 is a photograph of the Comscan image screen displaying level 1, the

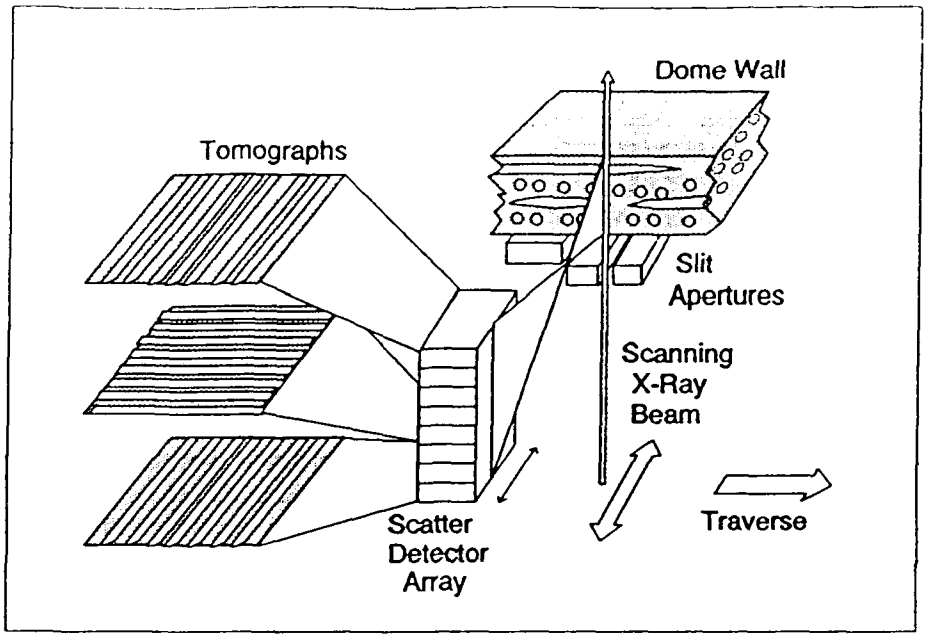

Figure 4. Diagram of the Philips Comscan XBT method applied to SRD wall.

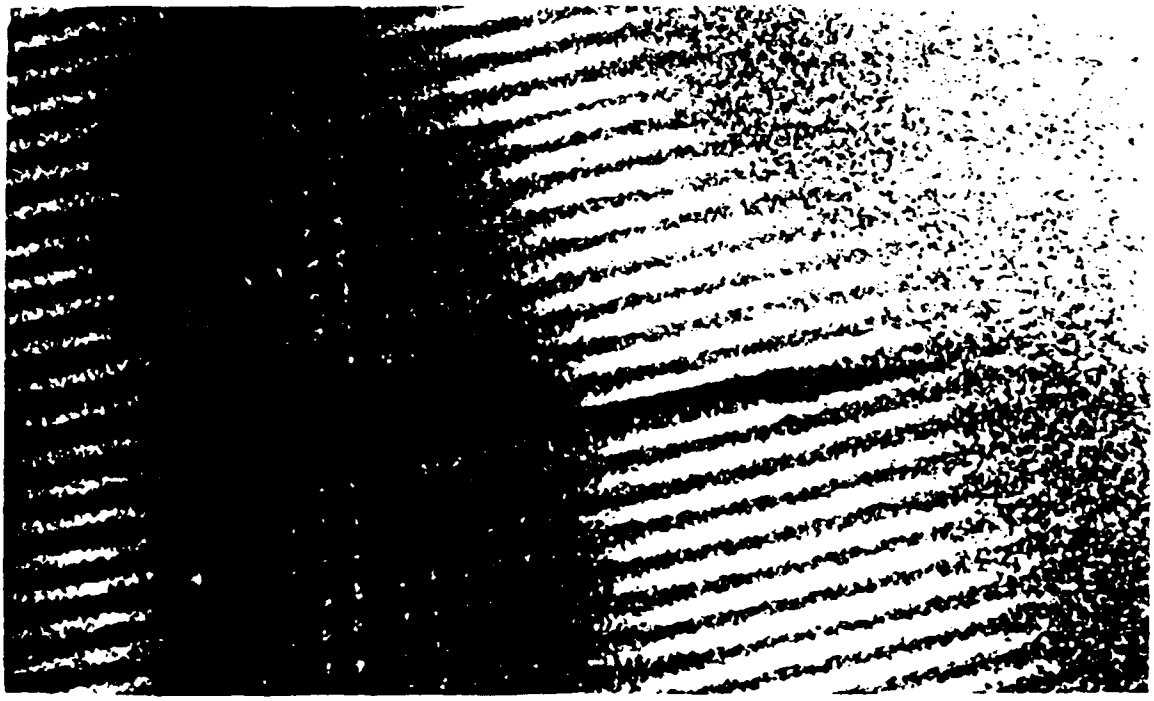

Figure 5. Comscan image display screen showing image level 1 of a damage site on the SRD removed from the USS Clark. The dark horizontal feature is the damage site. The dome curvature produces the distinct vertical bands which are the different layers of the SRD wall.

tomograph nearest to the surface or 10 mm from the scanner head. A run of broken cords is seen in the #1 keel band. A crack in the rubber matrix of the #1 radial ply is also apparent. This rubber damage is not seen on the transmission radiographs from the original inspection. Other scans were able to identify broken cords in the #2 keel band as well, but with decreased sharpness and increased noise. The #2 bead band damage was not apparent on the deep level images where expected.

The preliminary scans illustrate two artifacts of the XBT process applied to SRDs. The "curvature artifact" is due to the intersection of the tomographic planes with the curved SRD features. XBT slices do not follow SRD plies, but cut across them. Interactively paging up and down through the levels, we have had little difficulty interpreting the images with respect to SRD structural features and damage, perhaps due to our experience with SRD radiography. This artifact is pronounced in Figure 5 where four distinct regions on the image correspond, from right to left, to the outer rubber ply, the first radial, first longitudinal, and first radial again. The narrow grey bands between the two reinforced regions represent the rubber thickness between the layers of steel cords.

The "cord shadow artifact" has more serious implications. The scanning x-ray beam must penetrate the overlying material to create scattered rays for measurement of a voxel's properties. This results in an attenuation of the beam and a corresponding lowering of backscatter from the voxel. With materials of constant thickness and homogeneous composition, this attenuation can be simply compensated. But with our structured material there is no similarly simple solution. The modulation of beam intensity due to cords in the outer plies is superimposed on images of the deeper plies. This effect can be seen in Figure 5. The dark region containing the failed #1 longitudinal (keel band) is seen to be striated in the same direction as the adjacent radial ply regions. Near the center of the image, the dark striations in the longitudinal ply image are aligned with the bright features of the radial ply. The same cords producing the bright scatter image are attenuating the beam and "shadowing" the ply below. (Near the top and bottom of the image the alignment of cords and "shadows" is altered by parallax due to the scanning beam angle.) A similar modulation of the detected scattered rays is lessened due to the integration of scattered rays over the angle subtended by the detector. Although this artifact appears to have little effect on the image of Figure 5, those of deeper structures, such as the #2 bead band, are nearly obliterated by the superimposed shadows of overlying plies.

Plans for Further Development

We have just completed a manipulator to allow us to more easily position the scanner at the SRD surface. We plan to scan several more removed SRDS for comparison with radiographic data and to determine the optimum orientation and sequencing for a routine inspection. We also want to compare data obtained using different aperture sets. (A 20mm set is on hand as well as the standard ones.) We will soon install the XBT system into a container to facilitate travel to shipyards for test scans of installed SRDs in drydock as well.

We plan to develop a fixture for mounting the scanner on the dome. This will be more practical for indexing a sequence of positions along the dome surface. Ultimately this will become a prototype for an underwater attachment fixture.

We will investigate the improvement of the XBT images using image processing techniques. We also plan to develop an algorithm to reconstruct the image by using the data from overlying levels to compensate for their effect on the deep levels. This is expected to greatly improve the deep layer images and eliminate the shadow artifact. A demonstration of three dimensional visualization of XBT data is also planned.

With continued success and support, we plan to develop an underwater XBT capability. The XBT system will continue to be used from its container, which will be placed on the pier. The scanner will be installed into a waterproof enclosure. Scanning will be conducted through the enclosure wall placed against the submerged dome surface. An extended length umbilical hose will contain all the necessary high voltage, power and signal lines as well as coolant and dry air hoses. An attachment and manipulation fixture on the dome will provide the capability to position the scanner enclosure.

OTHER NDE METHODS

Other NDE methods have been proposed as candidates for one-sided inspection of SRDs. Indeed, our XBT project has been criticized on the grounds that other methods are less expensive or easier to implement. Although we have placed our emphasis and resources on development of XBT due to our evaluation of technical NDE performance issues, we continue to investigate other methods as time and funds permit. Successful efforts at a resolution below that of XBT may be useful as a screening evaluation to identify the most seriously damaged SRDs. These can then be scheduled for a more detailed evaluation. We have considered or are currently investigating the following techniques.

Shearography

Electronic shearography is an optical NDE method which is sensitive to very small changes in surface strain due to subsurface flaws. Typically a reference image of the surface is stored electronically using a laser interferometer. Upon the application of a uniform stress by vacuum, pressure, vibration or heating/cooling, subsequent images are compared with the reference image. The resultant image contains indications of the flaw. This technique is used for NDE of large aircraft and heavy equipment tires, which have a structure similar to SRDs.

A section of a damaged AN/SQQ-23 SRD was submitted to Laser Technology, Inc., Norristown, Pa., for evaluation using their electronic shearography systems. The section measured approximately 5'8" by 2'. An initial test was conducted using an ES-9150 Electronic Shearography System with advanced imaging electronics and a zoom lens. The test sample was lightly coated with a dye-penetrant developer used to provide a uniform surface reflectivity. The

sample was positioned and secured in a vacuum chamber and a reference image recorded. The sample was then stressed by reducing the pressure by 25 inches of water. The development of shearographic fringes was observed in real time during the stressing. The resultant shearographic image was captured and a hard copy produced.

The shearogram contained bright areas which were interpreted as "disbonds" by Laser Technology. Some of these areas were near to the known damage sites. Others were near structural ply features. These results were considered encouraging. However, the need to place the sample within a vacuum chamber renders the technique useless for whole SRD inspection.

A portable shearography system under development at Laser Technology uses a small remote vacuum chamber to stress the test object from one side. Tests of our sample using this device produced poor results. The low reflectivity of the dark SRD surface produced a poor image with the lower power laser in the portable system. The high level of strain and creep of the rubber sample relative to the small flaw signal was also thought to contribute to the problem. We conclude that this method is not applicable to one-sided SRD NDE.

Magnetic Flux Leakage

The magnetic flux leakage (MFL) method is based on applying a magnetic field to a ferromagnetic component and detecting disturbances in the magnetic field caused by defects. Preliminary experiments were conducted by the Southwest Research Institute, San Antonio, Texas, to determine if the MFL method is capable of detecting broken steel cords in SRDs.

For tests on the SRD material a yoke-shaped electromagnet 4 inches long by 1.6 inches wide was used to magnetize the specimen with a DC field. A magnetic field sensor was used to sense the leakage field. The electromagnet was oriented so that the field direction was along the axis of the cords in the layer to be inspected. The electromagnet/sensor combination was scanned in a raster pattern over the surface of the specimen by a computer controlled, stepper motor driven, scanning system. The MFL signals were digitized as a function of probe position. These data were used to generate a color image of the scan area by converting the signal amplitude to color.

A phantom of the sonar dome layup was prepared using five 15 by 15 inch squares of the cured steel/rubber fabric. The squares were stacked with alternating cord orientations (adjacent layers perpendicular), simulating the orthogonal SRD wall structure. The outer cover ply was simulated by an air gap between the probe and the first ply.

Broken cords were simulated by cutting 7.5 inches across the cords in one of the 15 inch squares starting at approximately the center of one edge. The cut ply was placed in the second reinforced ply position from the top of the five ply stack. For one of the experiments, the third ply from the top was displaced so that one edge was parallel to the cut in the second ply to simulate a "ply drop" similar to SRD structural features.

The color images produced clearly indicated the cut ply in the second position, even with a ply drop immediately below the cut. The lift-off effect of the outer cover ply simulation does not significantly attenuate the MFL signals. Based on these results the MFL method appears promising for our SRD application. In addition to the scanning mode employed in these tests, Southwest Research Institute has suggested a hand operated probe to be used by a diver to inspect SRDs underwater.

Direct Stiffness Measurement

We have investigated the possibility that structural damage might produce a directly measurable effect on the local modulus of the SRD wall. Initial experiments were carried out on the removed USS Clark SRD in the damaged region of interest. Two methods were used to apply stress to the SRD: Pressing with a rod and load cell, and applying a vacuum. We have chosen to continue with the vacuum method. The application of a vacuum is expected to apply a tensile load to the structural plies, whereas the application of a force against the curved dome would result in compressive cord loads. In addition, the load magnitude and direction are easier to control with the vacuum method.

A vacuum chamber was fashioned using a polycarbonate bell jar fitted with a foam gasket. A linear position transducer is spring mounted against the SRD surface so as to be independent from gasket compression and the resulting jar motion. Readings are taken before and after applying vacuum to obtain the measured deflection, or strain, of the surface. A computer is used to trigger the strain measurement at a preset vacuum level and file the data for later processing. Measurements are taken at each point on a grid covering the region of interest. The data set is then plotted as a 3-d surface plot or a contour plot, representing the stiffness of the SRD surface.

The plots obtained so far indicate considerable structure rather than the smooth transition one would expect from dome curvature and thickness gradients alone. We plan to refine the apparatus some more and obtain data from a series of damaged and undamaged SRDs to determine whether it is worthwhile to develop an underwater version.

Microwave Testing

Microwave based NDE has not been very promising due to long wavelengths with respect to material defects. Microwaves have been used, however, for such applications as measuring polymer cure rates, locating large internal material flaws or structural elements such as steel bars in concrete, detecting mixture ratios, and detecting moisture. Typically, a microwave signal is transmitted into the material and the reflected signal is measured. In this way the dielectric properties of the material are measured in terms of their effect on absorption or reflectance. We have investigated the use of microwaves for detecting the presence of water within the structural plies.

A phantom was constructed of alternating steel reinforced rubber fabric

plies. A section of one of these plies was fitted with a connector potted on one end to enable the piece to be pressurized with water. Such an arrangement produces wicking through the cords within the piece, which can be verified by the appearance of water at the opposite end from the fitting.

The phantom was provided to Spatial Dynamics Applications, Inc.(SDA), Acton, Massachussets. Tests were conducted using SDA's M1800 Non-Destructive Tester. This instrument operates at 1800 MHz and measures amplitude and phase of reflected signals. The output power is less than 1 microwatt per cm^2 at 5 cm.

A series of tests was conducted which succeeded in demonstrating the detection of water in a variety of configurations. Water was detected when placed between the plies, as well as when wicked into five steel cords. Detection of internal water was also accomplished with a petri dish of water placed against the far side of the phantom to simulate a dome full of water. We plan to conduct further tests of this method using specimens from an SRD.

Ultrasound

Ten years ago our initial evaluation of ultrasound for NDE of sonar domes led to its application in finding large voids in the fill rubber areas. In areas where there were structural plies (steel cord reinforced), the technique was wholly inadequate. Since then there have been significant advances in resolution and data analysis and we are reviewing the application of ultrasound for structural regions. This work is in the initial stage of defining the material properties in order to determine the best approach. Some preliminary scans have resulted in images of the steel cords in a one ply layer of SRD fabric. We are not yet able to comment on the potential of ultrasound for this application.

CONCLUSION

From our progress so far, XBT remains a promising candidate for providing one-sided NDE for the SRD. We have demonstrated the imaging of SRD damage on one SRD removed for cause. We have established a project methodology and schedule for developing the required SRD inspection system, with the goal of providing a routine pierside inspection capability. A significant number of engineering problems will need to be worked out to provide a repeatable inspection approach, as well as the development of new data analysis methods for imaging the deep SRD layers. We will continue our investigation of other NDE methods as time and funding allow. Table 1 summarizes and compares the SRD inspection methods.

METHOD	ADVANTAGES	DISADVANTAGES	NOTES
X-Ray Radiography	Well developed. Large base of SDRW/SRD data. Quantitative cord damage data. Film record.	Requires drydocking and SRD removal.	In use. 651 SDRW, 164 SRD inspections completed.
X-Ray Backscatter Tomography (XBT)	One sided. Tomographic. Quantitative cord damage data. Data comparable to radiography. Discrimination of SRD structure.	Expensive. Image artifacts. Difficult inter-pretation of deep features.	Early gamma backscatter study. Recent feasibility study with 3 vendor's systems and SRD specimens. Philips scanner at NRL site.
Ultrasound	One sided. Underwater.	No penetration of structural plies demonstrated.	Prior tests negative. New tests underway.
Shearography	One sided.	Overly sensitive. Poor SRD reflectance. Qualitative. Interpretation difficult.	Old NRL study. Recent vendor's study of SRD section.
Microwave	One sided. Water detection demonstrated.	Qualitative. No cord damage detection demonstrated.	1 vendor's test results.
Magnetic flux Leakage	One sided. Detects cord ends in phantom.	Qualitative. Discrimination between flaw/ SRD structure difficult.	Prelim. study done (SWRI).
Mechanical (Direct Stiffness Measurement)	One sided. Simple. Low cost. Correlation between local modulus and damage.	Qualitative.	Prelim. study. Prototype inspection device in development.

Table 1. Comparison of NDE methods for Sonar Rubber Dome Inspection.

ACKNOWLEDGEMENTS

The authors acknowledge the sponsorship of the NAVSEA Naval Surface Ship ASW Group and the support of the NRL Materials Chemistry Branch under NRL contract number N00014-90-2269. Ultrasound data was provided by H. Chaskelis of NRL. Shearographic tests were conducted by B. Feferman of Laser Technology, Inc., Norristown, Pa. Magnetic flux leakage tests were conducted by C. Teller of the Southwest Research Institute, San Antonio, Texas. Microwave testing was arranged by C. Seward of Spatial Dynamics, Inc., Acton, Massachussets. Mechanical test data was provided by S. Katz of Geo-Centers, Inc.

REFERENCES

1. R. Falabella and R.D. Corsaro, "Nondestructive Testing of Sonar Dome Rubber Windows," Proceedings, 32nd Defense Conference on Nondestructive Testing, Akron, Ohio, November 1983, p 232.

2. N. Vagelatos, D. Thayer, K. Brown, and F. Howe, Jr., "Inspection of Sonar Dome Rubber Windows Using Collimated Photon Scattering," IRT-8226-001, IRT Corporation, June 1983.

3. D. Schafer, M. Annis, P. Bjorkholm, and W. Baukus, "Advancements in Applications of Backscatter Tomography," *Proceedings, 17th Symposium on Nondestructive Evaluation*, San Antonio, Texas, April 1989, pp 78-84.

4. R.H. Bossi, J.L. Cline, and K.D. Fridell, "X-Ray Backscatter Imaging With a Spiral Scanner," *Proceedings, 17th Symposium on Nondestructive Evaluation*, San Antonio, Texas, April 1989, pp 104-108.

5. C.F. Poranski, E.C. Greenawald, "NDE for Navy Keel Mounted Rubber Sonar Domes," *Proceedings, 39th Defense Conference on Nondestructive Testing*, Modesto, California, 1990.

APPENDIX F

QUANTITATIVE RADIOSCOPIC PROFILE ANALYSIS VIA NEURAL NETWORKS

GEO CENTERS, INC

QUANTITATIVE RADIOSCOPIC PROFILE ANALYSIS VIA NEURAL NETWORKS

Edward C. Greenawald

Geo-Centers, Inc.
10903 Indian Head Highway
Fort Washington, MD 20744

Chester F. Poranski
Materials Chemistry Branch
Naval Research Laboratory
Washington D.C. 20375

INTRODUCTION

Artificial neural networks have been studied over a 30 year period and are a well developed computational technology applicable to a variety of difficult problems [1]. All neural networks are simulations of neurons and synapses based upon a primitive understanding of these biological structures. The distinctive feature of these networks is that they are trainable. By various iterative schemes, a set of well characterized data can be used to create a network which will produce a correct output function of an input vector. The learning is generalized, resulting in the ability to provide correct results for input vectors not contained in the training data. The term neural network has become nearly synonymous with a particular type: the feed-forward backpropagation neural network. We will use the term network in that sense here.

A network is composed of layers of processing units called neurons and their interconnections. The connections allow data to move unidirectionally from an input layer through intermediate, or hidden layers, toward an output layer. Many problems can be solved by networks with only one intermediate layer. The input layer differs from other layers in that it only provides a distribution of each input node to the intermediate layer. Each neuron receives input from all neurons of the next higher layer and sends output to all neurons of the next lower layer. Neurons in the same layer are not connected. A diagram of this structure is included in Figure 1. The connections between neurons are modeled as arrays of values known as weights. Neurons process their inputs by means of an activation function, and a transfer function. The activation function is typically a summation of the weighted inputs. Variations sometimes used are the inclusion of a constant bias value or the previous state of the neuron in the summation. The transfer function is typically a sigmoidal, or s-shaped, function. This function serves as a limiting thresholding function, but it also provides the neuron with programmable, i.e. wieght dependent, non-linearity. Under this scheme, y_j, the output of neuron j, is a non-linear function of its total input:

$$y_j = \frac{1}{1 + e^{\left(-\sum_i y_i w_{ij}\right)}} \quad (1)$$

where i is over all neurons in the layer above j, and w_{ij} is the weight vector for connections with the preceding layer's outputs, y_i.

Network training is accomplished by an iterative gradient procedure known as backpropagation. In preparation for training, the weights are initialized with small random values. During training, the network is presented with an input and the output is compared with the known correct output vector, or pattern. The error at each output is determined and propagated backwards through the network to associate a square error derivative with each neuron. Finally, the weights of each neuron are adjusted according to the corresponding gradients. A new input is then presented and the process repeated until convergence upon a solution, or set of weights, producing correct responses to all training data within an acceptable tolerance for error. The implementation of backpropagation in a multilayer network is decidedly non-trivial. Even a superficial mathematical description of the process is beyond our scope here. Fortunately, several commercial software publishers have now made available user configurable network programs. Furthermore, network solutions in the form of weight arrays, can now be implemented in computer hardware by downloading into dedicated neural processors.

Networks have recently been implemented to solve a variety of pattern recognition problems in the field of nondestructive evaluation [2,3,4]. The applications have typically been qualitative in nature, providing recognition and classification of structural or material flaws. Our current objective is to demonstrate the potential of neural networks for obtaining quantitative dimensional measurements from radioscopic data. Such a capability would be useful for the automated real time inspection of manufactured parts. Measurements by real time radiography currently require accurate data registration, well controlled orientation of the parts and visual analysis by a skilled interpreter. The demonstrated capability of neural networks to detect moment invariant features [5,6] promises to afford an automated solution without sensitivity to registration or orientation errors.

In this paper we present a demonstration of shift and rotation invariant measurements using Brainmaker, a commercial feed-forward backpropagation network [7], and simulated x-ray attenuation profiles. Although our interest is in radiographic imagery, we have chosen one dimensional profiles for this preliminary study to reduce the complexity of the simulation and the size of the network. The profiles can be considered, however, as representing either line profiles from real time radiography or linear detector array output. The profiles were modeled using computer graphics methods. Figure 1 illustrates the relationships among the modeling, simulation, and network aspects of the demonstration. Solutions were developed for three feature measurement problems: Wall thickness of a circular (cylindrical) object, concentricity of a circular object, and thickness measurement of a square object. In the first two cases, random registration error was introduced and in the third case a random rotational orientation was introduced.

SIMULATION

The fundamental relationship between monoenergetic incident and transmitted x-ray intensities and a material's properties is described by the formula

$$I = I_0 e^{-\mu z} \quad (2)$$

where I and I_0 are the transmitted and incident intensity, μ is the linear absorption coefficient for the material, and z is the material thickness [8].

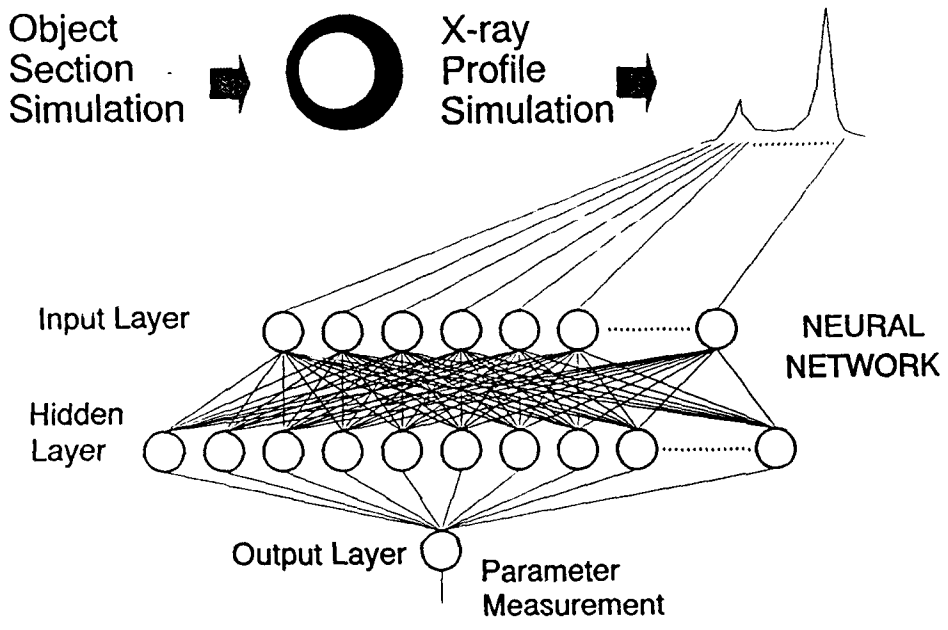

Figure 1. Schematic diagram of the profile simulation and neural network.

We modeled the part cross sections as filled (colored) areas on a computer graphics screen at a resolution of 5 pixels per millimeter. Normalized attenuation profiles, $P(x)$, were simulated by an algorithm implementing the equation:

$$P(x) = ke^{\gamma \sum_{z=0}^{T} \mu(x,z)\Delta z} \quad (3)$$

where T is the part thickness, $\mu(x,z)$ is the absorption coefficient for the part material (colored pixels) or for air (black pixels), Δz is the thickness represented by one pixel, and k and γ characterize the response of the detection system [9]. Values were calculated for the range of x over the part width plus the maximum programmed registration error. Then the profile data were normalized over the range 0 to 255, consistent with an 8 bit digitization of analog profile data. Output was in the form of disk files of numeric profile and measurement data. Graphics were also printed showing the part cross sections and associated profiles (prior to normalization). Figure 2 shows examples of the graphics output. Program input variables include the number of profiles to be generated in one run, material attenuation coefficients, and scaling and sampling parameters. We used the linear absorption coefficient for iron (1.85 cm^{-1}), obtained by multiplying published values of the density and the mass attenuation coefficient for 150 KeV radiation [10]. Our simplified attenuation model assumes monoenergetic x-rays and also ignores beam hardening, scatter, geometric unsharpness, and noise. Training data for a real inspection application would need to be generated using the real system and a set of real flawed parts.

NETWORK CONFIGURATION

We used a three layer network topology, with a sigmoid transfer function as described above. Inputs to the network consisted of alternate pixel samplings of the profile data (approximately 100 points). The intermediate layer was the same size as the input layer. One output neuron provided the desired parameter measurement. Two sets of 200 profiles were generated by the simulator for each case studied: one to be used for network training and the other for testing. Inputs

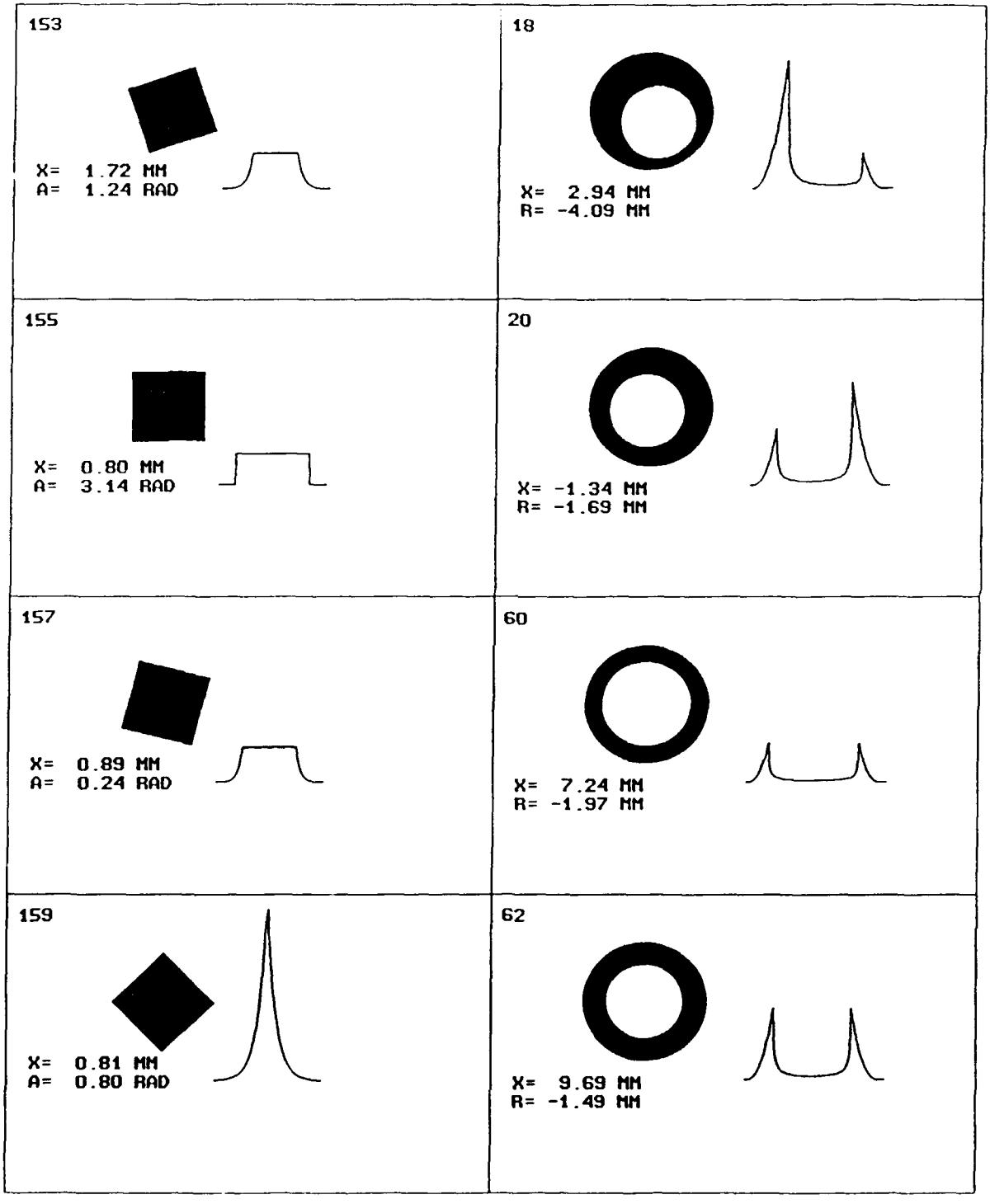

Figure 2. Examples of profile simulator output. Simulated cross sections are shown with their respective profiles (prior to normalization). Numbers 153, 155, 157, and 159 correspond to study case C, 18 and 20 to case B, and 60 and 62 to case A.

to the network consisted of the raw normalized profile data. No feature extraction pre-processing was done. Prior to training, neuron connection weights were randomized.

CASE A: CIRCULAR WALL THICKNESS

The part was modeled as a circular object with a 50 mm outside diameter and a nominal wall thickness of 10 mm. This could represent any tubular or cylindrical product. The wall was randomly thinned by varying the inside diameter over the range +0.00 mm to - 5.00 mm. Random registration error was introduced by varying the object center location over the range ±5.00 mm. The network training and testing data sets consisted of even indexed profile values (alternate pixel sampling) and the desired output value of the corresponding variation from nominal thickness. No registration information was provided to the network.

The network converged upon a solution after 353 presentations of the training data using a training tolerance of .05. The test data set was then run, producing correct measurements for 96% of the profiles using a tolerance of .1, equivalent to a wall thickness measurement tolerance of 1.0 mm.

CASE B: CIRCULAR WALL CONCENTRICITY

As in case A, the part was modeled as a circular object with a 50 mm outside diameter and 10 mm wall thickness. In this case, however, a random concentricity error was introduced by varying the juxtaposition of the two centers over a range of ±5.00 mm for both x and y axes. Again, random registration error of ±5.00 mm was introduced. The network training and testing data sets consisted of even indexed profile values and the desired output measurement of x axis eccentricity. (Analysis of y axis eccentricity would require a profile taken along the y axis.)

A network was successfully trained and tested, achieving 100% correct eccentricity measurement using a tolerance of 1.0 mm.

CASE C: SQUARE OBJECT THICKNESS

This part is modeled as an object with a 30 mm square cross section which may be presented to the detection system in any rotational orientation. Successive cross sections were randomly rotated up to 180 degrees. The square width was randomly varied by +0.00 to -3.00 mm. Network training and testing data sets consisted of even indexed profile values and the square width error measurement.

The network was trained in only 16 passes through the training data using a tolerance of .1. Testing was carried out using three different tolerances. With a tolerance of 0.3 mm, the same as that used in training, 89% of the measurements were correct. Using 0.6 mm, 98% were correct. At 1.2 mm, 99% were correct.

CONCLUSION

Using profile data from a simplified x-ray attenuation model, we have demonstrated the feasibility of obtaining quantitative measurements of object dimensions via neural networks. We have also demonstrated shift and rotational invariance. Our interpretation of this success is that the network is not obtaining a measurement in the usual sense, but is actually fulfilling its well established role as a pattern classifier. The dimensions are being recognized rather than measured. It is noteworthy in this regard that the normalization of each profile, while enhancing

contrast, deprives the network of some information relative to the measurement. The shape of the curve is emphasized at the expense of the quantitative information contained, for example, in the area under the curve. The function of the output neuron in this interpretation is analogous to that of a digital to analog converter. The hidden layer's outputs provide the pattern and the output neuron's transfer function provides an analog output. We suggest that the following areas are worthy of additional study: extension of the method to two dimensional x-ray imagery, improvement of accuracy, use of a better x-ray model, use of real inspection data, and verification of our interpretation.

ACKNOWLEDGEMENTS

We acknowledge the support of the NAVSEA Naval Surface Ship ASW Group and the NRL Materials Chemistry Branch under NRL contract number N00014-90-C-2269.

REFERENCES

1. B. Widrow and M.A. Lehr, "30 Years of Adaptive Neural Networks: Perceptron, Madaline, and Backpropagation," *Proceedings of the IEEE*, Vol. 78, No. 9 (1990), p. 1415.

2. D. Berry, L. Udpa, and S.S. Udpa, "Classification of Ultrasonic Signals Via Neural Networks," *Review of Progress in Quantitative NDE*, Vol. 10A, edited by D.O. Thompson and D.E. Chimenti (Plenum Press, New York, 1991), p. 659.

3. L.M. Brown and R. DeNale, "Classification of Ultrasonic Defect Signatures Using an Artificial Neural Network," *Review of Progress in Quantitative NDE, op. cit.*, p. 705.

4. R.S. Barga, M.A. Friesel, and R.B. Melton, "Classification of Acoustic Emission Waveforms for Nondestructive Evaluation Using Neural Networks," *Applications of Artificial Neural Networks,* SPIE Vol. 1294 (1990) p. 545.

5. A. Khotanzad and J. Lu, "Classification of Invariant Image Representations Using a Neural Network," *IEEE Transactions on Acoustics, Speech, and Signal Processing*, Vol. 38, No. 6 (1990), p. 1028.

6. R.J.T. Morris, L.D. Rubin, and H. Tirri, "Neural Network Techniques for Object Orientation Detection: Solution by Optimal Feedforward Network and Learning Vector Quantization Approaches," *IEEE Transactions on Pattern Analysis and Machine Intelligence*, Vol. 12, No. 11 (1990), p. 1107.

7. J. Lawrence and M. Lawrence, *Brainmaker User's Guide and Reference Manual* (California Scientific Software, Grass Valley, Ca, 1990).

8. R. Halmshaw, *Physics of Industrial Radiology* (American Elsevier, New York, 1966), p. 132.

9. E.C. Greenawald and C.F. Poranski, "Computer Simulation of Steel Cord Radiograph Profiles," *Review of Progress in Quantitative Nondestructive Evaluation*, Vol. 11, edited by D.O. Thompson and D.E. Chimenti (Plenum Press, New York, 1992), p. 2299.

10. *Handbook of Chemistry and Physics*, 52d Edition, edited by R.C. Weast (Chemical Rubber Co., Cleveland, Ohio, 1972).

APPENDIX G

REVIEW OF RECOMMENDATION TO PLACE SDRW N113 IN MONITOR STATUS

GEO CENTERS INC

DEPARTMENT OF THE NAVY
NAVAL RESEARCH LABORATORY
WASHINGTON, D.C. 20375-5320

IN REPLY REFER TO
9165/Prob 61-1549
Ser 6120/432
OCT 2 3 1996

From: Commanding Officer, Naval Research Laboratory
To: Commander, Naval Sea Systems Command (Code 06U1D, S. Silverstein)

Subj: REVIEW OF RECOMMENDATION TO PLACE SDRW S/N N113 IN MONITOR STATUS (USS TICONDEROGA CG47)

Encl: (1) Two copies of subject report

1. Enclosure (1) is forwarded your information and retention.

By direction

Blind Copies to:
NRL Code 6126, C. F. Poranski
NRL Code 6126, J. Nagode

Ser 6120/432A
17 December 1992

Subj: REVIEW OF RECOMMENDATION TO PLACE SDRW S/N N113 IN MONITOR STATUS (USS TICONDEROGA CG47)

Ref: (a) "SONAR DOME RUBBER WINDOW (SDRW) AND SONAR RUBBER DOME (SRD) RADIOGRAPHIC INSPECTION REPORTS (AUGUST - NOVEMBER 1992)," NRL Letter Report 6120/418, Dec. 4, 1992
(b) "SDRW RADIOGRAPH EVALUATION AND RECOMMENDATIONS," NRL Letter Report 6120-120, Feb. 20, 1986
(c) "REVISED NRL RECOMMENDATIONS FOR REPAIRED SONAR DOME RUBBER WINDOWS (SDRW)," NRL Letter Report 6120-53, Feb. 11, 1987

1. Introduction. The radiographic inspection of the subject SDRW, conducted on October 15, 1992, revealed a three inch damage site near the port splice edge. Approximately 30 of the steel cords are broken in one of the SDRW's three longitudinal plies. Reference (a) reports the details of the inspection and recommends that the damage be monitored by periodic radiographic inspection. NRL did not recommend that action be taken to repair or to replace the SDRW. NAVSEA 06U1D asked NRL to provide detailed information supporting this decision. This report provides additional support for the recommendation.

2. Recommendation Criteria. The criteria for our recommendations, given in references (b) and (c), have been formalized. They have evolved by making adjustments based on analyses of the cumulative inspection and failure data, new procedures and design changes, and events. The goal is to prevent SDRW failures at sea by detecting incipient corrosion-fatigue damage while also deferring costly actions such as SDRW replacement. Early damage detection also facilitates planning for SDRW procurements and change-outs.

The extent of SDRW damage is measured in terms of damage "sites", or sequential runs of broken cords within the SDRW wall. In addition to the number of sites, the individual site length (inches) and depth (number of plies) are also measures of severity. Damage growth is also measured in these terms.

SDRWs are routinely inspected at prescribed intervals of two or four years. Those found to be damaged can be inspected annually in order to monitor the damage growth. We recommend the repair of SDRWs considered to be at risk of failure before their next monitoring inspection. Replacement is recommended for SDRWs damaged beyond repair. The criteria for these categories are in

terms of the number of damage sites, length of damage, depth (i.e. the number of damaged longitudinal plies), and location. Currently, repair is recommended if any of the following conditions are met:

More than three damage sites.
A site greater than 18 inches in length.
A site involving two longitudinal plies.
A site in the bottom half of the SDRW.
A total damage length (sum of all sites) greater than 36 inches.

Replacement is recommended in cases of two or more "repair" indications, loss of SDRW pressure, or multiple 2-ply sites.

In addition to the many damaged SDRWs successfully managed by this method in the past, forty percent of the SDRWs currently in service contain monitored damage, including those with repairs. Only one failure of a timely monitored SDRW has occurred using the current criteria. In that case, the USS STUMP SDRW S/N N91 radiographs, obtained in February, 1989, contained an unusual feature: widespread indications of individual cord damage. Since the significance of this feature was unknown, the recommendation to monitor the SDRW was based only upon the three clearly identified runs of broken cords. The dome failed three months later (See Figure 5). SDRWs have also failed while overdue for inspection or while being monitored after NRL recommended repair or replacement.

3. Discussion of CG47 SDRW Damage. The criterion which applies to the CG47 SDRW damage site is the 18 inch one-ply site length threshold for repair recommendations. This threshold is based upon the observation that, whether damage growth proceeds rapidly or slowly, a limit exists at about 18 inches. Our interpretation of this fact is that as 1-ply damage progresses, loads are transferred to adjacent plies. Near 18 inches, the adjacent plies have assumed the directional loads causing the site growth. In the case of the CG47 SDRW, there are two additional longitudinal plies. Most of our data is from SDRWs with only one additional longitudinal ply.

In order to place the CG47 SDRW damage within the context of our experience with similar damage, it is instructive to consider several representations of the SDRW inspection data "space". Figure 1 is a histogram showing the distribution of all damage lengths measured throughout the 9 years of the radiographic inspection program, including those on SDRWs subsequently removed. All of these SDRWs were in service at the time of the measurement. Only the most recent measurement of each site is represented. The CG47 SDRW's place in this distribution is indicated by an arrow. Figure 2 shows similar data, but only for SDRWs currently in service. This represents the population of currently monitored SDRWs. Repaired SDRWs have been left out.

To determine the rate at which an SDRW damage site grows, we need an initial date to represent the onset of damage and one or more dates associated with subsequent measurements of site length. Figure 3 is a scatter plot of all site length measurements in the SDRW inspection database which meet this requirement. Damage onset dates were approximated by using the known undamaged dates nearest to the first damage measurement. These undamaged states were determined by inspection results when possible. If damage was detected on the first inspection and the SDRW was installed within two years prior to that inspection, the installation date was used as the undamaged date. Site length is plotted as a function of the number of months from the known undamaged condition. The solid square indicated by the arrow represents the datum from the damaged CG47 SDRW.

Nine SDRWs in the database have damage sites with five or more measurements and a known undamaged date. These damage growth data are plotted in Figure 4 along with the CG47 datum for comparison.

Only two SDRWs have failed while in a "monitor" state (disregarding repaired SDRWs and those that NRL recommended for repair or replacement). These were the USS STUMP (DD978) SDRW, discussed above, and the USS FIFE (DD991) SDRW S/N L31. The latter was overdue for inspection and failed in February, 1989. Although we do not have baseline inspection data for these SDRWs, we can plot the damage growth from the installation of the STUMP and from the first inspection of the FIFE. Figures 5 and 6 show the growth of damage to these two SDRWs. In each case, three damage sites are seen to develop. The right border of the graphs represents the time of SDRW failure.

4. Conclusion. We confirm our previous recommendation to monitor the damaged CG47 SDRW, rather than take other action. Our assessment of the reported CG47 SDRW damage and comparison with nine years of SDRW inspection and failure data leads to the conclusion that this SDRW is at a very low risk of failure within the recommended annual inspection interval. Furthermore, we can expect several more years of service from the SDRW, assuming that the typical, well-behaved damage growth pattern occurs.

Chester F. Poranski, Jr.
Materials Chemistry Branch
Chemistry Division
Code 6126

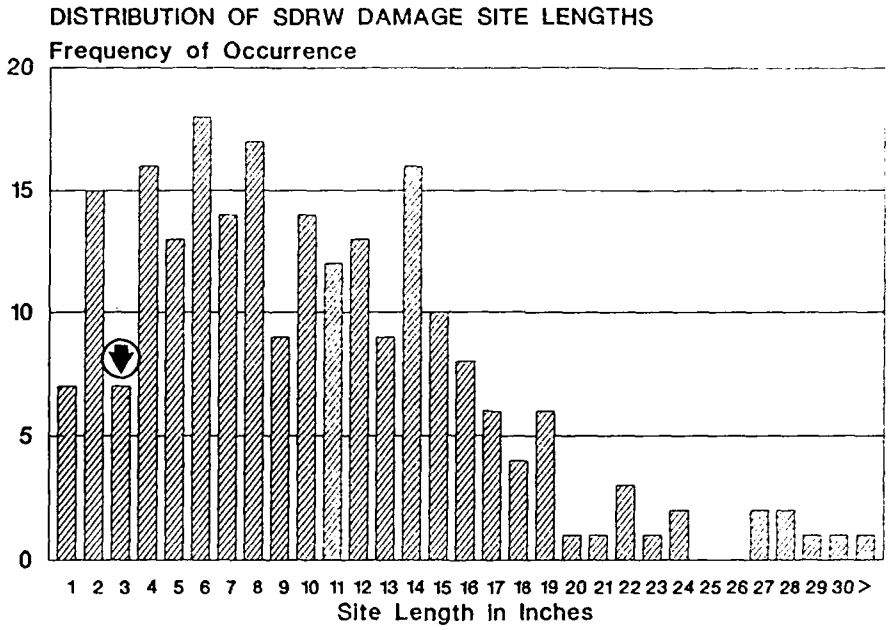

Figure 1. Distribution of most recent damage site length measurements for all SDRWs. The arrow indicates the place of the current CG47 damage site.

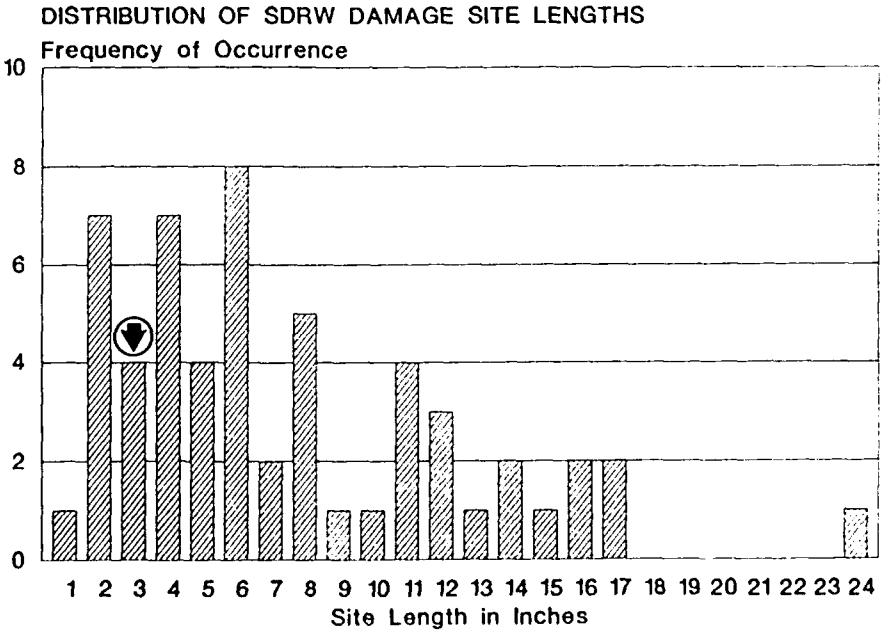

Figure 2. Distribution of most recent damage site length measurements for SDRWs currently in service. The arrow indicates the place of the current CG47 damage site.

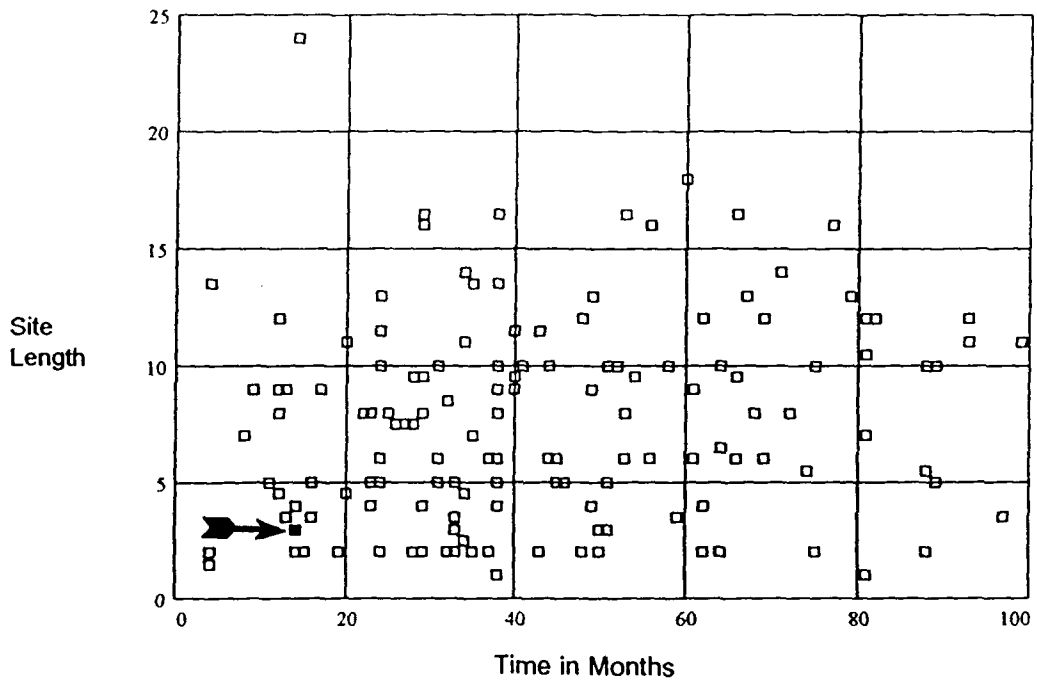

Figure 3. Plot of SDRW damage site length measurements as a function of time. This indicates the "space" within which damage growth is expected to occur. The current CG47 SDRW damage (solid) is indicated by the arrow.

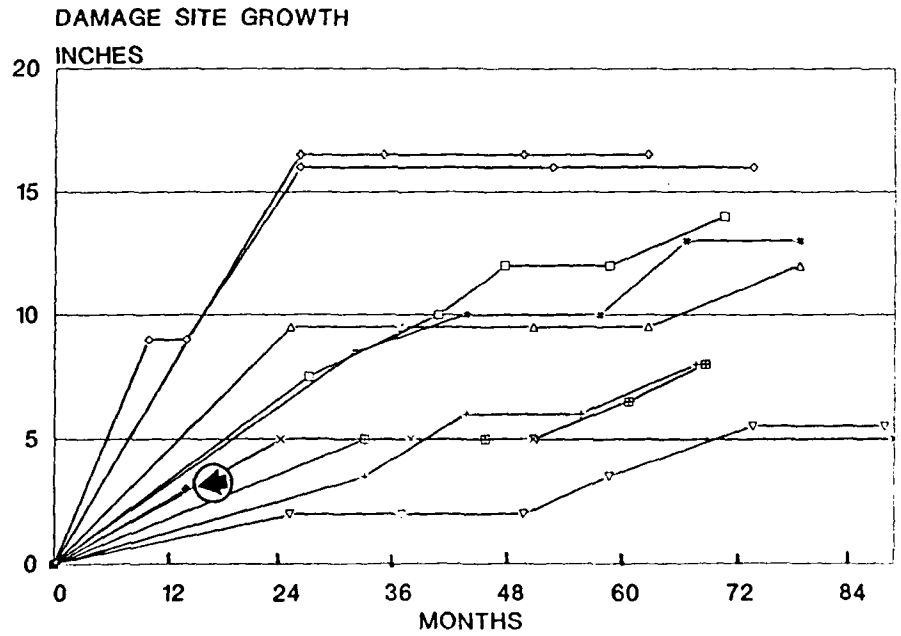

Figure 4. Damage site growth plotted for several SDRWs for which multiple measurements exist and the current CG47 SDRW (Arrow).

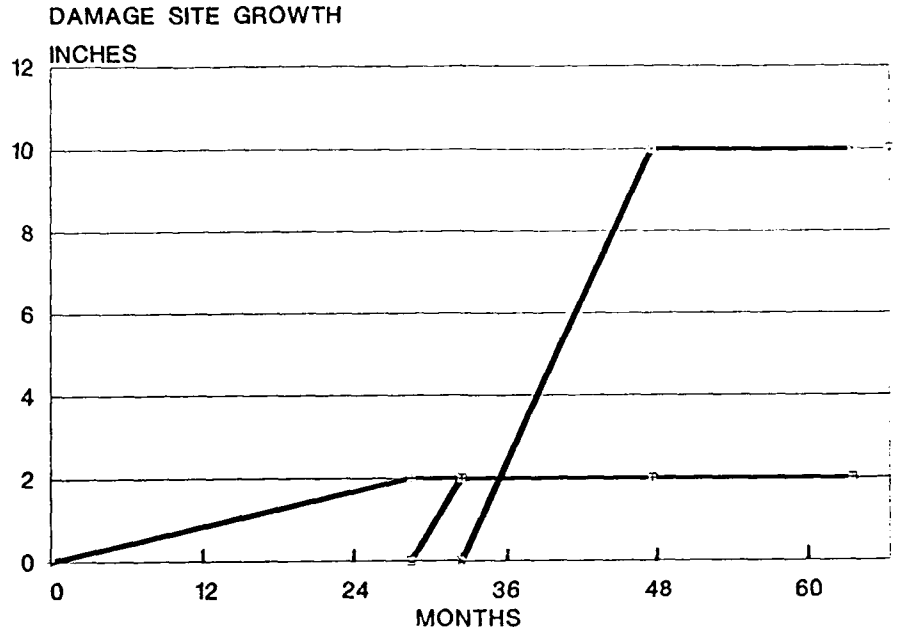

Figure 5. Plot of damage site lengths on the USS STUMP SDRW S/N N91 vs. the SDRW service life. The right border indicates the SDRW failure at 67 months.

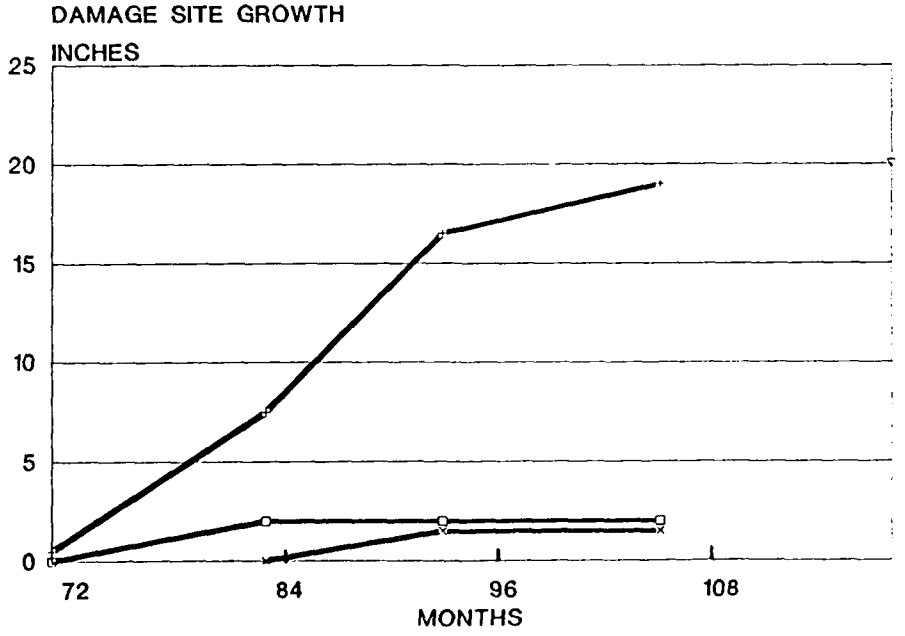

Figure 6. Plot of damage site lengths on the USS FIFE SDRW S/N L31 vs. the SDRW service life. The right border indicates the failure at 118 months.

APPENDIX H

FAILURE ANALYSIS REPORT FOR SRD S/N:B017

GEO-CENTERS, INC.

FAILURE ANALYSIS REPORT
FOR THE SONAR RUBBER DOME S/N:B017

BACKGROUND:

The AN/SQQ-23 SRD measures 400"L x 119"W x 98"H, and is constructed of neoprene and neoprene-steel wire cord fabric. The SRD is attached to the ship's hull through a steel casting. The wire cord fabric is laid-out in five layers with two alternating orientations. In the radial orientation steel wire cord fabric runs port to starboard. The longitudinal orientation is forward to aft, and the fabric is laid as three separate parts; keel band, bead band, and bi/tri-sectors. The keel band is laid-out adjacent to the keel line for both port and starboard sides. The bead band is located along the upper perimeter of the dome. Bisectors and trisectors fill the area between the keel band and bead band. A steel bead cable is attached to the open circumference of the dome with a steel wire cord fabric "tie-in". The tie-in wraps around the bead cable and runs in the radial direction.
The SRD is attached to the casting at the bead.

Sonar rubber dome (SRD) S/N:B017 was never placed into service. This dome was declared unsuitable due to higher than normal insertion loss (IL) measurements. IL inspection was performed by NRL Acoustics on 9 August 1985.

Two samples measuring 5'x 8', and 5'x 4' were removed from the upper port aft, and forward center sections, respectively. Visual inspection prior to sample removal did not reveal any external anomalies. Dome inspection and sample removal were performed on site at Norfolk Naval Ship Yard (NNSY) December, 1988.

AFT SAMPLE ANALYSIS FINDINGS:

The Aft sample was located from 5' port to 13' port of the aft center line. The sample incorporated the bead neck, bead cable, bead cable coupling, and associated structure. The sample was cut into 3" wide specimens in preparation for dissection.

Areas of adhesive failure between the nylon mesh and neoprene in the tie-in were observed. Failure between these substrates is typical, and could have been occurred during sample removal.

A black tacky substance was observed on the bead neck and on the adjacent areas of the casting. Once exposed to air, the substance dried within 72 hours. Chemical analysis using spectrometry showed the substance to be a polychloroprene rubber, however the variety is unknown.

The outline of each individual ply is prominent throughout the cross section on all samples. This is not a typical feature of a fully cured dome. During the cure process the neoprene layers are subject to temperatures that allow a certain amount of flow between plies, creating a more homogenous structure. Differentiating between the plies on a properly cured dome normally requires irradiating the interply layers of adhesive with a UV light source. The technique was not necessary in this case.

Examination of the cross sections revealed voids 1" below the upper rubber line, running parallel to the bead cable. These voids were located along the ends of the bead bands, measuring 1/4" to 1/2" in width by 1/32" to 1/16" in height. Small voids were also observed running along the ends of the bead ply tie-ins. Voids along the 26" bead band were illuminated with UV light to reveal areas where adhesive had been applied. Indications showed that the glue had been applied at some point, but contact between plies never developed.

FORWARD SAMPLE ANALYSIS FINDINGS:

The forward sample was located approximately 1' below the upper rubber line and 2.5' to either side of the centerline. The sample included the bead band/keel band intersections and associated structure. The sample was cut into 3" wide strips for dissection.

No broken cords or corroded areas were found. This SRD was never placed into service; therefore, there was no exposure to stress and corrosion. The only anomalies found indicate a construction or curing problem, or a combination of both.

As observed in examining the aft sample, the outline of each individual ply is prominent on all specimen cross sections. A large amount of voids and delaminated areas were also observed.

Small sections of polyethylene film, used for the packaging and storage of uncured fabric, were scattered among the plies. The film likely added to problems of poor adhesion and delamination characterizing this sample. This feature has been previously observed on both SRDs and SDRWs. The delaminations seen here are unlikely to affect the structural performance of the dome.

Numerous voids were observed throughout the sample. Most of these voids were running between ply butt joints along the bead band/keel band directions. A typical void cross-sectional area measured .01-.12 square inches. Most of the voids observed traversed the entire sample length. Since a majority of the butt joints are in the vicinity of the band intersections, voids were concentrated here as well. This region indicated high insertion loss. We now believe that higher than normal insertion loss

readings can be attributed to voids within the dome's structure.

CONCLUSIONS:

The large amount of voids found caused the high insertion loss readings. The voids found were caused by improper ply placement and inadequate neoprene flow during cure. Apparently SRD S/N:B017 was improperly cured.

APPENDIX I

FAILURE ANALYSIS REPORT FOR SRD S/N:B022

GEO-CENTERS, INC.

FAILURE ANALYSIS REPORT
FOR THE SONAR RUBBER DOME S/N:B022

BACKGROUND:

The AN/SQQ-23 sonar rubber dome (SRD) serial number B022, was cured in June 1985 and installed on the USS Pratt in December 1985. The dome developed a perforation in the aft port bead neck while in service on the *USS PRATT* (DDG-44). The dome was removed from service June 6, 1988 due to its inability to hold operational pressure. Service life of B022 was 30 months. Subsequently the dome was shipped to the Naval Research Laboratory for inspection and failure analysis.

DISSECTION:

Post removal measurements showed the perforation to be 7 inches long. Surface anomalies were found on both the inner and outer surfaces of the bead neck along the dome's perimeter. In-service radiographic inspection of the affected area was not available. Sections measuring 7'x4' and 7'x3' where cut and removed from the aft port and starboard sides, respectively. Both samples included the bead neck, bead cable, and associated structure 20" below the bead neck. Sample removal was accomplished by dry abrasive cutting using a gasoline powered rotating saw.

Specimens measuring 2" x 20" were cut from both main samples for detailed analysis. Each specimen was separated into individual plies that make up the SRD's structure. The specimen is then checked for broken, kinked, and deflected cords, as well as corrosion by-products, adhesive integrity, structural form, and construction anomalies.

LABORATORY OBSERVATIONS/DISCUSSION:

The bead neck perforation is located 8'6" Port of the aft centerline, continuing forward for 7 inches. On-site inspection of the inner marriage line and the bead sealing flap revealed several locations containing cracks and delaminations. Traces of rust where found beneath the sealing flap. The most severe of these cracks was a perforation located eight feet to port from the aft center line. A screw driver could be inserted through the perforation and light seen adjacent to the screw driver. In addition, small surface perforations (diameter < 1/8") were observed sporadically along the bead neck.

Discussion with the SRD's manufacturer revealed that during the construction processes a plate is used to hold the neck in place. This plate is positioned on the lower half of the neck, holding the bead neck plies in place. This action creates a groove around the perimeter of the SRD. Observation of the bead

area in cross-section revealed that the neck was compressed into a thin volume. Plies were pressed tightly together, forcing cords along the bead neck to contact each other. Plies at the extreme ends of the neck were within 1/32" of the outer surface. The groove seen along the bead neck is the area of reduced volume, and was created during the construction process. The reduction of cross-sectional area may have caused a decrease in bead neck strength and an increase in neck flexure.

Corrosion was observed on the bead cable, bead neck plies, and radial plies. Main sea water entry points seem to be through the bead neck groove perforations, and through the part of the bead neck adjacent to the casting. A laboratory experiment revealed that the nylon mesh contained in the bead casing wicked water; the mesh also comes in contact with the first and sixth bead plies at random intervals. It is also noted that the mesh is exposed along the surface facing the lower portion of the bead casting which, is exposed to the dome's internal water supply through cracks on the bead sealing ply. As a result, bead and radial plies often come in contact in the bead neck, which readily abets sea water migration in the structure.

Cohesive failure was observed in the bead's outer casing, as evidenced by the presence of rubber adhered to the casting. We believe this occurred during sample removal. Rust is apparent along the bead neck area of the casting. Cohesive failure in this region is typical, since the bead is securely clamped to the casting for sealing purposes. Adhesive failure at the bead shim/bead flap interface was observed in several locations as well.

Ripples on the bead shims running perpendicular to the bead cable were observed in several locations. The ripples were probably caused by the sample removal procedure that required pulling on the bead cable.

CONCLUSION:

Failure of SRD S/N: B022 occurred when the aft port bead neck developed a perforation. The damage is located along the compressed area of the bead neck. The resultant groove depth on the bead neck, a construction anomaly, varies throughout the dome's perimeter. Small diameter holes were found along the inside of this grooved area. The reduction of cross sectional area may have decreased the strength of the neck allowing excessive flexure and fatigue to occur. Seawater infiltrated the neck through the small holes located on the groove, and the cracks located on the bead sealing ply. Final failure of B022 was due to a combination of corrosion and fatigue.

APPENDIX J

PROCESSABLE FLUOROPOLYMERS WITH LOW DIELECTRIC CONSTANTS: PREPARATION AND STRUCTURE-PROPERTY RELATIONSHIPS OF POLYACRYLATES AND POLYMETHACRYLATES

GEO CENTERS, INC

PROCESSABLE FLUOROPOLYMERS WITH LOW DIELECTRIC CONSTANTS: PREPARATION AND STRUCTURE-PROPERTY RELATIONSHIPS OF POLYACRYLATES AND POLYMETHACRYLATES

Henry S.-W. Hu
Geo-Centers, Inc., Fort Washington, MD 20744
and
James R. Griffith
Naval Research Laboratory, Washington, D.C. 20375

Introduction

Capacitance is directly proportional to the dielectric constant of a material. Present computer operations are limited by the coupling capacitance between circuit paths and integrated circuits on multilayer boards. The computing speed between integrated circuits is reduced by this capacitance and the power required to operate is increased.[1] A reduction in dielectric constant can allow lower thickness of dielectric, for equivalent capacitance, and enable the ground plane to be moved closer to the line. Additional lines can therefore, be accommodated for the same cross talk. Thus, the effect of a lower dielectric constant is to increase speed of signal, improve density of package and result in improved system performance.[2]

Reductions in such parasitic capacitance can be achieved in a number of ways through the proper selection of materials and the design of circuit geometry. In 1988 St. Clair *et al.*[3] reported a reduction of dielectric constant to 2.39 by chemically altering the composition of a polyimide backbone to reduce the interactions between linear polyimide chains and by the incorporation of fluorine atoms. In 1991 Cassidy *et al.*[4] reported a reduction of dielectric constant to 2.32 for the hexafluoroisopropylidene-containing polyacrylates and copolyacrylates.

Very recently we[5] reported a class of processable heavily fluorinated acrylic resins which exhibit dielectric constants as low as 2.10. In this paper we report the preparation of a series of processable heavily fluorinated acrylic and methacrylic homo- and co-polymers which exhibit dielectric constants as low as 2.06 which is very close to the minimum known values[6,7] of 2.0-2.08 for PTFE (Teflon) and 1.89-1.93 for Teflon AF. The factors which affect the reduction of dielectric constants from structure-property relationships are elucidated.

Experimental Section

Only one typical example in the preparation of monomers is described here; the others will be reported elsewhere.

Materials. Triethylamine was fractionally distilled from lithium aluminum hydride under nitrogen. Acryloyl chloride and methacryloyl chloride were distilled under nitrogen. 1,1,2-Trichlorotrifluoroethane (Freon 113) was distilled from phosphorus pentoxide under nitrogen. Azobisisobutyronitrile (AIBN) was used as received. Methyl ethyl ketone peroxide (MEKP) (9% A.O. Max., Organic Peroxide VN 2550) was obtained from Witco. Alumina (neutral, Brockman activity 1, 80-200 mesh) was obtained from Fisher Scientific Co. All other reagents were used as received or purified by standard procedures.

Preparation of etherdiacrylate 6. 1,3-Bis-(2-hydroxy-hexafluoro-2-propyl)-5-(4-heptafluoro-isopropoxy-1,1,2,2,3,3,4,4-octafluoro-1-butyl)benzene, bp 95°C/1.0mm, was prepared by the multistep route reported by Griffith and O'Rear.[8]

The etherdiacrylate 6 was prepared by a modification of the procedure of Griffith and O'Rear.[8] To a solution of etherdiol (3 g, 3.78 mmol) in Freon 113 (10 mL) in an ice-water bath under nitrogen, triethylamine (0.791 g, 7.81 mmol) in Freon 113 (5 mL) was added dropwise in 10 min. After 10 more min, acryloyl chloride (0.707 g, 7.81 mmol) in Freon 113 (5 mL) was added dropwise in 20 min; a precipitate formed immediately. After stirring 2 hr at room temperature, filtration through Celite to remove the solid, followed by evaporation at room temperature *in vacuo*, 3.02 g of a viscous liquid was obtained.

The liquid was dissolved in a mixture of methylene chloride (20 mL) and Freon 113 (10 mL); filtration through neutral alumina (1 g) gave a clear filtrate. It was cooled in an ice bath, washed twice with 1.3N sodium hydroxide 10 mL, washed with water 10 mL, dried over anhydrous sodium

Scheme I

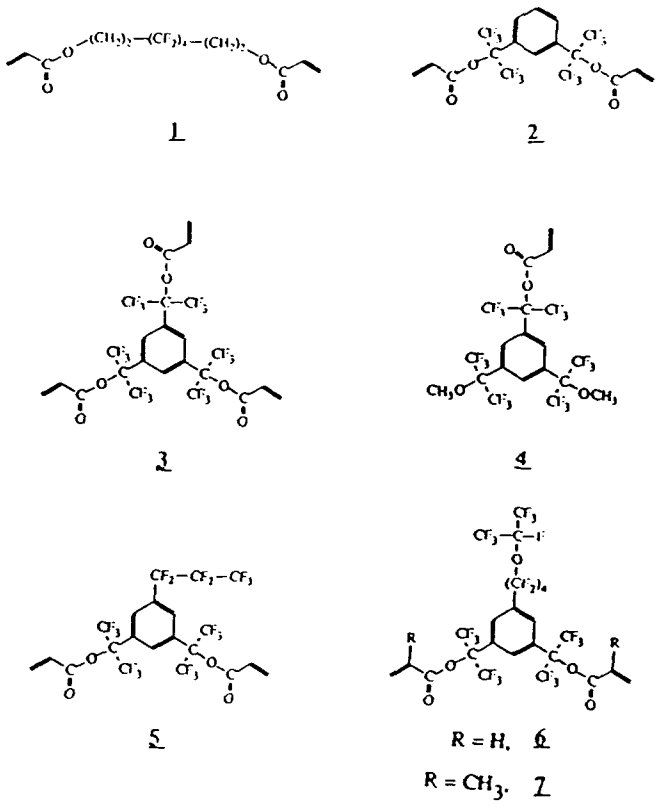

Table I

Summary of Data for Dielectric Constant Measurements[a]

Monomer used	Fluorine content (%)[d]	Dielectric Constant, Frequency (GHz)			
		0.0	3.0	9.0	15.0
1	38.17	2.37	2.41	2.36	2.36
2	43.99	2.26	2.25	2.28	2.27
3	46.32	2.23	2.23	2.23	2.22
(3 + 6)[b]	51.58	2.22	2.23	2.24	2.22
(4 + 5)[b]	52.27	2.21	2.22	2.22	2.19
5	52.60	2.18	2.21	2.16	2.15
6	56.85	2.11	2.10	2.12	2.13
7	55.14	2.07	2.06	2.08	2.10
PTFE[c]	75.98	1.96	1.98	1.99	----

[a]See Experimental Section for details.
[b]50/50 (w/w).
[c]Polytetrafluoroethylene (MMS-636-2) from Gilbert Plastics & Supply Co.
[d]Calculated.

sulfate, percolated and washed through a column of neutral alumina (3 g) twice, and evaporated *in vacuo* at room temperature for 3 hr to give a colorless viscous liquid **6** 1.38 g, yield 40%.

Preparation of polymer "cylindrical donuts" from monomers. The liquid monomer was mixed with a trace amount of AIBN at room temperature in a cylindrical donut mold made from General Electric RTV 11 silicon molding compound. Donuts had an outer diameter of 7.0 mm, inner diameter of 3.0 mm and a thickness of 3.0 mm. The semisolid monomer was mixed with a trace amount of liquid methyl ethyl ketone peroxide (MEKP) with some heating to obtain a clear liquid.

For polymerization the filled donut molds were kept under an inert atmosphere and the temperature was raised to 85°C over 2 hr, then kept at 85-100°C for 20 hr.

Dielectric constant (DE) measurements. Dielectric constant values are reported as "Permittivity" with the symbol ε or K_s. The polymer cylindrical donuts were used for the measurement of DE on a Hewlett Packard 8510 Automated Network Analyzer with conditions and calibration as described before.[5]

Results and Discussion

Monomers and polymers. In proton-1 NMR spectra, the acrylates showed a characteristic ABX pattern in the region of δ 6.8-6.0 with a pair of doublet couplings for each vinyl proton while the methacrylates showed a characteristic AB pattern in the region of δ 6.5-5.8 with an equivalent singlet peak for each vinyl proton. The monomers purified by percolation over alumina contained no detectable hydrate water or polymerized impurities.

As expected, the homopolymers and the 50/50 (w/w) copolymers are semitransparent, hard solids and some shrinkage in volume is observed during curing. In an undercured state they are frangible, but when totally cured they acquire a more resilient character. The degree of polymerization or conversion of monomers can be easily monitored with fourier transform infrared spectrophotometer, for example, by examining the intensity of the absorption frequencies at 1635 and 1410 cm^{-1} which are assigned to the acrylate functional groups.

Dielectric constant (DE) and structure-property relationships. In order to validate the accuracy of our measurements, three samples of virgin PTFE in the same cylindrical donut size were measured and found to have average DE values around 1.96-1.99, which are close to the reported values 2.0-2.08.[6] Summarized results of the DE measurement on the polymer donuts are shown in **Table I**. All the new polymers exhibit unusually low DEs around 2.06-2.41 over a wide frequency region of 500 MHz to 18.5 GHz; the variation of DE values over the measured frequency region is within 0.03 which indicates a wide range frequency independence.

Basically, the effect of a higher fluorine content from either the polymer backbone or sidechain, will be the reduction of polymer chain-chain electronic interactions, which further results in a reduction of DE. This effect was observed by St. Clair *et al.*[3], but only on the polymer backbone.

In comparison of **5** with **6**, the existence of a perfluoroalkyl ether linkage seems to play an important role in further reducing the dielectric constant values. This ether linkage is structurally similar to the dioxole ring which exists in the Teflon AF terpolymer of 2,2-bis(trifluoromethyl)-4,5-difluoro-1,3-dioxole, perfluoropropylene and tetrafluoroethylene. The Teflon AF has been reported by Resnick[7] as the lowest dielectric constant (1.89-1.93) of any polymer thus far.

It has been reported[10] that in the preparation of polyimides the more flexible *meta*-linked diamine systematically gave lower DE values than the corresponding *para*-linked system and that this may be related to free volume in the polymer since the *meta*-substituted systems should have a higher degree of entropy. Therefore, the symmetrical *meta*-substitution in our aromatic structure may result in a reduction of DE.

In comparison of **6** with **7**, a reduction of DE was observed when acrylate was replaced by methacrylate and this may be related to the free volume in the polymer since the bulkier methacrylate should have more steric hindrance than the acrylate.

Lower dielectric constants ? Dielectric constants of these materials can be further lowered by known means such as by incorporating air bubbles in the materials, or by inhibiting the crystallization. Recently Singh *et al.*[11] calculated the dielectric constants of polyimide films from the measured free volume fraction and found that the calculated values for the dielectric constants are close to the experimental results.

In 1991 Groh and Zimmermann[12] estimated the theoretical lower limit of the refractive index of amorphous organic polymers by using the Lorenz-Lorentz equation and reported the lower limit to be very close to 1.29, while in 1979 Dislich[13] proposed a lower limit of about 1.33 from a screening of published polymer data.

The amorphous Resnick Teflon AF terpolymer is reported with the lowest refractive index in the range of 1.29-1.31 and also with the lowest dielectric constant in the range of 1.89-1.93. Furthermore, Groh and Zimmermann[12] reported that functional groups with a high fluorine content, like CF_3 and CF_2, have the lowest refractive index contribution. The value for the ether group is also remarkably low, while the values for the carbonyl and carboxyl groups are high. In view of the good agreement between the refractive index and the dielectric constant on amorphous organic polymers, the opportunity to obtain the dielectric constants in the range of 1.89-2.06 by modifying our synthesis is high.

Conclusions

In this work we have demonstrated that a new class of heavily fluorinated acrylic and methacrylic resins can be efficiently synthesized and then cured to solid form with a catalyst at elevated temperatures. These cured resins were found to have unusually low dielectric constants, which are close to the minimum known values for PTFE and its Teflon AF terpolymers. In contrast to tetrafluoroethylene, our monomers are processable under normal conditions due to the fact that they are liquids or low melting solids, and moreover are soluble in common organic solvents. Lower dielectric constants are obtained as fluorine contents from polymer backbone or sidechain increase, when acrylate is replaced by methacrylate, when ether linkages are present in the fluorocarbon and when aromatic structure is symmetrically *meta*-substituted.

Acknowledgement. We are indebted to Mr. Jonas K. Lodge of SFA, Inc. for the dielectric constant measurements. Partial funding support from the Office of Naval Research is gratefully acknowledged.

References and Notes

(1) Licari, J. J.; Hughes, L. A. *Handbook of Polymer Coating for Electronics*; Noyes Publications: Park Ridge, NJ, 1990; p 114. The relationship of capacitance C with dielectric constant K_s can be expressed as $C = AK_s\varepsilon_o/d$ where A is area, d is distance, and $\varepsilon_o = 8.85418 \times 10^{-14}$ F/cm.

(2) Tummala, R. R.; Keyes, R. W.; Grobman, W. D.; Kapur, S. In *Microelectronics Packaging Handbook*; Tummala, R. R., Rymaszewski, E. J., Eds.; Van Nostrand Reinhold: New York, NY, 1989; p 691.

(3) St. Clair, A. K.; St. Clair, T. L.; Winfree, W. P. *Polym. Mater. Sci. Eng.* **1988**, *59*, 28.

(4) Kane, K. M.; Wells, L. A.; Cassidy, P. E. *High Perform. Polym.* **1991**, *3(3)*, 191.

(5) (a) Hu, H. S.-W.; Griffith, J. R. *Polym. Mater. Sci. Eng.* **1992**, *66*, 261. (b) Hu, H. S.-W.; Griffith, J. R. In *Polymers for Microelectronics*, Willson, G.; Thompson, L. F.; Tagawa, S. Eds., *ACS Symposium Series*, in press.

(6) see Ref. (1), pp 378-379, Table A-13: Dielectric Constants for Polymer Coatings (at 25°C).

(7) Resnick, P. R. *Polym. Prepr.* **1990**, *31(1)*, 312.

(8) Griffith, J. R.; O'Rear, J. G. *Polym. Mater. Sci. Eng.* **1985**, *53*, 766.

(9) Griffith, J. R.; O'Rear, J. G. In *Biomedical and Dental Applications of Polymers*; Gebelein, C. G., Koblitz, F. F., Eds.; Plenum: New York, NY, 1981; pp 373-377.

(10) St. Clair, T. L. In *Polyimides*, Wilson, D., Stenzenberger, H. D., Hergenrother, P. M., Eds.; Blackie: Glasgow, U.K., 1990; pp 58-78. see p 74.

(11) (a) Singh, J. J.; Eftekhari, A.; St. Clare, T. L. *NASA Memorandum* 102625, **1990**. (b) Eftekhari, A.; St. Clare, A. K.; Stoakley, D. M.; Kuppa, S.; Singh, J. J. *Polym. Mater. Sci. Eng.* **1992**, *66*, 279. The calculation was based on the relation: $1/\varepsilon = (1-f)/\varepsilon_o + f/\varepsilon_\infty$ where ε_o is the value of ε for zero free volume fraction which can be obtained from the plot of ε vs f.

(12) Groh, W.; Zimmermann, A. *Macromolecules* **1991**, *24*, 6660.

(13) Dislich, H. *Angew. Chem., Int. Ed. Engl.* **1979**, *18*, 49.

APPENDIX K

PROCESSABLE FLUOROPOLYMERS WITH LOW DIELECTRIC CONSTANTS: PREPARATION AND STRUCTURE-PROPERTY RELATIONSHIPS OF POLYACRYLATES AND POLYMETHACRYLATES

GEO-CENTERS, INC.

PROCESSABLE FLUOROPOLYMERS WITH LOW DIELECTRIC CONSTANTS: PREPARATION AND STRUCTURE-PROPERTY RELATIONSHIPS OF POLYACRYLATES AND POLYMETHACRYLATES

Henry S.-W. Hu, Geo-Centers, Inc., Fort Washington, MD 20744 and James R. Griffith, Naval Research Laboratory, Washington, D.C. 20375

The preparation of a series of processable heavily fluorinated acrylic and methacrylic homo- and co-polymers with low dielectric constants is carried out to elucidate the structure-property relationships. The monomers were prepared through the condensation of the respective alcohols with acryloyl and methacryloyl chloride. Unlike tetrafluoroethylene, these monomers are easy to process into transparent polymers under normal conditions due to their liquid or semisolid nature. All polymers exhibit dielectric constants around 2.06-2.41 with variation within 0.03 over a frequency region of 500 MHz to 18.5 GHz. These values are very close to the minimum known dielectric constants of 2.0-2.08 for Teflon and 1.89-1.93 for Teflon AF. The factors which affect the dielectric constant include the fluorine content, the polymer type and molecular features. Lower dielectric constants are obtained as fluorine contents from polymer backbone or sidechain increase, when acrylate is replaced by methacrylate, when ether linkages are present in the fluorocarbon and when aromatic structure is symmetrically *meta*-substituted.

APPENDIX L

L-PROLINE MODIFIED NYLONS

GEO-CENTERS, INC.

L-PROLINE-MODIFIED-NYLONS: THE FORMATION OF MOLECULAR TURNS FROM INTRAMOLECULAR HYDROGEN BONDING IN A COPOLYAMIDEUREA.

Henry S.-W. Hu, Geo-Centers, Inc., Fort Washington, MD 20744; James R. Campbell and James R. Griffith, Naval Research Laboratory, Washington, DC 20375-5000

The inclusion of L-proline into nylon has the potential for creating resilient polymers with beta bend structure like those existing in the naturally occurring L-proline-rich proteins, such as elastin. In carrying out the multistep preparation of an alternating copolyamide **1** from L-proline and 11-aminoundecanoic acid (Polym. Prepr., 32(1), 543-544 (1991)), the monomer 11-aminoundecanoyl-L-prolyl azide hydrobromide was found to form the alternating copolyamideurea **2** at ambient temperature and without the addition of an amine acid trap. A three-step reaction mechanism involving the emission of nitrogen, followed by a Curtius rearrangement to yield an isocyanato group with subsequent addition of an amino group is proposed. The formation of a six-member-ring "molecular turn", due to the intramolecular hydrogen bonding between urea and amide groups, is characterized by infrared and NMR spectroscopies.

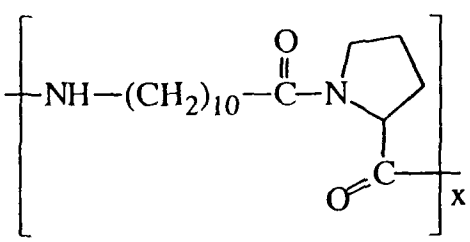

1

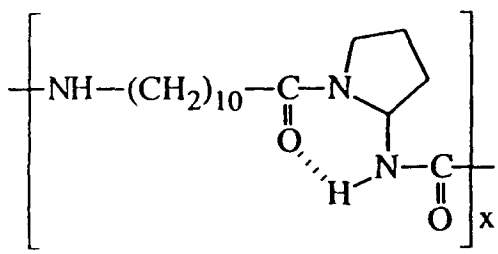

2

APPENDIX M

PHASE TRANSITIONS IN POLYMER BLENDS VIA ^{129}XE NMR SPECTROSCOPY

GEO-CENTERS, INC.

Phase Transitions in Polymer Blends via ^{129}Xe NMR Spectroscopy

J. H. Walton, J. B. Miller*, C. M. Roland
Chemistry Division, Code 6120
Naval Research Laboratory
Washington, D.C. 20375-5342

and

J. B. Nagode
Geo-Centers Inc.
Fort Washington, MD 20744

Abstract

We present ^{129}Xe NMR results on xenon dissolved in a blend of cis -1,4-polyisoprene (Mw = 115,000) and 1,4-polybutadiene (Mw = 23,600). Annealing above the blend's lower critical solution temperature (LCST) induces spinodal decomposition; subsequent quenching yields a metastable phase-separated morphology. The ^{129}Xe NMR lineshape is used to follow the mutual interdiffusion of the two constituent polymers as the system returns to a homogeneous structure. The domain size induced by the heating is measured and a polymer diffusion coefficient extracted from the NMR experiment. This work demonstrates the feasibility of using ^{129}Xe NMR for studying the phase behavior and dissolution kinetics of binary blends. For the materials studied herein, ^{129}Xe NMR was found to be a significantly higher resolution probe of the blend morphology than DSC.

Introduction

Recently ^{129}Xe NMR has been used to study polymer blends [1,2]. The inertness of xenon and the dependence of its chemical shift on local environment make it an attractive probe of morphology. It is particularly advantageous for blends whose components have nearly identical glass transition temperatures, which are difficult to study with conventional

techniques [2]. For a phase-separated, two-component blend, the ^{129}Xe NMR spectrum will exhibit two resonances, whereas the homogeneous morphology of a miscible blend results in a single NMR peak. In this work ^{129}Xe NMR is applied to mixtures of polyisoprene (PIP) and polybutadiene (PBD), which have been studied extensively in this laboratory [3-6] and elsewhere [7-10]. When the polybutadiene has a vinyl content of less than about 75%, mixtures with 1,4-polyisoprene exhibit a lower critical solution temperature (LCST), which has been attributed to equation of state effects [3] or to the copolymer effect [10]. By selecting components of the appr ·ate molecular weights, the phase transition can be made to occur at readily accessible temperatures, allowing study of the kinetics of phase separation or component dissolution.

Experimental

The blend was comprised of 34% by volume of 1,4-polyisoprene and 66% polybutadiene (8% vinyl content), mixed by dissolution in cyclohexane followed by vacuum drying. The PIP and PBD, from Scientific Polymer Products, had weight average molecular weights equal to 115,000 and 23,000 respectively (polydispersities < 1.1).

NMR samples were sealed in a xenon atmosphere (details given elsewhere [2]) for measurement at the ^{129}Xe frequency of 83 MHz. Free Induction Decays (FIDs) were generated with a 30 degree pulse and a high repetition rate. A mild exponential filter was applied to the FIDs prior to Fourier transformation. The reported chemical shifts are relative to gas at 0.5 atm. and are precise to +/- 0.2 ppm. All spectra were obtained at room temperature (<LCST), since at higher temperatures the decreased solubility of xenon in

these polymers resulted in weak signal intensities.

A Perkin-Elmer DSC-2 was used for calorimetry. Specimens 5-7 mg in weight were heated at 320°C/min to 100°C; after a 30 min dwell time, they were quenched at >200°C/min. The heat capacity was then measured in the conventional manner by cooling to -125°C, followed by heating back to room temperature. The scan rate was 20°C/min, with the data measured during the heating cycle.

Results and Discussion

In order for ^{129}Xe NMR to be applied to a given blend, the chemical shift must be different for xenon dissolved in the pure components. In Fig. 1 is shown the ^{129}Xe NMR spectrum obtained for pure PIP and PBD, simultaneously in the sample chamber but physically separated. Two resonances are seen with a separation of 8 ppm. The spectrum of the mixed polymers, prepared by solution blending or annealed at room temperature for several weeks, reveals a single peak indicative of a homogeneous phase morphology. (Fast diffusional exchange of the xenon between small phase-separated domains was ruled out using the technique described in ref. 2.) This result agrees with the known miscibility of the blend under these conditions [3]. When the sample is heated to 100°C for 30 min, followed by quenching to room temperature, splitting of the resonance is observed. This clearly demonstrates that phase separation has occurred, consistent with the previously reported LCST = 70°C for this mixture [3]. As the sample is maintained at room temperature (< LCST), the splitting of the resonance and its breadth is reduced over time, reflecting redissolution of the components.

In Fig. 2 are shown the DSC results obtained on the same blend subjected to an equivalent thermal history. While the phase separation effected by heating to 100°C causes a smearing out of the thermal transition, this evidence of a phase separated structure is not as distinguishing as the xenon NMR spectrum. Moreover, after only 45 min annealing at room temperature, distinct indication of a multi-phase structure is gone; the DSC thermogram has nearly assumed the appearance seen for the original homogeneous sample. Notwithstanding the persistence of a phase separated structure as directly evidenced by the NMR data in Fig. 1, the DSC measurement no longer senses the presence of distinct phases. At least for this particular blend, the xenon NMR experiment provides a higher resolution probe of phase morphology than the more conventional DSC technique.

The detailed relationship between the phase morphology and the NMR spectrum is described by theories for chemically exchanging systems [11,12]. In the slow exchange limit (whereby a xenon atom remains in a particular domain for a time long on the NMR time scale), the observed chemical shifts will be exactly equal to the chemical shifts of xenon in the respective pure environments. This is the situation prevailing in previous studies of blends lying well within the two-phase region of the phase diagram [1,2]. However, xenon diffuses rapidly between smaller domains, reducing the separation of the respective NMR resonances as given by

$$\delta\omega = \delta\omega_{\infty}\sqrt{1 - \frac{2}{\tau^2(\delta\omega_{\infty})^2}} \qquad (1)$$

where τ is one half the average time the xenon atom resides in a given domain and $\delta\omega_{\infty}$ is the frequency difference between the sites when there is no exchange. This relation

explicitly assumes $\delta\omega_\infty$ is much larger than the linewidth of the individual resonances and the xenon populations in the two domains are equal, with the xenon spending equal time in each domain. As seen in Fig. 1, for these polymers $\delta\omega_\infty$ is about six times the natural linewidths, so that the first assumption is valid. Although the polybutadiene is present in approximately twofold excess, the xenon populations in the two polymers are nearly equal, as determined by the relative integrated intensities of the two peaks at the top of Fig. 1; thus, the second assumption is also valid. The third assumption is valid because the rapid diffusion of xenon between the two domains and the slow change in composition of the domains maintains an equilibrium with respect to the two xenon populations.

The exchange mechanism for xenon in polymers is fickian diffusion. In three dimensions the root mean square distance a xenon atom travels in a time period t is given by

$$X_{RMS}=(6Dt)^{1/2} \tag{2}$$

where D represents the xenon diffusion coefficient in the polymer. Identifying t as 2τ and combining eqs. 1 and 2, an average domain size is calculated to equal

$$X_{RMS}=\left[\frac{288D^2}{(\delta\omega_\infty)^2-(\delta\omega)^2}\right]^{1/4} \tag{3}$$

In the fast exchange limit there is no splitting, while in the slow exchange limit the splitting approaches its maximum and is insensitive to domain size. Since the diffusion coefficient of xenon is temperature dependent, when either limiting condition prevails, experiments can be conducted at another temperature in order that the intermediate exchange regime is attained.

It is tempting to suggest that equation 3 allows the measurement of domain size as a

function of time. However, this implies the unphysical situation that the domains of the two phases are simply getting smaller. In fact the two polymers are recombining by interdiffusion, creating a concentration gradient between the phase separated domains [13]. Thus, there is a smooth variation in the polymer composition as a function of distance, with the densities evolving continuously in time. This time dependent density variation makes proper mathematical treatment of the ^{129}Xe NMR lineshape as a function of time extremely difficult. Since the xenon chemical shift is sensitive to its local environment, knowledge of the average local environment during the course of the xenon diffusion would be required. Furthermore, the average local environment (morphology) in a blend is not the average of the environments of the two pure components due to concentration fluctuations [14,15] and, for example, non-zero excess mixing volumes [1,3]. Nonetheless, if the polymer blend remains above the LCST long enough for substantial phase separation to occur, initially a two phase model is appropriate.

We assume complete phase separation into the pure polymer components as the initial condition. From the chemical shifts of the two peaks in the xenon spectrum a value of X_{RMS} can be obtained. Using the appropriate values in eq. 3 ($D = 1.4X10^{-7}$ cm^2/s in polyisoprene; $\delta\omega = 2100$ rad/s; $\delta\omega_\infty = 4200$ rad/s), an initial average polyisoprene domain size produced by the annealing at T>LCST is calculated to be on the order of 0.3 μm. This is sufficiently large that distinct glass transitions can be resolved using DSC [16-18], as was observed herein. The polymers then interdiffuse. When the polymer composition within a defining (?) volume, whose diameter is given by the distance over which xenon can diffuse on the time scale of the experiment, is the same for all defining (?) volumes within the sample, the

NMR spectrum will exhibit one line.

The time required for a single resonance to appear in the NMR spectrum is in a convoluted way related to the diffusion constants of the polymers. As has been addressed in studies of the rate at which adhesion develops via interdiffusion across an interface, this is a complicated problem [19-23]. If we assume that the time required for collapse of the NMR lines, 60 hours, is roughly the time required for diffusion over approximately 0.3 μm, from eq. 2 a value for an average polymer diffusion coefficient of $\approx 5X10^{-15}$ cm^2/sec is obtained. This certainly represents an lower bound, since the 60 hours is a measure of the time for homogenization of the morphology, not simply polymer translation. Note also that if the assumptions that the blend phase separates into the pure polymer components and that phase separation was complete after heating above the LCST are incorrect, the estimate of X_{RMS} will be too low. This would also lead to underestimation of the diffusion constant of the polymers.

Conclusions

For the polyisoprene/polybutadiene blend studied herein, the resolution advantage of ^{129}Xe NMR over a more conventional method such as DSC for probing blend morphologies has been demonstrated. The time scale over which the ^{129}Xe NMR can distinguish separate domains is remarkably longer than by DSC. The relative insensitivity of DSC is due, in part, to the difficulty in detecting changes in slope in the DCS curves (as opposed to peak separation in the NMR) and, in the present case, the relatively small differences in T_g of the two polymers (app. 30 K). In general, the relative merits of xenon NMR spectroscopy will

vary according to the magnitude of $\delta\omega_\infty$ and the diffusion coefficient of xenon in the particular system of interest. However, the latter quantity is not expected to vary greatly among polymers, and recent measurements in our laboratory reveal a wide range of values for the chemical shift for xenon dissolved in various polymers [24]. This indicates that $\delta\omega_\infty$ will be large for many blend systems, suggesting that ^{129}Xe NMR can be usefully applied.

Herein we have used xenon NMR to follow, at least in a qualitative fashion, the kinetics of phase redissolution following a temperature jump. A previous study [2] demonstrated how upper bounds on domain sizes can be extracted from xenon NMR data when the system is in the slow exchange limit; i.e., the lifetime of a xenon atom in a particular domain is long on the NMR time scale. Although domain sizes can also be determined from 2-D NMR experiments [25] when the domain sizes are static, the method is difficult to employ when domain sizes are changing over time.

Acknowledgements

J. H. W. thanks the National Research Council and the Naval Research Laboratory for an NRC/NRL postdoctoral associateship. This work was partially supported by the Office of Naval Research.

References

1. S.K. Brownstein, J.E.L. Roovers, and D.J. Worsfold, *Magn. Reson. Chem.* 26, 392 (1988).

2. Walton, J. H.; Miller, J. B.; Roland, C. M. *J. Poly. Sci. Part B: Poly. Phys.* 30, 527

(1992).

3. Trask, C. A.; Roland, C. M. *Poly. Comm.* 29, 332 (1988).

4. Roland, C. M.; Trask, C. A., in *Advances in Polymer Blends and Alloys Technology* M. A. Kohudic, K. Finlayson, Eds. (Technomic Publ., 1989), pg. 100.

5. Roland, C. M. *Rub. Chem. Tech.* 62, 456 (1989).

6. Tomlin, D.W.; Roland, C.M. *Macromol*, 25, 2994 (1992).

7. Bartenev, G.M.; Kongarov, G.S. *Rub. Chem. Tech.* 36, 668 (1963).

8. Cohen, R.E. *Adv. Chem. Series* 193, 489 (1982).

9. Kawahara, S.; Akiyama, S. Ueda, A. *Polymer J.* 21, 221 (1989).

10. Sakurai, S.; Jinnai, H.; Hasegawa, H.; Hashimoto, T.; Han, C.C. *Macromol.* 24, 4839 (1991).

11. Gutowsky, H. S.; Holm, C. *J. Chem. Phys.* 25, 1228 (1956).

12. Pople, J. A.; Schneider, W. G.; Bernstein, H. J., *High Resolution Nuclear Magnetic Resonance* (McGraw-Hill, New York, 1959).

13. Hashimoto, T.; Tsukahara, Y.; Kawai, H. *Macromol.* 14, 708 (1981).

14. Roland, C.M.; Ngai, K.L. *Macromol.* 24, 2261 (1991).

15. Roland, C.M.; Ngai, K.L. *J. Rheology* 36, 1691 (1992).

16. Kaplan, D.S. *J. Appl. Poly. Sci.* 20, 2615 (1976).

17. Braun,H.G.; Rehage, G. *Angew. Macromol. Chem.* 131, 107 (1985).

18. Roland, C.M. *Rub. Chem. Tech.* 62, 456 (1989).

19. Skewis, J.D. *Rub. Chem. Tech.* 39, 217 (1966).

20. Kramer, E.J.; Green, P.F. *Polymer* 25, 473 (1984).

21. Green, P.F.; Doyle, B.L. *Phys. Rev. Lett.* 57, 2407 (1986).

22. Roland, C.M. *Macromol.* 20, 2557 (1987).

23. Roland, C.M.; Nagode, J.B. *Polymer* 32, 505 (1991).

24. Miller, J. B.; Walton, J. H.; Roland, C. M. *Macromol.*, submitted.

25. Ernst, R. R.; Bodenhausen, G.; Wokaun, A., *Principles of Nuclear Magnetic Resonance in One and Two Dimensions* (Clarendon, Oxford, 1987).

FIGURE CAPTIONS

Figure 1. ^{129}Xe NMR spectra of xenon dissolved in the miscible blend (bottom), at various times after phase separation by heating, and corresponding to complete phase separation (top). The latter was actually obtained by placing physically distinct pieces of the respective pure polymers in the NMR tube. Redissolution of the components is not complete even after 64 hours.

Figure 2. DSC results for the blend annealed at room temperature for the indicated time periods subsequent to a 30 min period at 100°C. The latter is above the LCST and thus gives rise to a phase-separated morphology. The redissolution of the components is reflected in the DSC data; however, after just 45 min annealing the thermogram suggests homogeneity, notwithstanding the NMR data in Fig. 1.

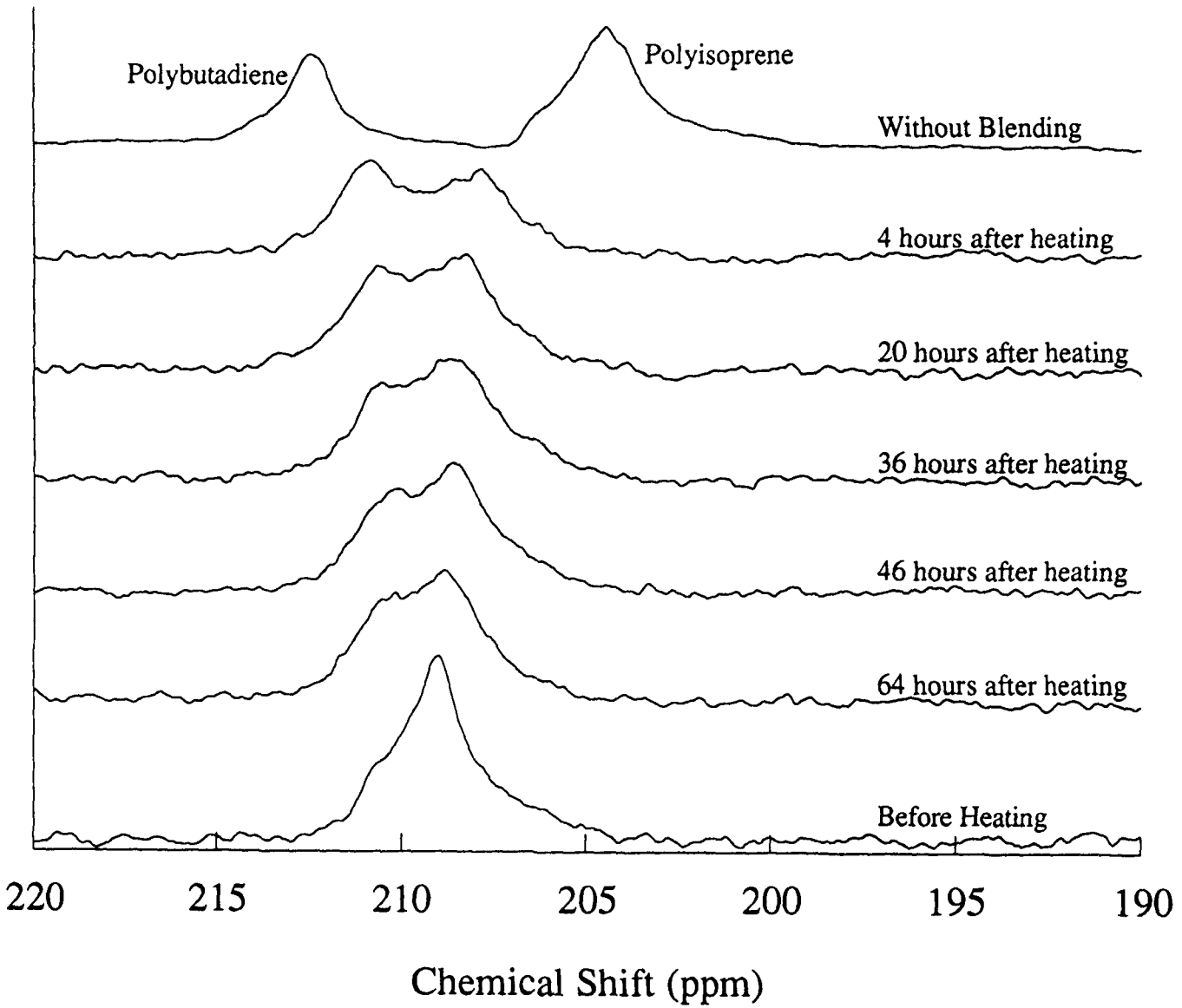
Polybutadiene
Polyisoprene
Without Blending
4 hours after heating
20 hours after heating
36 hours after heating
46 hours after heating
64 hours after heating
Before Heating
220
215
210
205
200
195
190
Chemical Shift (ppm)

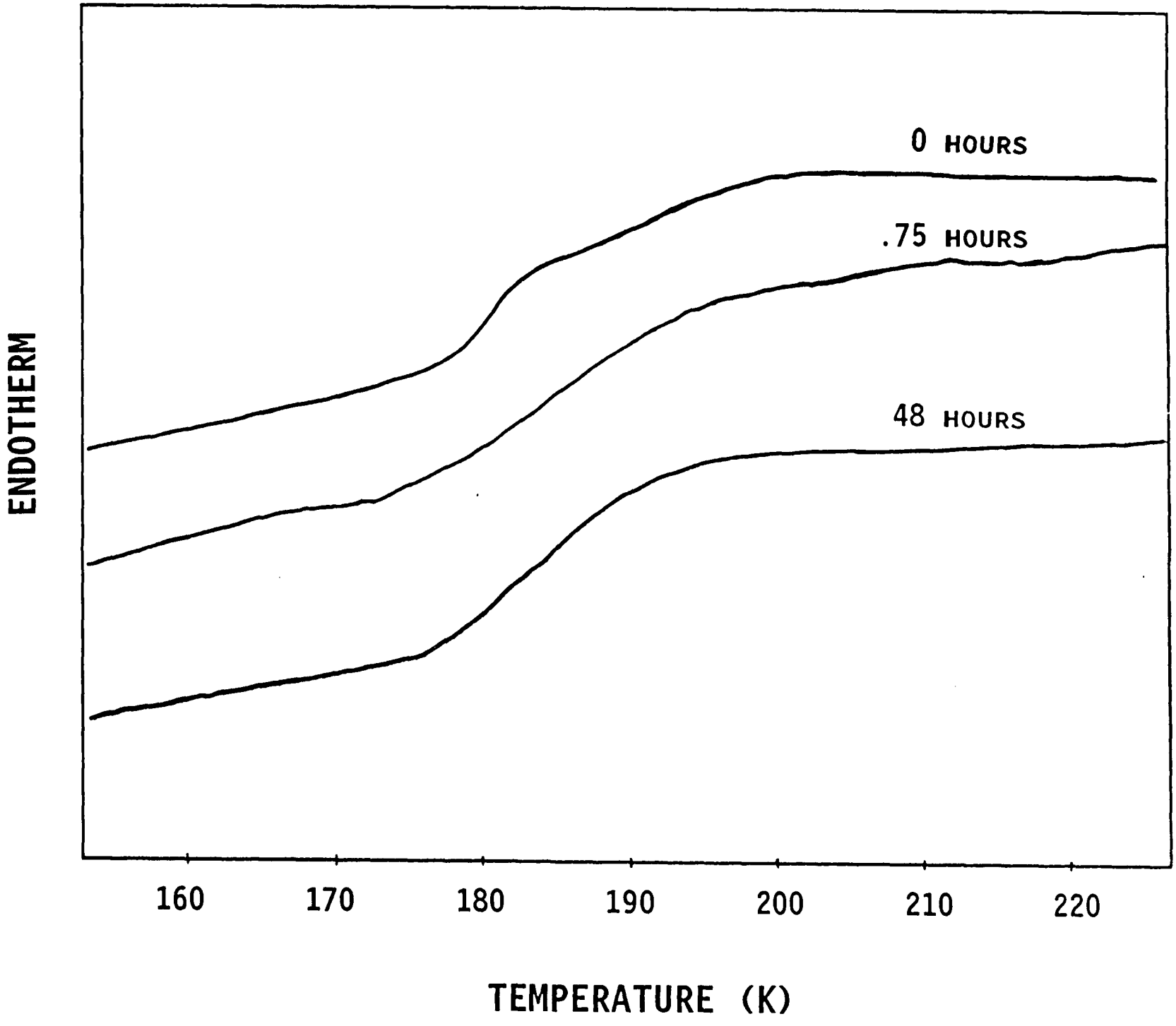
0 HOURS
.75 HOURS
48 HOURS
ENDOTHERM
160
170
180
190
200
210
220
TEMPERATURE (K)

APPENDIX N

BIODEGRADABLE PACKAGING MATERIALS

GEO-CENTERS, INC.

INTERIM PROGRESS REPORT

on

Starch Based Biodegradable Packaging Materials:

Compatibilized Blends/Alloys
Characterization Processing
Physical Properties

Prepared For

Biodegradable Packaging Program
The Biotechnology Division
Soldier Science Directorate

U.S. Army Natick RD&E Center
Natick, MA 01760

Prepared By

Stanley Bedell
Elizabeth Welsh
Paul Dell
Renay Pollier
GEO-CENTERS, INC.
Newton Centre, MA 02159

MARCH 1993

GEO-CENTERS, INC.

TABLE OF CONTENTS

Introduction 1

Biodegradable Program 1

Expectations 2

Equipment 3

- Brabender Extrusion Unit
- CSI-Max Mixing Extruder
- Mini-Max Injection Molder

Project Plan 10

Project Process 12

- CSI-Max Mixing Extruder
- Experimental Mixes
- Differential Scanning Calorimetry (DSC)
- Fusion
- Water
- Twin Screw Extruder

Injection Molded Biodegradable Materials 20

- Study of Physical Properties as a Function of Water Content
- Starch Blend Rheology Study

Conclusions and Future Plans 24

- Extrusion Work
- Future Investigation of Physical Properties as a Function of Water Content
- Future Investigation of Starch Blend Rheology

References 27

LIST OF TABLES

1. Qualitative Comparisons of Various Compositions and Water Percentages 15

2. Comparison of Old and New Formulations 17

3. Formulations Processed on Twin Screw Extruder Using Ribbon Die 18

4. Mechanical Property Data on Polymer Tapes 19

5. Weight Gain Due to Water Sensitivity 19

LIST OF FIGURES

1. Standard Extruder Dies 4
2. Twin Screw Extruder Using a Blown Film Die 5
3. Twin Screw Extruder Using a Vertical Ribbon Die 6
4. Schematic of the CSI-Max Mixing Extruder 7
5. Schematic of the CSI-Max Extruder Ribbon Die 8
6. Schematic of the CSI-Max Mini-Max Injection Molder 9
7. Tensile Properties of Novamont Resins 21
8. Tensile Properties of In-House Blends 23

INTRODUCTION

The signing of the MARPOL Treaty brought a great deal of attention to the problem of plastic waste disposal in the Armed Services. The Navy's interest is acute, due to the impending constraints which will be placed on sea disposal when the treaty is implemented after 1993. Packaging materials, just as they do in the civilian world, constitute a large proportion of such waste. The development of packaging materials which are biodegradable in the sea, as well as, on the land would go a long way toward satisfying this Treaty's requirements. The economic potential of such a development is obvious and there are a number of large companies (Warner-Lambert, Novamont, ICI) actively engaged in this endeavor.

The materials which are currently available and for the most part, may not have been developed for packaging applications, are blends of starch with other polymers. These blends, both commercially available and proprietary, generally contain 50% starch by weight and usually biodegrade to the extent that they contain this starch. In addition, they may also suffer from property instability and lack adequate water resistance. Such shortcomings represent serious limitations for a packaging material. Since packaging represents a large volume application, the economics of the material is important and must be competitive with conventional packaging materials.

The technology of making polymer blends and alloys has been developed to a high degree. The enhanced physical properties of such materials, which often result, have been utilized in many polymer applications. It is the intention of this program to utilize this basic technological approach to meet the goals which have been set forth.

BIODEGRADABLE PROGRAM

The Biodegradable Packaging Program involves a joint effort between the Soldier Science Directorate (SSD), the Food Engineering Directorate (FED), the Individual Protection Directorate (IPD), and outside contracting for special services. This report is concerned with the research being conducted within SSD and more specifically what contributions GEO-CENTERS, INC. has made to it.

Several people within SSD are directly involved with the study of starch-based biodegradable materials. There is a Cooperative Research and Development Agreement (CRDA) between the U.S. Army Natick Research, Development and Engineering Center and Glenn Elion, owner of International Communications & Energy (IC&E). Jean Mayer (Natick) and Glenn Elion (IC&E) work together in testing various kinds and amounts of biodegradable polymers, fillers and plasticizers to give a biodegradable formulation to produce blown film.

Peter Stenhouse (Natick) is also involved with the biodegradable materials. Some of his work involves the extrusion of the material, as well as, the actual testing of blown film or tape materials for their thermal properties. He is currently working on a joint project involving his work at Natick and work being done at the Warner-Lambert Company.

Stanley Bedell (GEO-CENTERS, INC. principal investigator) is working to incorporate the use of shellac into starch-based biodegradable formulations. Elizabeth Welsh (GEO-CENTERS, INC.) has been doing extrusion work involving the unknown formulations that Natick and Natick/IC&E are processing to produce blown film. Paul Dell's (GEO-CENTERS, INC.) work involves studying the physical and thermal properties of the starch blends and Renay Pollier (GEO-CENTERS, INC.) is involved in data entry and secretarial support.

The materials used in the biodegradable formulations, such as corn starch, synthetic polymers, nucleating agents, water, plasticizers, and other additives are mixed together without prior processing. It is possible to produce starch-based blown film by first gelatinizing or destructuring the starch, but the current method being used does not require these steps to be done.[6] They are then fed into a Twin Screw Mixer (TSM) Extrusion Unit with either a blown film or ribbon die attached. The use of the ribbon die enables the degree of fusion (melting of the polymers by heat) which has taken place within the resulting tape to be studied. It can also show any nondispersed materials which might still be in the processed tape. For the majority of biodegradable materials processed, however, the blown film die is used to produce blown film.

From October to the present, there has been approximately one hundred (100) biodegradable formulations run on the twin screw extruder in an attempt to produce blown film or make a tape from the ribbon die.

EXPECTATIONS

This paper is expected to address some of the shortcomings which starch-based materials currently possess as they relate to this packaging application. To do so, it will examine the usefulness of potential compatibilizers, modifiers, and other related polymers in starch-based polymer systems. It will examine means of enhancing the hydrophobicity of starch blends without unduly compromising its biodegradability. Furthermore, it will elucidate the role of water and the water-to-glycerine (plasticizer) relationship, so as to better control water up-take and water loss.

These efforts are directed toward developing a packaging material which is 100% biodegradable and which can meet the service requirements of such materials while, at the same time, exhibiting a certain level of economic competitiveness.

EQUIPMENT

Brabender Extrusion Unit

The formulations were processed on a Brabender 42 mm counter-rotating (towards each other) Twin Screw Mixer (TSM) fitted with either a blown film die (2.54 cm I.D. with a 0.05 cm gap) or a vertical ribbon die (2 inch width with a 0.020 inch gap)(See Figure 1). The extrusion system contained three (3) heated zones located on the twin screw barrel area (referred to as Zone 1, 2, and 3) and a fourth heated zone (Zone 4) at the die. The formulations were manually fed into the extruder. Zone temperatures and the extruder speed were adjusted to give a smooth melted material coming out the blown film or ribbon die. When using the blown film die, the blown bubble was taken up through rollers while internal and external air was used to blow and cool the film.[3] As material exited the ribbon die, the ribbon was fed through squeeze rolls to keep the material flat and prevent curling of the edges (See Figures 2 and 3).

CSI-Max Mixing Extruder

The CSI-Max Mixing Extruder is a laboratory bench top Model CS-194AV fitted with a 5 inch conventional single screw. The equipment was initially modified with this type of screw because the existing screw did not meet the needed requirements for processing the type of material which was to be used. This new single screw was made to give more mixing action to the material and be able to move the material down the barrel of the screw. Once work was started using this screw, it was then modified to change the flight depth and flight edges to improve its feeding characteristics. The unit contained two (2) heated zones located on the single screw barrel area with two separate temperature controllers, each zone had its own heater switch for the rotor and the header (die) areas, it had a variable speed rotor control used for mixing the polymer melt, and a ribbon die 3/4 inches wide with a gap setting of 0.020 inches (See Figures 4 and 5).

Mini-Max Injection Molder

To make samples for tensile testing or for degradation studies, formulations were processed on the Mini-Max Injection Molder, Model CS-183 MMV using a 4 cubic centimeter (cc) capacity cup. The unit contained a temperature controller, a variable speed rotor control, used for mixing the polymer melt, an open/shut valve, and a mold clamping device (See Figure 6). Once the polymer material had been in the cup long enough to sufficiently melt and mix the polymer material, it could be injected into the desired mold shape:

standard extruder dies

RIBBON DIE

For evaluation of quality of fusion and presence of "fish eyes", non-dispersed ingredients and contaminants.

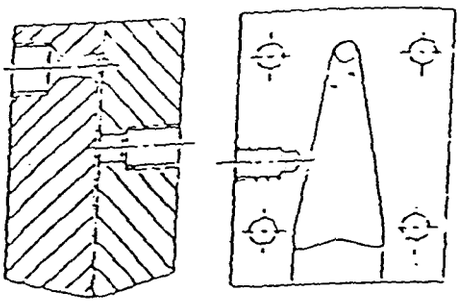

VERTICAL

CENTERING VERTICAL BLOWN FILM

For extrusion and study of blown films.

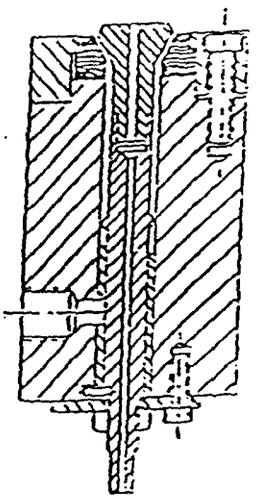

C.W. Brabender®
INSTRUMENTS, INC.
50 East Wesley Street / P.O. Box 2127 / South Hackensack, New Jersey 07606
Telephone (201) 343-8425 / Telex: 13-4466 / Facsimile-Telefax #201-343-0628

FIGURE 1. STANDARD EXTRUDER DIES

GEO-CENTERS, INC

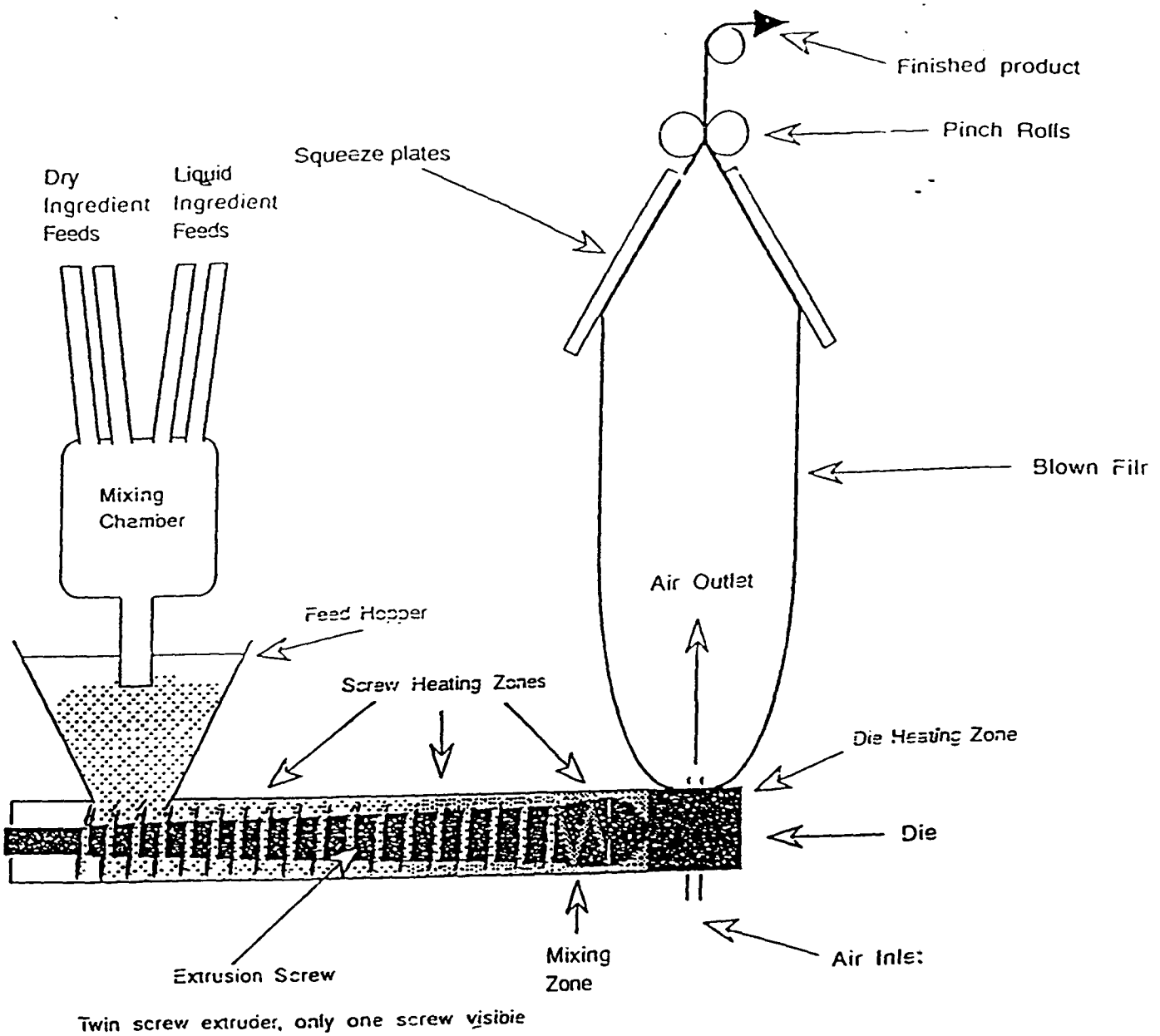

FIGURE 2. TWIN SCREW EXTRUDER USING A BLOWN FILM DIE

GEO-CENTERS, INC

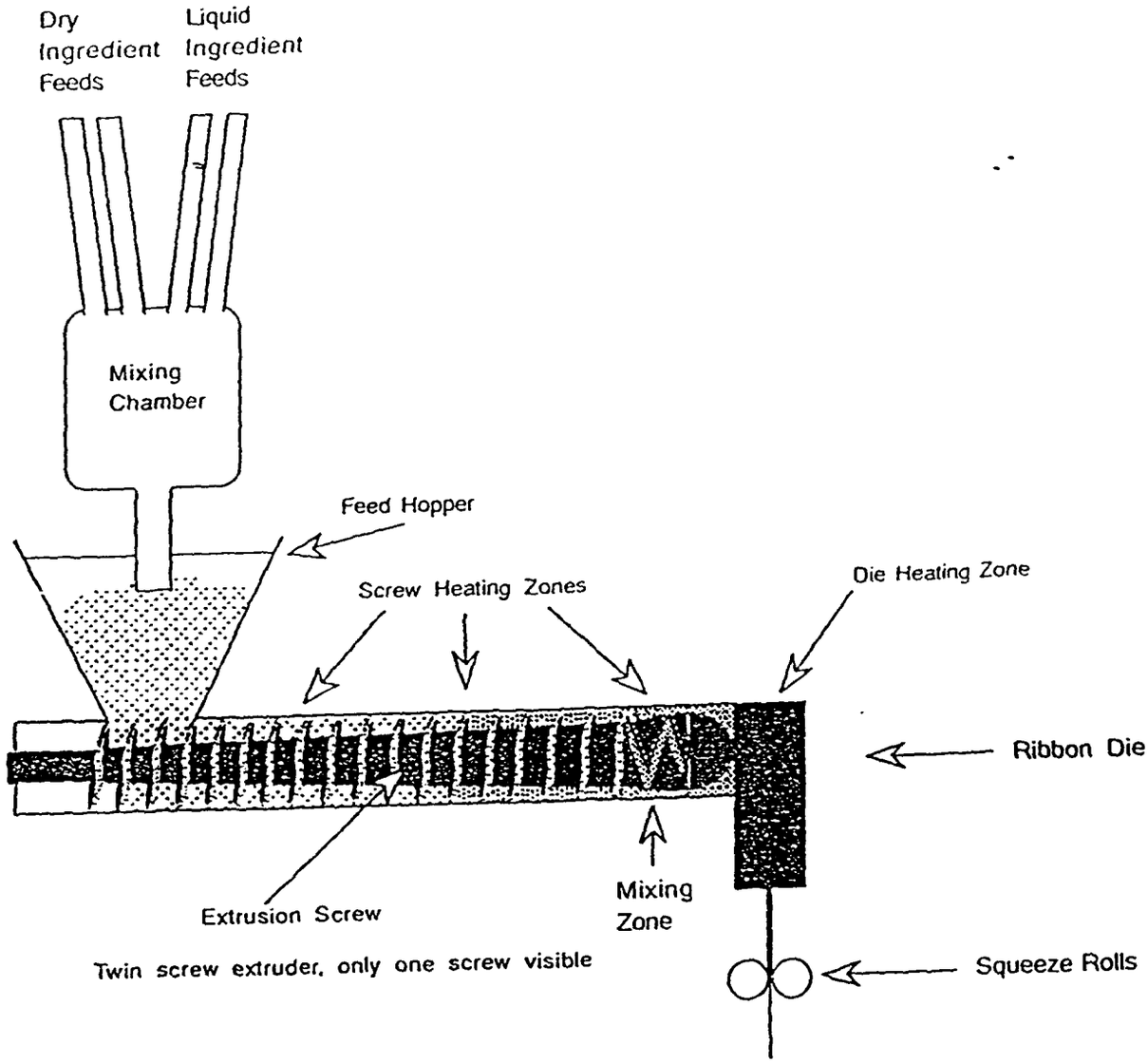

FIGURE 3. TWIN SCREW EXTRUDER USING A VERTICAL RIBBON DIE

GEO-CENTERS, INC.

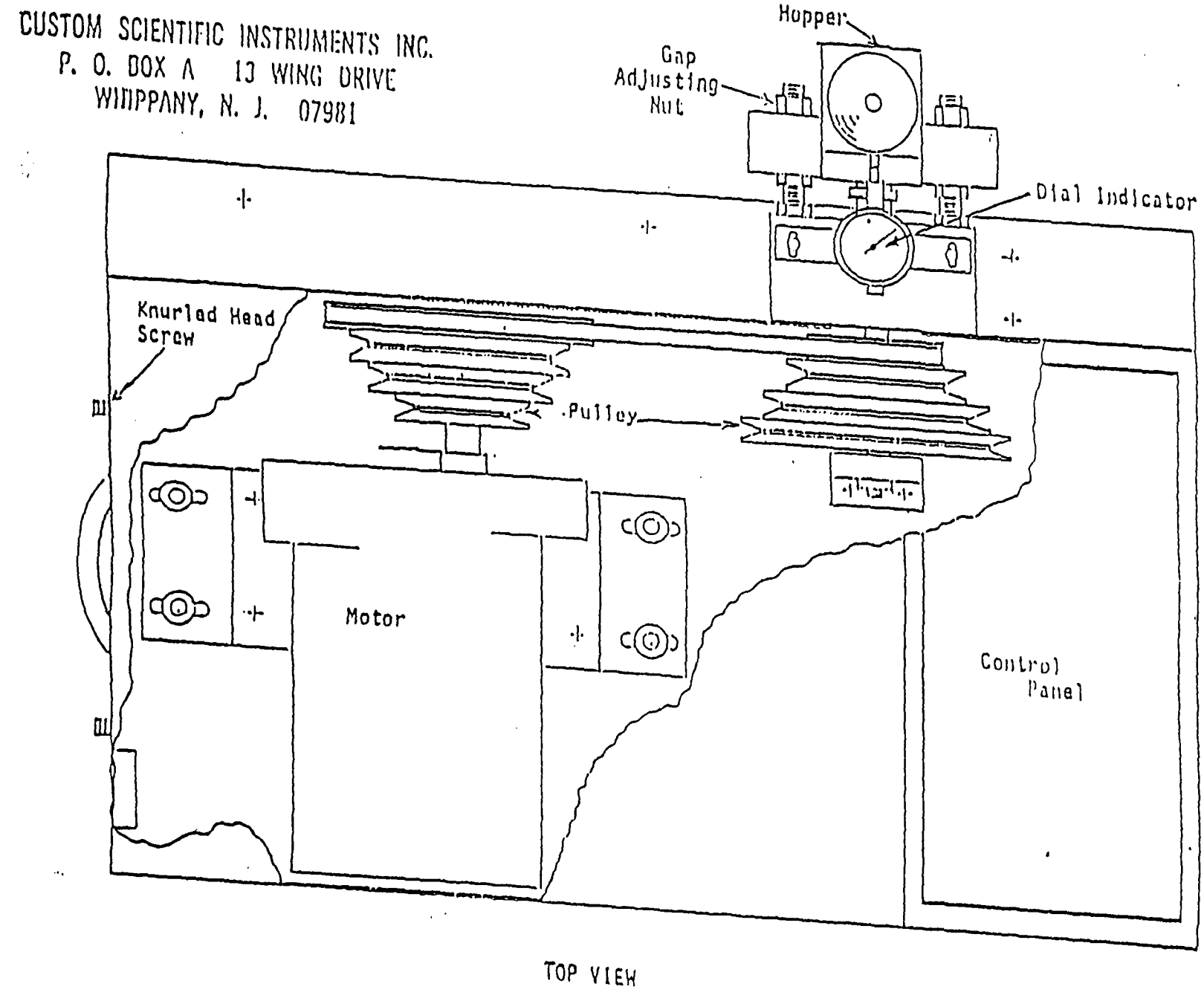

FIGURE 4. SCHEMATIC OF THE CSI-MAX MIXING EXTRUDER

CUSTOM SCIENTIFIC INSTRUMENTS INC.
P. O. BOX A 13 WING DRIVE
WHIPPANY, N. J. 07981

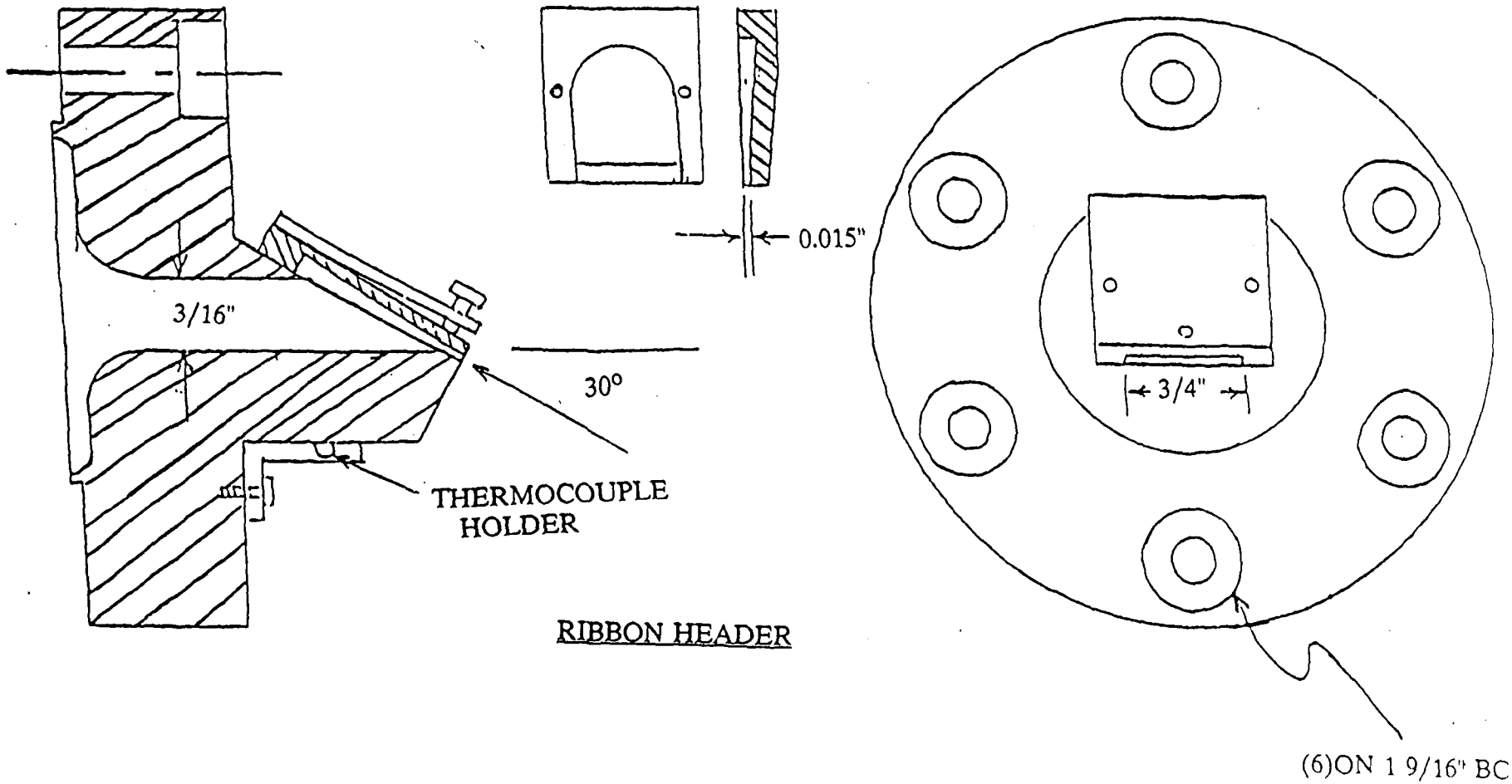

FIGURE 5. SCHEMATIC OF THE CSI-MAX EXTRUDER RIBBON DIE

FIGURE 6. SCHEMATIC OF THE CSI-MAX MINI-MAX INJECTION MOLDER

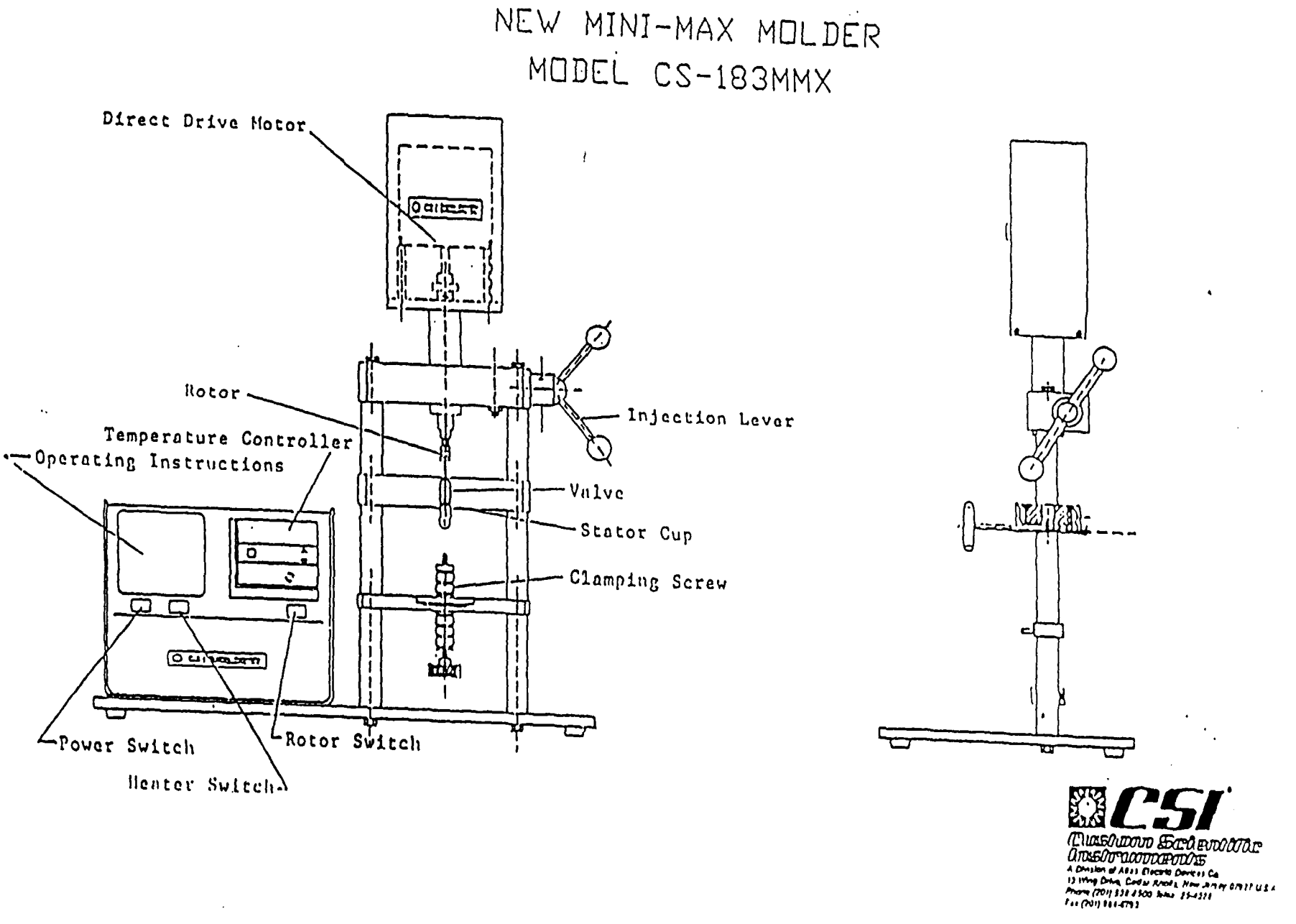

rectangular 1/16" thick x 1/2"W x 2 3/4"L
(used for degradation studies)

dog-bone ASTM D-1708, 1/8" thick 1.0" Total Length
(used for tensile and elongation studies)

PROJECT PLAN

An enhancement of physical properties over those of the constituent polymer components often result when either the miscibility of the components is improved or in the case where the components remain immiscible, the dispersed phase dimensions are reduced and the adhesion between the phases is improved.

The effect of compatibilizers on the properties of a blend of starch and ethylene-vinyl alcohol copolymer will be examined first by direct addition of such species of well-defined structure to the blend and second by generation of such materials "in situ" via a grafting mechanism (reactive processing).

The goals that have been set in terms of the level of biodegradability and cost, places the ultimate focus on substantially increasing the level of the starch in the composite. Initially, the impact of such additives will be examined on a 50/50 starch/EVOH blend, since a lot of information on this composition is already available and its characteristics and shortcomings have been well-defined.

In addition to compatibilizers, which are often effective at the 1-2% weight level, a second type of additive, known as a modifier, will also be examined. These materials can be copolymers which contain a rubbery component and an interactive one. In such cases compatibilization, as well as toughening, may occur. Modifiers are more apt to be useful in the 20-40% by weight range and could include a number of alternative plasticizers. Long chain aliphatic mono-glycerides or sorbitans, although not polymeric, might be useful in this regard.

In addition to the functional additives described, a number of other variables will be examined and their impact on process and performance characteristics assessed. The effect of water content and fusion temperature on the water resistance of the processed blend will be determined.

The amylose content of the starch, as well as, the ethylene content and melt index of the ethylene-vinyl alcohol copolymer are variables which also need to be given consideration. The amylopectin content, which is the semicrystalline starch component,

will have a significant impact on the crystallizability of the starch phase and hence, its tendency to retrograde. It's likely to have a beneficial impact, though, on water resistance. The EVOH copolymers contain all the elements of the modifiers previously described (i.e., rubbery component as ethylene and an interactive component as polyvinyl alcohol). Since the rate at which the thermodynamic equilibrium can be achieved depends on the driving thermodynamic force, which is the polymer-polymer interaction coefficient and the resisting rheological forces, such as the ability of the polymer to diffuse (diffusivity), the viscosities of the polymeric components are relative. As a result, lower viscosity grades of EVOH (higher ethylene concentration and higher melt index values) could be helpful in achieving this equilibrium. Similarly, lowering the starch phase viscosity might also be desirable.

Finally, the factors which influence the extent of gelatinization during processing and the effect of this destructuring on properties and on the stability of those properties over time will also be investigated.

The program, as outlined, is an ambitious one and one which could involve a great many experimental trials. It was initially planned to use the available CSI-Max Mixing Extruder, which had been fitted with a 5-inch conventional single screw to evaluate the compatibilizers and modifiers and to examine the other variables which were of interest. This laboratory instrument offered the advantages of easy access and would have relatively small material requirements. A large number of experiments could be carried out in a timely manner and with the use of the ribbon die, tapes could be obtained on which meaningful measurements could be made. Selected compositions would then be run on a twin screw extruder located in the Fiber Plant (IPD) to produce either blown film or tapes.

Mechanical properties, such as tensile strength and percent elongation, would be measured and polymers characterized by thermal (Differential Scanning Calorimetry (DSC)) and thermo mechanical (low frequency storage modulus) techniques. The Morphology of processed blends would be examined by Scanning Electron Microscopy (SEM) and/or Scanning Tunneling Electron Microscopy (TEM) optical techniques.

The question then arises as to what type of polymers might be effective as compatibilizers for this system. A literature search turned up a number of clues. Maxwell[1,2] found that an ethylene acrylic acid copolymer, containing 20% by weight acrylic acid, gave transparent cast films with starch and polyvinyl alcohol. Otey, Westhoff, and Doanne[4,5] also reported similar results with starch. This evidence of miscibility suggests that polymers containing groups like carboxyl, which are capable of interacting (hydrogen bond) with starch and/or polyvinyl alcohol, would be good candidates as compatibilizers for the subject polymer blend. A number of copolymers, containing

carboxyl groups, are commercially available. Some, like styrene maleic anhydride or maleic acid are hydrophobic enough to have an effect on the water resistance of the blend as well. Ethylene maleic acid or anhydride and methylvinyl ether maleic acid or anhydride polymers would also be worth evaluating. However, since such materials are not likely to be biodegradable they would be considered as secondary candidates.

Jean Mayer has been interested in looking at shellac as an additive, with such blends, for some time. Its water insolubility and biodegradability make it a very attractive candidate in this application. It does contain acid functionality, which could confer compatibilizing characteristics. Its low molecular weight (1,000), however, may compromise its efficiency as a compatibilizer. On the other hand, a low molecular weight immiscible "compatibilizer" can act as an adhesive for a pair of mutually immiscible polymers and so enhance compatibility.

Since the compatibility of such carboxyl, containing polymers with both starch and polyvinyl alcohol, have been found to be improved, significantly, by the presence of ammonia (a fugitive base), our evaluation of shellac will be carried out with and without ammonia.

Since ammonia is also an effective accelerator for the polymerization of shellac, it might result in some polymerization of the shellac during processing. Polymerization could result in an increase in water resistance, toughness, and better compatibilization. Attempts will be made to utilize this potential polymerizability.

The early experiments will involve hand blending of the dry ingredients, the addition of these solids to the mixed liquids, and then hand mixing the blend. Whether or not this will result in the degree of dispersion and uniformity that is necessary for the efficient action of the compatibilizer will remain to be seen. Some type of efficient mixing, particularly when using a compatibilizer, may be necessary prior to processing. This may be particularly true in the presence of ammonia, since some dissolution and swelling of the shellac particles takes place.

PROJECT PROGRESS

CSI-Max Mixing Extruder

It soon became clear that the available 5-inch laboratory screw would have limited utility. Even after the modification of the flight depth and flight edges improved its feeding characteristics, the screw still exhibited some serious disadvantages. Short residence time, limited amount of shear, and the lack of any real mixing all served to restrict the amount of quantitative information that could be generated.

The need to use two passes at 10 RPMs for adequate fusion made it impossible to use the mechanical take off, so that tapes with the smoothness and uniformity of dimension necessary for mechanical measurements, were not possible.

Experimental Mixes

The compositions which were examined, were based on a formulation with which Jean Mayer and Peter Stenhouse had had a great deal of success. A 50/50 starch/EVOH blend containing 3% zinc stearate, 10% water, and 22% glycerine was modified by the replacement of 20% of the EVOH with an equivalent weight of shellac. The overall shellac content was 10%, based on the weight of the polymer components. The shellac, containing compositions, were examined with and without ammonia, the water content being held constant. Although the amount of added water represented about 10% by weight of the mix, if one includes the water content of the starch (8%) and EVOH F101 (2.8%), the total water content is about 13.6%.

The experimental mixes containing shellac, would be fairly dry, up to thirty minutes after mixing, but then would go through a sticky, gummy stage and then become fairly dry again after approximately 16 hours. Heating the mix under sealed conditions (no water loss) for one hour at 115^{o}C hastened the process, with the mix becoming very dry after the heat treatment occurred. It appears the heat treatment results in surface liquid moving into the polymer particle. This is seen by the heated mixes fusing much more readily and with much less vapor loss than their unheated counterparts. Similar results are obtained if the mix is allowed to sit for a number of days at room temperature before extrusion.

Later mixes, in which, the EVOH F101 was replaced with EVOH H101 and, in which, the glycerine was reduced to 14%, did not show such marked changes in "wetness" over the short term. They do, however, become significantly drier over the long term (one week).

The "dryness" of a mix is not a significant factor in the laboratory screw, since the material is forced through with a plunger. However, in the twin screw, the bulk density (dryness) determines the rate at which the material will pass and, hence, its residence time. This can certainly influence the mechanical properties of the processed blend.

Differential Scanning Calorimetry (DSC)

The presence of water and/or glycerine transforms starch into a thermoplastic polymer. Starch consists of amylopectin and amylose fractions. Amylopectin is semicrystalline, it contains regions of low order (areas where branch points are

amorphous) and regions of high order (branched areas are crystalline). Normally, corn starch contains 70% amylopectin. In a 50/50 blend of starch and EVOH, the contribution of starch to crystallinity may be expected to be large. However, in the absence of external forces, its tendency to crystallize on rapid cooling may be small, particularly in the presence of water and glycerine. The DSC of a starch-water or starch-glycerine mixture will support this contention. A very small melting endotherm can be seen in first heating, but no evidence of crystallization can be seen in the cooling curve and no melting occurred in the second heating. Upon the addition of 3% zinc stearate (m.p. 130°C), a nucleating agent, a small crystallization peak appears in the cooling curve and this time, melting is seen in the second heating. These peaks arise not from the presence of zinc stearate per se, but rather because as a nucleating agent it causes the semicrystalline amylopectin fraction to crystallize.

Water and/or glycerine depresses the melting point of EVOH as well. Although it is not clear how, in a mixture of starch and EVOH, the water and glycerine will partition, there will be two plasticized components produced with different melting points. Because of its short residence time, the laboratory screw, under certain conditions, can produce a fused starch continuum containing a large number of unmelted EVOH swollen (plasticized) particles.

Fusion

The laboratory screw has produced a good deal of qualitative information on fusion temperatures and the impact that the water content has on these temperatures. Generally speaking, the higher the water content at a given glycerine level, the lower the temperature needed for fusion. The temperature range over which fusion will occur in this screw is narrow, due to the short residence time. The loss of water can rapidly change the fusion temperature. This sensitivity to water loss is particularly acute at high water levels. All the water present does not seem to be held to the same extent. Water loss is particularly noticeable when water content is high and glycerine content is low. The rates of water to glycerine, therefore, needs to be considered.

The presence of 10% shellac, by weight, significantly reduces the fusion temperatures. The presence of ammonia also reduces the process temperature whether or not shellac is present. It is not likely, therefore, that the shellac, containing composition, will be able to be processed at the same temperatures as the control.

Table 1 gives a qualitative comparison of process temperatures for various compositions with varying water contents. These are given in order of decreasing process temperatures.

TABLE 1. Qualitative Comparisons of Various Compositions and Water Percentages

Composition	Water Content(%)	Temperatures
No Shellac/No ammonia	13.6%	Highest
No Shellac/Ammonia	11.4%	
Shellac/No ammonia	9.3%	
Shellac/Ammonia	10.5%	Lowest

The impact of shellac and ammonia on process temperature is real, although at present, the reasons for this effect are not known.

Water

As was previously shown, water plays a significant role in the fusion process. The presence of water in the extruded polymer also has an impact on the mechanical properties of the polymer tape and their stability over time. As in the case of cellophane, water contributes to the strength of the polymer and to its extensibility as well.

Tapes with water contents in the 4-5% range or less are stiff and can become brittle with time. On the other hand, tapes containing 7 to 9% water have been found to remain flexible after 3-4 months whether stored in a desiccator or on a laboratory bench. Their water contents seemingly remained constant, under either condition during this time. It appears that the processing conditions can have significant effect on the ability of the processed blend to hold its water.

The water to glycerine ratio, as previously noted, is also important in the ability of the polymer to retain its moisture. The water content of the tapes containing shellac after extrusion, over a range of 5-10% has had very little effect on the water up-take of tapes upon total immersion, for seven (7) days, at room temperature. All samples produced on the laboratory screw take up about 20% of their weight, in water, whether or not they contain shellac. The shellac, at least in the manner added and under the conditions processed, has not had an impact on water resistance. It does continue, however, to reduce the processing temperatures needed.

Twin Screw Extruder

The twin screw extruder became available on an intermittent basis in November 1992. Early attempts to blow film with shellac, containing compositions in one pass, were not successful, although reintroducing two and three strands of polymer together in a second pass usually produced film. The early experiments showed that in order to blow film it was absolutely necessary to have enough material and enough pressure in the screw to cause fusion. Temperature alone was not sufficient. The feeding characteristics of the mix are very important in this regard and the screw speed needs to be matched to the "dryness" of the mix. If the mix is wet and feeds slowly, the screw speed needs to be increased so that enough material gets into the screw.

Since the shellac, containing mixes, were wetter than those without and tended to get stickier with time, a heat treatment was used (1 hour at 115°C) to produce a mix with more desirable feeding characteristics. At screw speeds between 30 and 50 RPM's and with the drier mixes, it was possible to blow film, in one pass, using the shellac compositions. It became apparent that the introduction of shellac into the standard formulation significantly altered the processing characteristics. Based on this, it was not likely that both types of mixes would give their optimum properties under the same set of processing conditions. As a result of the heat treatment the shellac, containing mixes, became so dry that they would feed in about half the time the control mix took. This substantially shorter residence time in the screw further emphasized the need for different processing conditions.

In order to minimize these differences, it was felt a reduction in the amount of water present in the shellac containing mixes, might allow us to process at temperatures closer to those used for the control. At the same time the EVOH F101 was replaced by EVOH H101 (Jean Mayer had gotten better results with this EVOH which has 38% PE) and the glycerine level was reduced to 14% (36% reduction). A comparison of the new formulations versus the old ones can be seen in Table 2.

TABLE 2. Comparison of Old and New Formulations

Control Material	Old Control Formulation	New Containing Formulation	Shellac Containing Formulation	Modified Formulation
Argo Starch	20g	20g	20g	20g
EVOH F101	16g	---	16g	---
EVOH H101	---	16g	---	16g
Zinc Stearate	2g	2g	2g	2g
Shellac	---	---	4g	4g
Water	6.3g	5.3g	5.6g	2.9g
Glycerine	13.7g	8g	13.7g	8g
Ammonium Hydroxide	---	---	1.0g	1.0g
% Water	14.4%	14.3%	13.6%	10.5%

The percent water includes the water actually added and water present in both the starch and EVOH. In reducing the level of water, the ratio of water to glycerine is kept nearly the same. In order to focus on the fusion process and to more carefully monitor sample homogeneity, a ribbon die was used on the twin screw extruder. It was hoped that such a die could produce samples for mechanical measurements which were not stressed or oriented in any way.

The following formulations in Table 3 contained EVOH H101 and a decreased level of glycerine were processed on the twin screw extruder using a ribbon die. A single set of processing conditions were used (Zone 1-4: 104-114°C, 125°C, 130°C, 130°C, extruder speed: 40 RPM).

TABLE 3. Formulations Processed on Twin Screw Extruder
Using Ribbon Die

Material	I	III	IV
Argo Starch	200g	200g	200g
EVOH H101	160g	160g	160g
Zinc Stearate	20g	20g	20g
Shellac	---	40g	40g
Water	53g	29g	29g
Glycerine	80g	80g	80g
Ammonium Hydroxide	---	10g	---
% Water	14.3%	10.5%	9.3%

Formulations 3 and 4 had been heated for one hour at 115°C prior to use. Table 4 presents the mechanical property data on the polymer tapes obtained. The specimens were conditioned at 20% and 80% relative humidity (RH) but the measurements were made at 50% relative humidity. There was only one set of processing conditions used (*Zone* 1-4: 104-114°C, 125°C, 130°C, 130°C, extruder speed: 40 RPM).

TABLE 4. Mechanical Property Data on Polymer Tapes

Formulation	Initial Water in Formula	Water In Tape	Conditioned at 20% RH: Tensile Strength (MPa*)	Conditioned at 20% RH: Percent Elongation	Conditioned at 80% RH: Tensile Strength (MPa*)	Conditioned at 80% RH: Percent Elongation
I	14.3%	9.3%	94.6	250%	66.8	190%
III	10.5%	8.0%	8.1	55%	4.5	45%
IV	9.3%	7.1%	8.4	55%	4.9	70%

* MPa = MegaPaschal

The water sensitivity of the processed mixes, as measured by water up-take after total immersion in water at room temperature for seven (7) days, appears in Table 5.

TABLE 5. Weight Gain Due to Water Sensitivity

Formulation	Composition	Weight Gain (%)
I	No Shellac	17.1%
III	Shellac/Ammonia	14.1%
IV	Shellac	12.6%

There seems to be a significant effect here, relative to the presence of shellac and water resistance. The difference between ammonia and no ammonia may be reflective of a difference in degree of fusion rather than anything else. A difference in "dryness" and hence, residence time is likely to result in a difference in fusion. If these are poorly fused, then weight gain numbers are even more significant since formulation I (control) is extremely well fused. Shellac may, indeed, be having an effect. Before any assessment can be made, the homogeneity of the mix, the homogeneity of the shellac in the extruded polymer and the morphology, which has been coated, needs to be examined.

The processing of formulation III on the twin screw extruder at slightly higher temperatures (Zone 1-4: 90°C, 135°C, 135°C, 130°C, extruder speed: 40 RPM) resulted in an increase in the stress at maximum load to 14.5 MPa and elongation of 40%. Again, a response to process conditions occurred.

The mechanical properties of formulation I (control) were quite impressive and even conditioning at 80%, RH did not seriously compromise the properties. It should be noted, however, that because of its "wetness" the feeding rate was quite slow and so, its residence time in the screw was as much as 3-4 times longer than the accompanying mixes. When the mix was allowed to sit in a sealed bag for a week and was then extruded (Zone 1-4: 100°C, 125°C, 125°C, 125°C, extruder speed: 40 RPM), the stress at maximum load was only 8.8 MPa. The mix had become much drier and so, fed very quickly through the screw (much shorter residence time). Since the dryness of the mix has a profound influence on the feeding rate and hence, residence time, its potential impact on final properties needs to be kept in mind.

The mechanical properties of formulations III and IV are poor, relative to control. There may be other causes, but it seems the materials are not fused, which may just be reflective of the very short residence time.

INJECTION MOLDED BIODEGRADABLE MATERIALS

Work has been done involving the injection molding of biodegradable materials. This is accomplished by using the Mini-Max Injection Molder and forming tensile bars (dog-bones) for tensile strength and percent elongation studies, and rectangular bars for biodegradation studies. This is a bench top model, which enables the making of small samples and thus, requires very small amounts of material to be used. The injection molder can process material in pellet or powder form. The formulations used on the mini-injection molder can be the same formulations that are processed on the twin screw extrusion equipment. Samples have also been made using corn starch in pellet form, supplied by the Novamont Company. These resins were tested on the injection molder in both pellet and powder form. Tensile and elongation properties of the dog-bone samples can be studied through the use of this equipment, as well as, the feasibility of scaling up to run bigger amounts of material on the twin screw extruder.

Study of Physical Properties as a Function of Water Content

A series of tests has been completed to determine the relationship of water content to the physical properties of a commercially available starch-based resin. This research was first conducted because there had been a dramatic change in the tensile properties of the Novamont corn starch resins, known as A106H and SA038, when they where made into a dog-bone from the resin pellets and from a milled powder on the mini-injection molder. Figure 7, shows approximately a 300% increase in displacement at maximum load and a slight 20% decrease in maximum load sustained in the milled powder versus the pellet resin.

FIGURE 7. TENSILE PROPERTIES OF NOVAMONT RESINS

Since the composition of the two Novamont resins are not available, studies are being repeated by using in-house blends of starch, EVOH, and plasticizers. This study will measure the water content of the blends and relate it to the tensile and rheological properties. There will also be some data taken on the melt and crystallization temperatures and a few images of the material may be taken using a Scanning Electron Microscope (SEM).

Tentative results showed a definite relationship between water content and physical properties. In Figure 8, one can see that as the percent of water increases, the displacement at maximum load also increases, while the maximum load sustained decreases. This relationship continues until around 10% water, the point where it is believed that the water content becomes so great that too much strength is lost. At that point, the displacement peaks then decrease.

Starch Blend Rheology Study

The factors necessary for a starch blend to be melt processable in a twin screw extruder are not well-defined at this point. Two obvious characteristics necessary are that the blend melts at the processing temperature and that the blend is able to flow through the extruder. These two characteristics are being investigated. Through the study of these characteristics of the preprocessed blends and through the later analysis of blown film after processing, the hope is to incorporate that data into a model or simulation of twin screw blown film polymer processing.

The first characteristic necessary to process a blend, is that the blend melts at the desired processing temperature. The melting temperature and crystallization temperature are measured by using Differential Scanning Calorimetry (DSC). A DSC measures the changes in heat flow as a function of a heating cycle. The curves produced by the DSC's software shows peaks that can be associated with points of melting, crystallization, and destructuring of the starch blend. A difficulty in taking these readings, are that sealed pans must be used to keep blend components from volatilizing out and there must also be a preliminary heating, to melt and mix the blend sufficiently.

The second characteristic necessary in processing, is that the blend must flow through the extruder. Using a Capillary Rheometer (CR), the hope is to characterize the flow behavior necessary to process the blends. In order to test the blends, a solid rod of the material is made by packing it into a mold and then heating the mold to melt the blend. The cooled rod is removed from the mold and tested in the CR. The CR calculates the viscosity and shear stress over a given range of shear rates. This data is used to produce curves that will be used to characterize the flow behavior. Thus far, the data has been reproducible, is distinguishable from blend to blend, and appears to fall in a quantifiable region. After sufficient supplies and materials are available (target is April), a systematic study on various preprocessed blends will be conducted.

FIGURE 8. TENSILE PROPERTIES OF IN-HOUSE BLENDS

GEO-CENTERS, INC

CONCLUSIONS AND FUTURE PLANS

Extrusion Work

The 5-inch laboratory single screw does not exhibit the necessary mixing, shear, and residence time to produce samples which could be considered to have representative mechanical properties. It can be, however, useful in examining the parameters which influence fusion temperature, embrittlement, and water resistance. Screening experiments relative to the evaluation of new plasticizers, such as monosubstituted fatty acid glycerides and sorbitans and their mixtures with water, will be carried out. The qualitative information regarding fusion temperature, plasticizer action, and stability obtained will be useful in designing the twin screw experiments.

The question as to whether or not shellac imparts water resistance on the polymer blend has not been completely answered. Mixed results have been obtained. Although several heat treated mixes that were processed on the twin screw extruder have shown some reduction in water up-take relative to a control, the results have not been conclusive. Before a realistic assessment of its effect can be made, it is necessary to know something of the nature of the morphology that has been created in terms of the dimensions and the stability of the dispersed phase. In order to be effective, the size of the dispersed phase needs to be submicron. It is also important to know where the shellac is. It needs to be at the starch-EVOH interface. This morphology will be examined by Scanning Electron Microscopy (SEM) and Transmission Electron Microscopy (TEM). Mixes which contain shellac, particularly those with ammonium hydroxide, contain a large number of inhomogeneities. Any additive has to be uniformly dispersed throughout the mix if it is to be effective. Although mixing does occur in the twin screw, the extent to which it occurs using the present configuration is uncertain. The fact that the addition of shellac has had no significant effect on water resistance in tapes produced in the laboratory screw where no mixing occurs, may be more indicative of the fact that the lack of homogeneity in the mix is a problem. High shear mixing of the blends will be examined as a means of overcoming this difficulty.

That the presence of water and glycerine serves to plasticize the EVOH fraction, as well as, the starch portion of the blend, is well established. How the liquids are partition between them is not known. When the liquids and shellac are added to each polymer component separately but in the same proportion as they are in the final blend, allowed to equilibrate for a period of time and then combined and extruded through the laboratory screw, the extrudate has significantly different water resistance than previously seen. A 50% decrease in water up-take is noted compared to the same polymer mix blended in the conventional way. Perhaps using this technique gives better interaction of the shellac with one or the other of the polymeric components. Other modifications to the blending process will be pursued in order to enhance the possibility of interaction.

Another method that is commonly employed to enhance the effectiveness of the polymeric additive, is to actually process it with one of the major polymer components and then look at the effect of adding increasing amounts of the second polymer to the previously processed blend. This approach will also be pursued. Using this technique, often times enhances the properties, which can be achieved using much smaller amounts of the second component.

The rate at which the thermodynamic equilibrium of the morphology, which is created, can be achieved depends on the magnitude of the polymer-polymer interactions and the resisting rheological forces (i.e. diffusivity). The rate at which they diffuse into each other depends on the viscosities of the polymers. For this reason, the higher melt index (lower viscosity) versions of EVOH F101 and EVOH H101 will be examined.

The water content of the processed polymer blends is a very important factor in the strength of the materials and contributes to the flexibility (extension) of the blends as well. In addition, at low water contents (5% or less) embrittlement occurs. If there is a stable water content of between 7-9%, the polymer blend retains its extensibility over long periods at time. Stable, here, refers to the ability of the blend to retain its water content under a number of diverse conditions (desiccator). This ability to retain moisture under varied circumstances seems to depend on the water to glycerine ratio and process conditions. Some evidence even suggests that shellac, or more specifically, shellac/Ammonium Hydroxide, may play a role. The role of shellac in this regard will also be investigated. The dramatic effect that water has on the properties of starch blends emphasizes the importance of the presence of a humectant like glycerine in the system.

Higher molecular weight humectants while still efficient retainers of water may offer advantages in terms of their plasticizing action. In addition, those that combine higher molecular weight with an interactive group may be less susceptible to extraction due to this interaction and chain entanglement. Such materials as highly sulfonated tallow, polyethoxylated and polypropoxylated glucose will be evaluated. Other materials similarly interactive but with surfactant-like properties (monosubstituted fatty acid glycerides and sorbitans) will be used in an attempt to stabilize the phases. The role of water not withstanding, the presence of an unstable morphology, which may have the tendency to coalesce with time, may by responsible for the deterioration of properties which often occurs. Under stress (extension) this instability may lead to the whitening (crystallization) that is often seen.

A stable dispersed phase submicron, in dimension that has shellac at the interphase, may exhibit biodegradable characteristics not normally seen with petroleum-based polymers. Surface area and the nature of that surface can often times dramatically influence biodegradation.

The twin screw extrusion trials, for the most part, have concentrated on water content and processing temperatures keeping screw speed constant. Hence, residence time depended strictly on the feeding characteristics of the mix. A specific look at resonance time, within the temperative parameters established, will be taken. This will not only include screw speed but mix dryness as well. This ability to control the width of residence time is an important feature of the twin screw extruder (positive pumping), as is the ability to adjust the ratio of dispersive to distributive mixing. It is intended that this advantage be explored to its fullest.

Future Investigations of Physical Properties as a Function of Water Content

The gathering, compiling, and analysis of data is planned to be completed in the next 3-4 months. A total of 6-10 blends will be examined during that time. The tensile data is planned to be completed by the middle of April. A few DSCs will be conducted in March and April, and rheological data will also be completed in that time period. Microscopy may be done on 2-10 samples in the coming months. If data collection is successful and the information significant, then all the information will be collected and written up for possible publication.

Future Investigation of Starch Blend Rheology

After sufficient data is gathered on melt and crystallization temperatures and on the rheological behavior of the blends, correlations will be examined between those characteristics and the physical properties of blown film. Selected blends will be extruded and blown into film. These films will be tested on an Instron to measure the tensile properties. If correlations are found between the preprocessed blend characteristics and the blown film physical properties, then a decision in how to proceed with the research will be made. The continuation of the research may consist of expanding the number of components and concentration of components and/or by developing a model or simulation of the blends studied.

REFERENCES

1. Maxwell, C.S. Tappi 53; 1464 (1970).

2. Maxwell, C.S. Tappi 54; 568 (1971).

3. Mayer, J.M., J.E. McCassie, D.H. Ball, R.E. Stote, J.R. Wright, A.E. Shupe, P.J. Stenhouse, P.A. Dell, M.J. Hepfinger, E.A. Costa, E.T. Reese, and D.L. Kaplan. BIODEGRADABLE POLYMERS FOR PACKAGING. U.S. Army Natick RD&E Center, Natick, Ma 01760-5020.

4. Otey, F.H., R.P. Westhoff, and W.M. Doane. Ind. Eng. Chem. Prod. Res. Dev.. pp. 19, 592 (1980).

5. Otey, F.H., R.P. Westhoff, and W.M. Doane. Ind. Eng. Chem. Prod. Res. Dev. pp. 26, 1659 (1987).

6. Stenhouse, P.J., J.M. Mayer, M.J. Hepfinger, E.A. Costa, and D.L. Kaplan. BLOWN FILM FROM STARCH/POLY (VINYL ALCOHOL) AND STARCH/ETHYLENE-VINYL ALCOHOL BLENDS. U.S. Army Natick RD&E Center, Natick, Ma 01760-5020.

Effects of Water Content on the Properties of Starch/Poly(ethylene vinyl alcohol) Blends

Paul A. Dell

Geo-Centers Inc., 7 Wells Avenue, Newton Centre, Massachusetts, 02159

Synopsis

The physical properties of unmodified starch, poly(ethylene vinyl alcohol), glycerol, and water mixtures are reported. Thermal and melt flow properties of the pre-processed, physically mixed materials were determined along with the tensile properties and morphology of injection molded microtensile samples. Melt flow properties were measured by a capillary rheometer, and the water content was varied from 4-18%. The morphology, rheology, and tensile properties are all highly related to the percentage of water present. A transition in the tensile properties and morphology of the blends was observed at approximately 11% moisture content.

INTRODUCTION

The effects of water and other plasticizers on starch have been studied previously,[1-3] and a comprehensive review of various starches and their structures is given by Zobel.[4] There has been little reported work on starch/EVAL blends, specifically in the area of plasticizer content and its effect on physical properties. In this study, the effects of water content on changes in the thermal, melt flow, and tensile properties of the polymer blends, along with morphology, are examined. A number of thermal and rheological measurement methods such as TGA, cone-and-plate viscometers,

and rotating cylinder viscometers could not be used at temperatures above 100 C since the water would volatilize off and change the composition of the mixtures.

Starch/EVAL and other polymer blends are important for possible use in biodegradable materials.[5,6,7,8,9] Starch is of interest because of its low cost, availability as a renewable resource, and its established biodegradability. Studies have been conducted with various starches on the effects of water, glycols, and other plasticizers, but these have been mostly on unmodified starches in doughs for the food industry[10,11,12] or on pre-treated starches[13,14,15,16] for the plastics industry. The use of starch as a component for plastics has often focused on modified or pre-treated starch and poly(vinyl alcohol) blends or starch as a filler in polyethylene (PE).[17,18,19,20,21] Some research has also been conducted on starch-poly(ethylene-co-acrylic acid) (EAA) blends.[22] The disadvantages of the EAA films are: they require pre-mixing with large amounts of water, which adds to processing costs; they require urea, which decomposes into ammonia; and they are not 100% biodegradable (100% mineralization). Starch/EVAL blends do not need to be premixed with a large amount of water, there is no need for urea, and data suggests EVAL is biodegradable.[23] EVAL is also of interest due to its excellent oxygen barrier properties. In addition to injection molding, starch/EVAL blends can be processed into blown film.[24] The properties of both the pre-processed mix and the injection molded microtensile samples of starch, poly(ethylene vinyl alcohol)(EVAL), glycerol, and water are reported here.

EXPERIMENTAL

Materials

EVAL was provided by Eval Company of America (Lisle, IL) with a melt index of 1.6 at 190 C and 38 mol % ethylene. The starch used was food grade Argo corn (maize) starch produced by CPC International (Englewood Cliffs, NJ), with approximately 30% amylose and 70% amylopectin. The glycerol was purchased from Sigma Chemical Company (St. Louis, IL). The water was deionized by a Millipore Milli-Ro system (Bedford, MA).

Mixing

A typical starch/EVAL blend consisted of 40g of starch, 40g of EVAL, 30g of glycerol, and an appropriate amount of water to achieve the desired moisture content. Blends were prepared by combining the dry materials (starch and EVAL) in a sealable polyethylene bag, adding the glycerol and the water, and mixing by hand until a uniform consistency was established. The blend was left in the sealed bag for 24 hours before testing began, to allow for the starch to absorb the glycerol and/or water.

Moisture Analysis

Water content was determined with a model 903H Moisture Evolution Analyzer (TA Instruments, Inc., New Castle, DE) which uses an electrolytic cell to conduct a coulombic measurement of water content. The instrument was calibrated with 2 mg of water at 150 C for 40 min. Each sample was run twice to ensure accuracy. The moisture levels reported are the average values.

Mechanical Properties

A bench-top injection molder (model CS-183, Custom Scientific Instruments, Inc., Cedar Knolls, NJ) was used to mold the microtensile specimens. The dimensions of the microtensile specimens were in accordance with the ASTM method D1708 (38.1 mm-length, 15.88 mm-width, 3.2mm-thickness). The specimens were processed at 185 C and injected into a room temperature mold. The microtensile bars were stored in polyethylene bags and tested within 48 hours to minimize possible aging effects. Tensile properties were measured using the Instron Universal Testing Machine (Canton, MA) model 4204 with a 200 lb. (90.7 kg) load cell and a 0.05 in/min (0.127 cm/min) crosshead speed.

The tensile values given are calculated at the maximum load sustained during the testing profile. The maximum load sustained was generally near the breaking point of the material. The stress is calculated from the load at maximum load divided by the initial cross-sectional area of the

specimen. The elongation is calculated from the cross-head distance traveled to the poin maximum load sustained.

Thermal Properties

Differential scanning calorimetry (DSC) measurements were conducted on TA instruments (mc 910 and 912, New Castle, DE). Large volume stainless steel pans were filled with material then sealed along with a Viton rubber O-ring (Perkin Elmer, Norwalk, CT) in the top portion o pan to suppress vaporization and water loss. The thermal cycle was from ambient to 200 C, l to ambient, again to 200 C, and back to ambient, all at 10 C/min. The results given are fron second heating and cooling cycle. The first cycle was used to melt the blend to i..p homogeneity, and to impart a known thermal history to the sample. The melting and crystalliz values were taken at the peak of the exotherms or endotherms.

Melt Flow Properties

Melt-rheological measurements were conducted on a constant shear rate type capillary rheo (Instron-model 3213 Capillary Rheometer running RheoSoft software, Canton, MA). The cap was circular, with a length/diameter ratio of 40 (5.0897 cm. - length, 0.127 cm.- inner diam The materials were tested at 135 C over identical velocity profiles, but some blends could r

tested at the highest shear rates due to high load values. The Rabinowitsch correction metho calculated by the RheoSoft software was used to correct the shear rate, shear stress, and visco values.

To minimize water loss, a preform was made of the material (a cylinder of approximat 0.953 cm-diameter and 20.3 cm- length) of each blend to expedite the loading of the blends into capillary rheometer. The blends were packed into glass tubes, which were sealed at one end. tubes were then sealed at the other end and heated at 120 C for two hours, followed by coolin room temperature for two hours. Then the glass was fractured to remove the starch/EVAL prefo and the preform was sealed into a polyethylene bag until loading into the capillary rheometer. O loaded, the material was compressed slightly with the plunger and then allowed to equilibrate five minutes.

Microscopy

Samples for optical microscopy were viewed and photographed using a Zeiss (Thornwood, model 61455 optical microscope at 400x magnification. The samples were cut from an end o microtensile samples, placed on a glass slide, and stained with Melzer's reagent, which is a solu containing iodine and ethanol. The iodine permits visualization of the starch granule size dispersity by causing the starch to appear dark.

Scanning Electron Microscopy (SEM) was conducted on a Zeiss (Thornwood, NY) n CSM 950 Computerized Scanning Microscope. The samples were mounted and sputter coated

a gold palladium alloy using a Balzers Union (Liechtenstein) model MED 010 sputter coater. T samples were not dried or treated in any other way before coating and viewing.

RESULTS AND DISCUSSION

Mechanical Properties

Water content affects the tensile properties of microtensile starch/EVAL specimens. In Figure the stress at maximum load is plotted versus water content for the microtensile samples. There an inverse relationship between the maximum stress and the water content. The relationship n be described by a second order equation. The deviation from linearity may result from process in which the higher moisture content blends have a greater moisture loss.

The elongation at maximum load of the starch/EVAL blend specimens (Figure 2) increa steadily with the water content until approximately 11% moisture. Above 11% moisture the d becomes erratic. An elongation maxima is expected at some point due to the decreasing stren of the material exhibited in the stress curve (Figure 1). This elongational maxima at approximat 11% water region also appears to correlate with a transition in the surface structure of microtensile specimens which will be discussed later.

The transition at 11% water in the starch/EVAL blends may be the result of two compe forces. The transition may be due to the water playing a dual role as both a plasticizer and a blow agent.[5] The plasticization role of the water will lower the melting temperature of the blend (Fi

3). lower the viscosity (refer to "Melt Flow Properties" section) and permit a more thorough mixin of the blend under the processing conditions. The water's plasticization of the blend will increas the elongation. Water's effect as a blowing agent would create defects that would likely lower th maximum tensile strength and the maximum elongation of the specimens. The competing roles c water as a plasticizer and blowing agent may be the explanation for the apparent transition in th elongational values around the 11% water region.

Thermal Properties

The melting and crystallization temperatures versus water content are given in Figure 3. Increasin the water content lowers both the melting and crystallization temperatures of the starch/EVA blends. The relationship between the thermal behavior and water content is linear between 4-18% The equation of the fitted curve for the melting temperature as a function of the water content is

$$T_m = 144.20 - 162.61x$$

with a correlation value (R^2) of 0.976. The equation for the crystallization temperature as a functi of the water content is:

$$T_c = 97.93 - 270.68x$$

with a R^2 value of 0.988. It should be noted that the y-intercepts give theoretical values for the T_m and T_c for 0% moisture.

Glycerol also contributes to lowering the melting and crystallization temperatures of EVAL. The effects of both water (Figure 4) and glycerol (Figure 5) over the range of 0-30% on EVAL alone are shown. The percent values given on the graphs in figures 4 and 5 are calculated from the composition of the ingredients, not from the moisture evolution analyzer measurements on the blends. Water has a greater effect than glycerol on reducing the melting and crystallization temperatures of the EVAL.

Melt Flow Properties

In Figure 6, the viscosity of the blends decreases as the water content increases. This is due to the water's plasticization effect on the EVAL. The melting point of dry EVAL is 175 C[20] and the melting point of the starch/EVAL blends with glycerol and water is 30-50 C lower. The starch/EVAL blends with glycerol and water are melt processable at 145 C or lower, as opposed to the 175 C and above needed to process the EVAL resin alone. This can be shown in the viscosity curves, the curve of the starch/EVAL blend at 135 C with 9.5% H_2O is comparable to the viscosity curve of EVAL at 200 C (Figure 6). This lowering of the processing temperature is beneficial because the lower temperatures would avoid degradation of the starch and save energy.

The flow behavior is of a highly non-newtonian pseudoplastic and can be approximated using the power law model. The power law factor varies greatly (0.25-0.5) with water content. I

the power law factor is plotted vs. percent H_2O (Figure 7), the result shows a scattered data set with a possible region of interest around 11-13% water. The data set may be approximated by a simple line which yields a R^2 value of 0.519, but a fit may also be made with a third order polynomial which yields a R^2 value of 0.625. There is no a priori justification for fitting a third order polynomial to the power law factor vs. water curve, but complex behavior would be expected from a blend of two polymers and two plasticizers.

In starch based materials, the shear history of the material is important. In the capillary rheometer studies reported here, no shear has been applied to the blends before testing. Further studies may be conducted using a pre-shearing capillary rheometer, such as the Rheoplast rheometer (COURBON Company, France). The Rheoplast device is capable of delivering a specific amount of shear to a material in a closed system.[27] Another option would be to measure the effects of the specific mechanical energy on the flow behavior by use of an in-line rheometer. The Rheopac is a slit die rheometer which has been used to measure the viscosity of maize and potato starches with moisture contents between 5-20%.[28,29]

Morphology

The optical photographs of starch/EVAL samples stained with Melzer's reagent show the morphology of the starch granules in the injection molded samples. In the microtensile sample containing 6.62% H_2O (Figure 8A), the starch granules are intact and apparently acting only as a filler in the EVAL. With 11.6% water (Figure 8B), the starch granules are fragmented and

dispersed. As the water level increases to 16.3% (Figure 8C), almost all of the starch granules are fragmented and more evenly dispersed. The water content greatly effects the morphology of the starch granules in the specimens.

The starch morphology changes may explain, in part, the decrease in the stress at maximum load (Figure 1). When the granules are intact (Figure 8A), the EVAL can form a continuous phase around the starch granules, which are acting only as a filler. As the moisture level is increased and the starch granules fragment, the starch may continue to act as a filler; but since the starch is finer and more dispersed, it produces more heterogeneity in the EVAL phase. Another possibility is that the starch may be forming its own continuous phase, which is a weaker network than the EVAL phase. If an interpenetrating polymer network of starch and EVAL is being formed, the starch phase of the system is reducing the maximum stress that the sample can sustain, and it is also creating a more elastic polymeric material (Figure 2).

SEM photomicrographs also provide insight into the materials. The photographs in Figure 9 are representative of the surface of the samples, although there was variability in the surface of all the samples. At 4-9% moisture contents (Figure 9A), the surface is rough with many holes and bumps on the order of 5-10 μm. In the 9-13% moisture region (Figures 9B and 9C), the surface appears smoother and the spherical surface features are on the order of 1 μm in Figure 9B, and are even smaller in Figure 9C. As the moisture level increases, the surface features change only slightly. Above 13% water (Figure 9D) the surface appears slightly rougher, but without holes or bumps. The larger surface features on the lower moisture content samples may be due, in part, to the higher viscosity, which would make it more difficult for the material to fully fill and form into the mold. Over the entire range of moisture contents, occasionally small holes (1 μ) appear which

seem to be the result of water volatilizing off during processing. The irregularity of these holes may be the result of temperature fluctuations or entrapped air.

SEM photomicrographs were also taken of the capillary rheometer extrudate. The morphology varied with the moisture content and the shear rate. At low shear rates (10-100 1/sec), small cracks were visible at 2000x magnification (Figure 10). The cracks were connected at slight indentations and gave the surface the appearance of an orange peel. At high shear rates (500-1000 1/sec), the cracks were not evident and the surface was smoother. A smooth surface also appeared on some low shear rate extrudate samples around the 11% moisture region.

CONCLUSIONS

Water content affects the physical and thermal properties of starch/EVAL blends. Based on the iodine stained photos and the thermal studies, the starch and EVAL are not miscible in the presence of glycerol and water. The effects of water on the tensile properties are likely due to the fragmentation of the starch and the plasticization of both the starch and EVAL as the water content is increased. The fragmentation of the starch is disruptive to the EVAL phase, which lowers its strength. The water's plasticization effect is imparting greater elasticity to the materials and aiding the processing of the blends by lowering the melting temperature. The lowering of the melting and crystallization temperatures of the EVAL is likely the result of the interaction of the hydroxyl groups of EVAL with the water. SEM photomicrographs confirm that the surface of the polymer blends also varies with water content. The larger surface features on the 4-9% moisture levels is

likely the result of incomplete melting and appearance of intact starch granules. As the water level increases, the surface is more uniform due to the lower melting temperature, which allows for a more thorough mixing; also, the fragmentation of the starch granules lends itself to a smoother and more uniform surface. The transition in the tensile properties and changes in morphology around the 11% moisture region suggest that this is an optimal value for the elongation properties and surface morphology of these starch/EVAL blends.

This work was performed in support of a U.S. Army Natick Research, Development & Engineering Center (Natick, MA) research program. The author would like to express his appreciation to Dr. William Kohlman for his guidance and input throughout many revisions of this paper. Also thanks to Mrs. Elizabeth Welsh, Mr. Robert Stote, and Ms. Renay Pollier for their assistance in sample preparation and testing. And thanks to David Kaplan, JoAnn Ratto, Peter Stenhouse, Jean Mayer, and Steve McCarthy for their input on this study.

REFERENCES

1. R. Shogren in *Fundamentals of Biodegradable Materials and Packaging*, D. Kaplan, E. Thomas, and C. Ching Eds., Technomic Publishing Co. Inc., Lancaster, Pennsylvania, in press (1993).

2. J. W. Donovan, *Biopolymers*, **18**, 263 (1979).

3. J. Levievre, *J. Appl. Polym. Sci.*, **18**, 293 (1974).

4. H. F. Zobel, *Starch/Stärke*, **40**, 44 (1988).

5. J. M. Mayer, A. L. Allen, P. A. Dell, J. E. McCassie, A. E. Shupe, P. J. Stenhouse, E. A. Welch, and D. L. Kaplan, *Polymer Chemistry Pre-Prints: Spring-Denver*, American Chemical Society, to appear.

6. J. M. Mayer, J. E. McCassie, D. H. Ball, R. E. Stote, J. R. Wright, A. E. Shupe, P. J. Stenhouse, P. A. Dell, M. J. Hepfinger, E. A. Costa, E. T. Reese, and D. L. Kaplan in *Fundamentals of Biodegradable Materials and Packaging*, D. Kaplan, E. Thomas, and C. Ching Eds., Technomic Publishing Co. Inc., Lancaster, Pennsylvania, in press (1993).

7. P.J. Stenhouse, J. Ratto, and P. A. Dell, *"Polysaccharide/Synthetic Polymer for Biopolymer Blends" symposium by Paper and Textile Division of ACS Chicago August 22-27 in press (1993).*

8. P. J. Stenhouse, J. Mayer, M. Hepfinger, E. Costa, P. Dell, and D. Kaplan in *Fundamentals of Biodegradable Materials and Packaging*, D. Kaplan, E. Thomas, and C. Ching Eds., Technomic Publishing Co. Inc., Lancaster, Pennsylvania, in press (1993).

9. S. Simmons, C. Weigand, R. Albalak, R. Armstrong, and E. Thomas in *Fundamentals of Biodegradable Materials and Packaging*, D. Kaplan, E. Thomas, and C. Ching Eds., Technomic Publishing Co. Inc., Lancaster, Pennsylvania, in press (1993).

10. K. L. Mackey and R. Y. Ofoli, *J. Food Science*, **55**,417 (1990).

11. R. Chinnaswamy and M. A. Hanna, *Cereal Chemistry*, **65(2)**, 138 (1988).

12. V. J. Davidson in *Food Extrusion Science and Technology*, J. L. Kokini, Chi-Tang Ho, and M. V. Karwe Eds., Marcel Dekker, Inc., New York, 1992, Chap. 17.

13. R. L Shogren, C. L. Swanson and A. R. Thompson, *Starch/ Stärke*, **44**, 335 (1992).

14. C. Basioli, V. Bellotti, L. Del Giudice and R. Lombi, *European Patent Application*, EP 400,532 (1990).

15. F. H. Otey, R. P. Westhoff, *U.S. Pat.*, 4,454,268 (1984).

16. R. J. Dennenberg, R. J. Bothast, T. P. Abbott, *J. App. Poly. Sci.*, **22**, 459 (1978).

17. R. P. Westhoff, W. F. Kwolek and F. H. Otey, *Starch/Stärke*, **31**, 163 (1979).

18. F. H. Otey, R. P. Westhoff, and W. M. Doane, *Ind. Eng. Chem. Prod. Res. Dev.*, **19**, 592 (1980).

19. R Chinnaswamy and M.A. Hanna, *Starch/Stärke*, **43**, 396 (1991).

20. W. Wiedmann and E. Strobel, *Starch/Stärke*, **43**, 138 (1991).

21. S. M. Goheen and R. P. Wool, *J. Appl. Polym. Sci.*, **42**, 2691 (1991).

22. F.H Otey, R. P. Westhoff, and W. M. Doane, *Ind. Eng. Chem. Res.*, **26**,1659 (1987).

23. J. M. Mayer, A. L. Allen, P. A. Dell, J. E. McCassie, A. E. Shupe, P. J. Stenhouse, E. A. Welsh, and D. L. Kaplan, in *Polymer Chemistry Pre-Prints (Spring '93-Denver)*, American Chemical Society, to be published.

24. P. J. Stenhouse, J. Mayer, M. Hepfinger, E. Costa, P. Dell, and D. Kaplan in *Fundamentals of Biodegradable Materials and Packaging*, D. Kaplan, E. Thomas, and C. Ching Eds., Technomic Publishing Co. Inc., Lancaster, Pennsylvania, to be published.

25. A. C. Smith, *Food Extrusion Science and Technology*, J. L. Kokini, Chi-Tang Ho, and M V. Karwe Eds., Marcel Dekker, Inc., New York, 1992, chap. 36 p.601.

26. EVAL Company of America product information sheets 1992.

27. B.Vergnes and J. P. Villemaire, *Rheologica Acta*, **26**, 570 (1987).

28. G. Della Valle, B. Vergnes and J. Tayeb, *ENTROPIE*, **169**, 59 (1992).

29. G. Della Valle, B. Vergnes, J. Tayeb and Y. Boché, in *Theoretical and Applied Rheology*, P. Moldenaers and R. Keunings (Eds.) Proc. XIth Int. Congr. on Rheology, Brussels, Belgium, August 17-21 1992, Elsevier Science Publishers, Brussels, 1992.

Legends for figures

Figure 1 Influence of water content on stress at maximum load (N=8-10, standard deviation is shown): (◊) starch/EVAL.

Figure 2 Influence of water content on elongation at maximum load (N=8-10, standard deviation is shown): (♦) starch/EVAL.

Figure 3 Influence of water content on melting and crystalization temperatures on starch/EVAL blends: (○) melting temperature; (□) crystalization temperature.

Figure 4 Influence of water content on melting and crystalization temperatures on EVAL: (○) melting temperature; (□) crystalization temperature.

Figure 5 Influence of glycerol content on melting and crystalization temperatures on EVAL: (●) melting temperature; (■) crystalization temperature.

Figure 6 Viscosity versus shear rate of EVAL at two temperatures, and starch/EVAL blends at three different moisture contents: (○) EVAL at 180°C (<1% H_2O); (●) EVAL at 200°C (<1% H_2O); (□) 9.5% H_2O starch/EVAL at 135°C; (◘)13.7% H_2O starch/EVAL at 135°C; (15.5% H_2O starch/EVAL at 135°C.

Figure 7 Influence of water content on the power law factor from capillary rheometry experiments:(+) power law factor.

Figure 8 Optical photographs of starch/EVAL microtensile at 400x magnification: (A) 6.62% H_2O; (B) 11.6% H_2O; (C) 16.5% H_2O.

Figure 9 SEM photographs of starch/EVAL microtensile samples at 1000x magnification: (A) 6.62% H_2O; (B) 9.22% H_2O; (C) 11.2% H_2O; (D) 16.5% H_2O.

Figure 10 SEM photograph of starch/EVAL capillary rheometry extrudate.

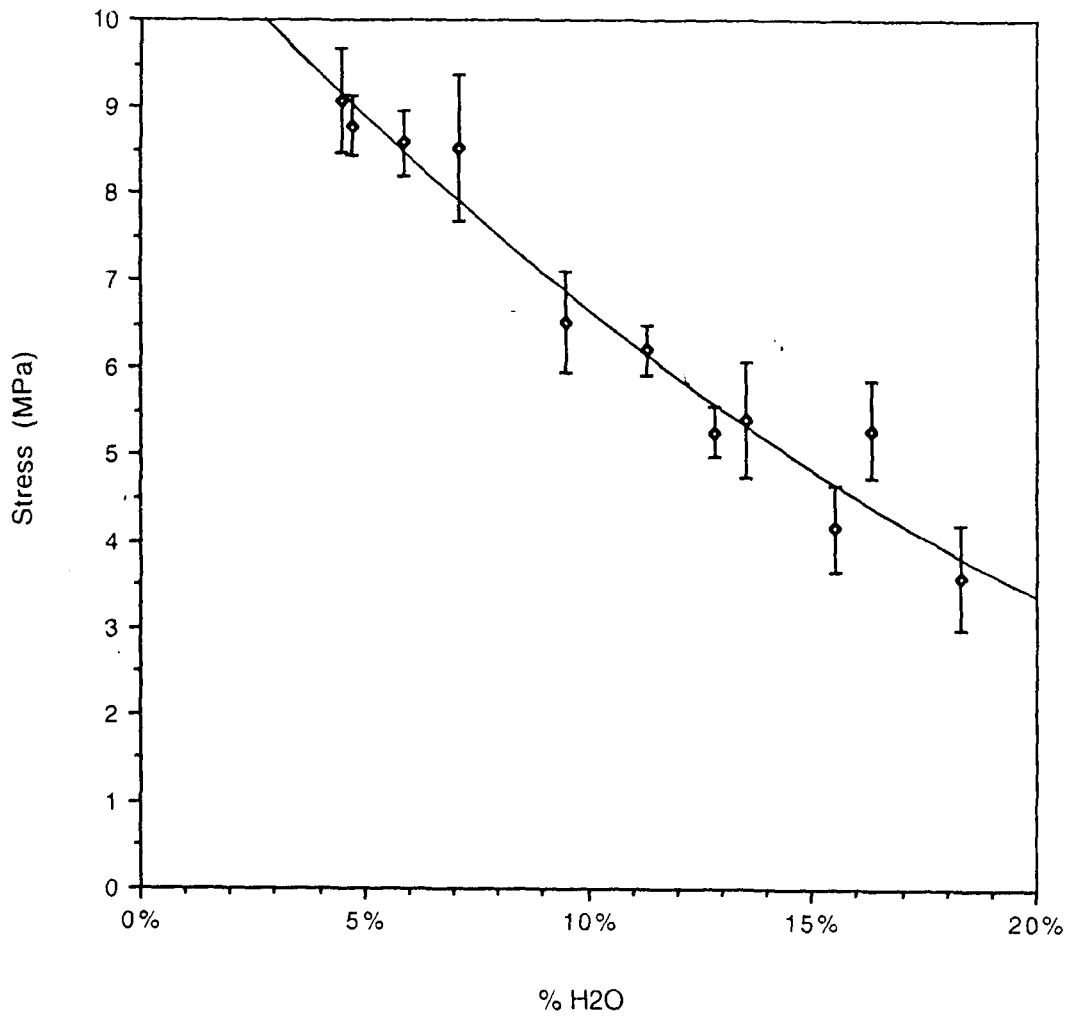

Figure 1 ◆ Stress (MPa)

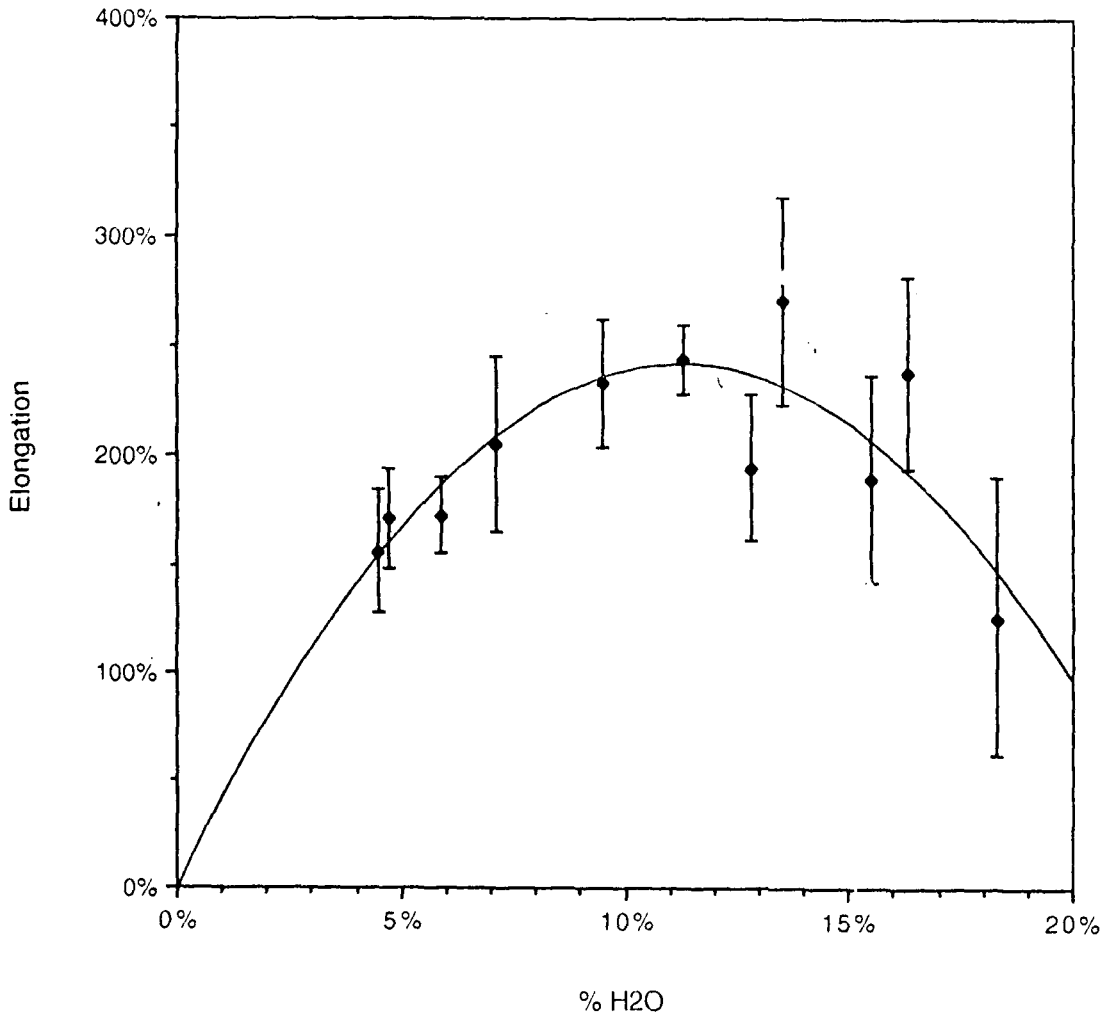

Figure 2 ◆ Elongation

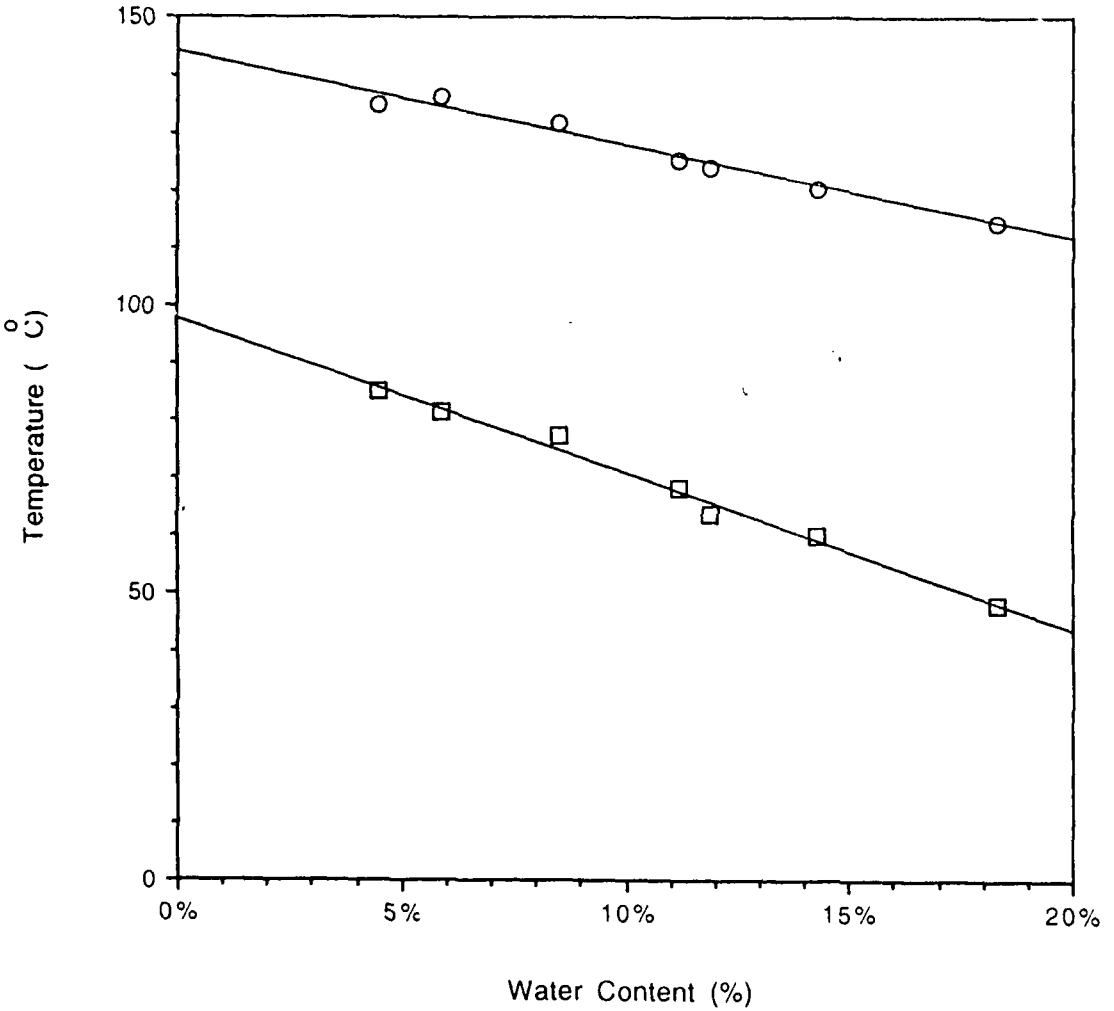

Figure 3

○ Melting Temp.

□ Crystalization Temp.

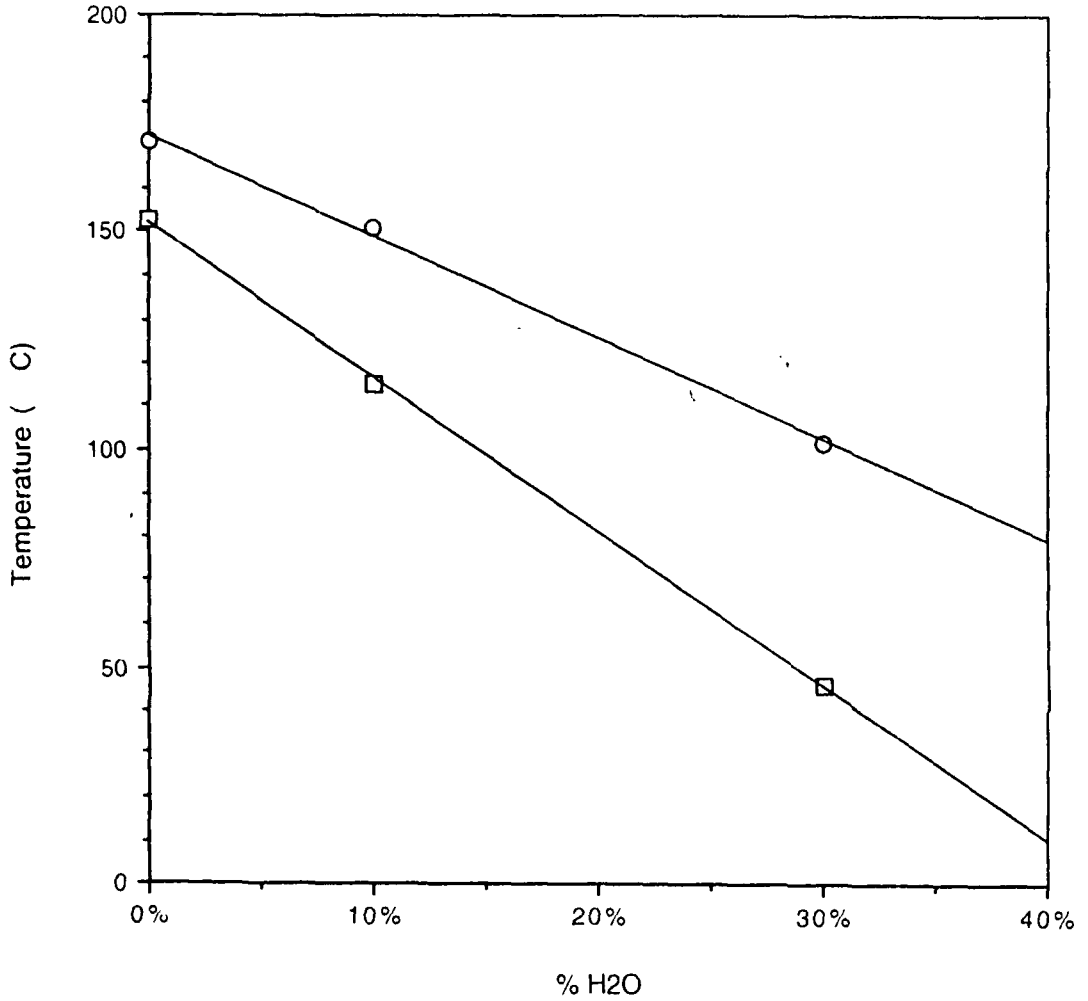

Figure 4

○ Melting Temp.

□ Crystalization Temp.

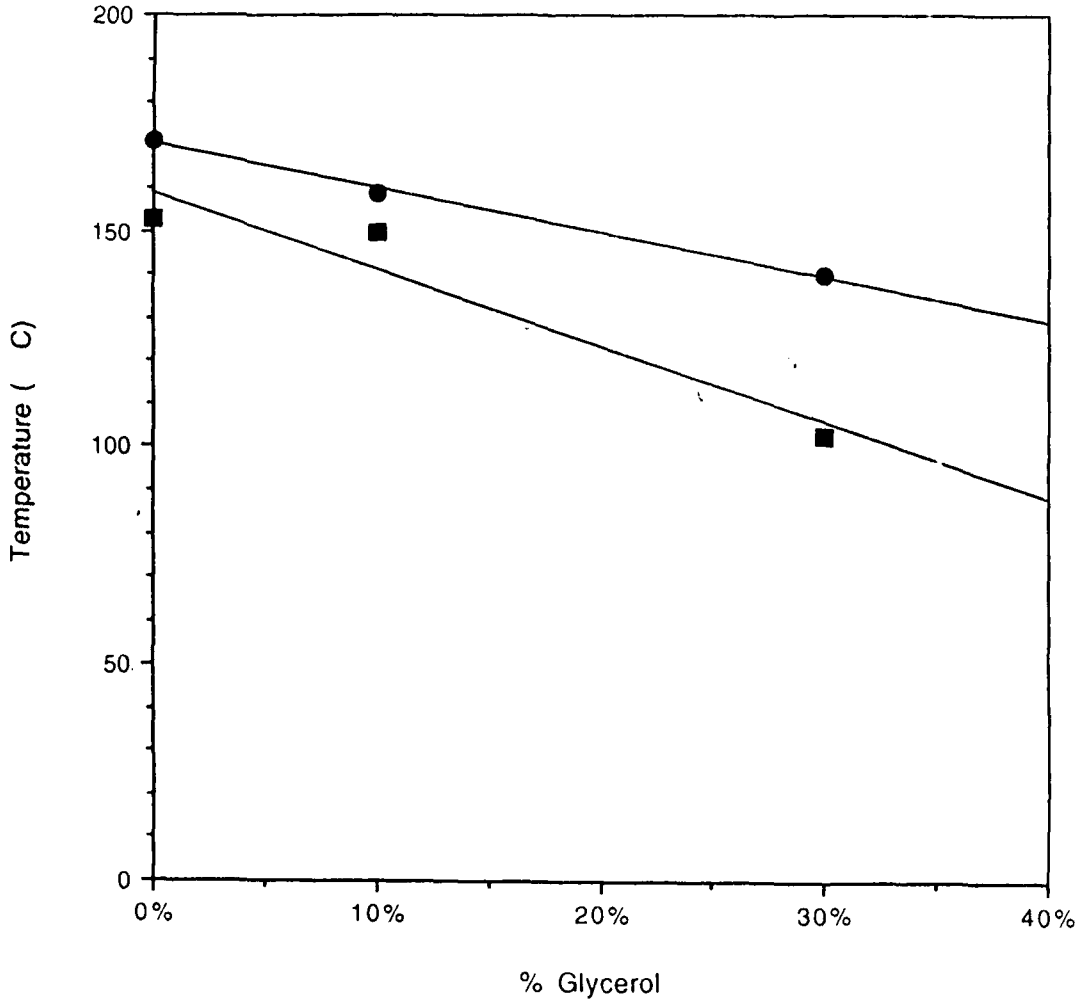
200
150
100
50
0
Temperature (C)
0%
10%
20%
30%
40%
% Glycerol
Melting Temp.
Crystalization Temp.

Figure 5

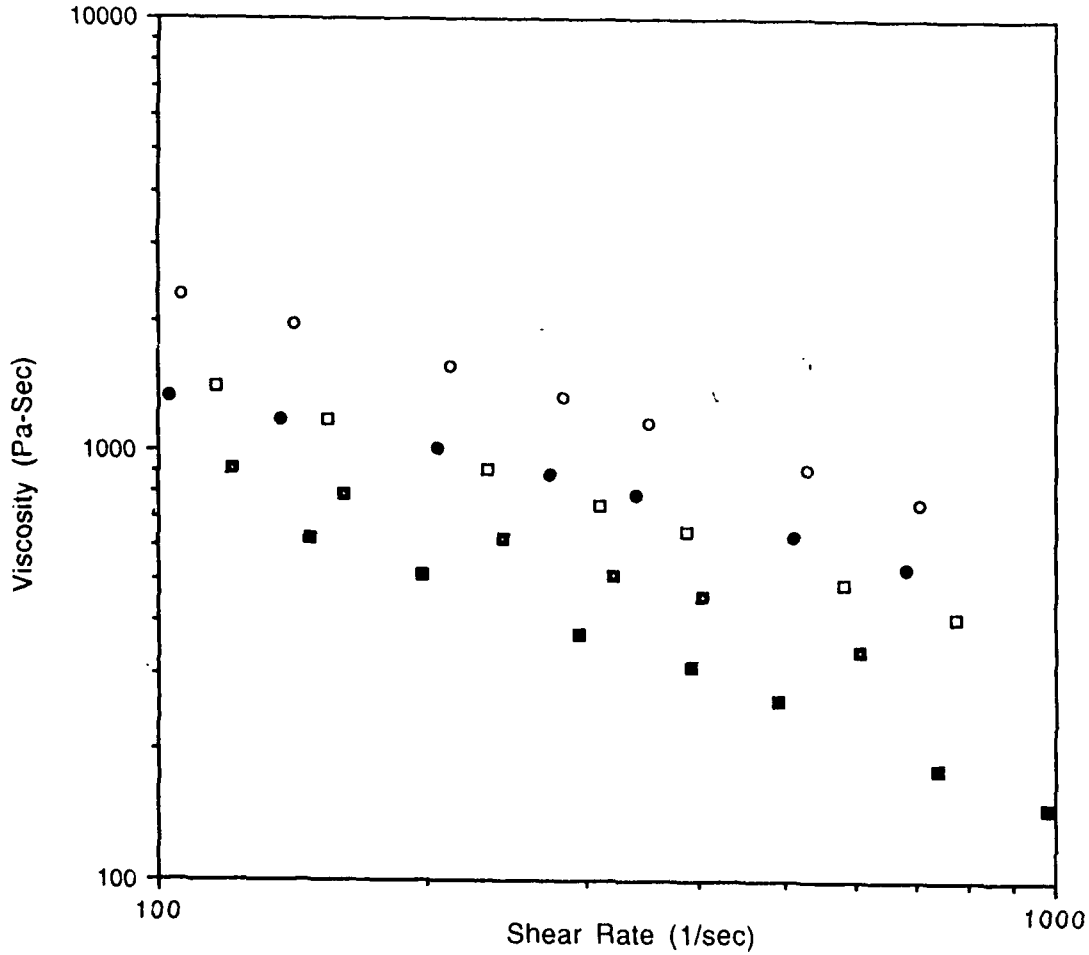

Figure 6

- ○ H101A @ 180 C
- ● H101A @ 200 C
- □ Starch/EVOH @ 135 C 9.5% H2O
- ▣ Starch/EVOH @ 135 C 13.7% H2O
- ■ Starch/EVOH @ 135 C 15.5% H2O

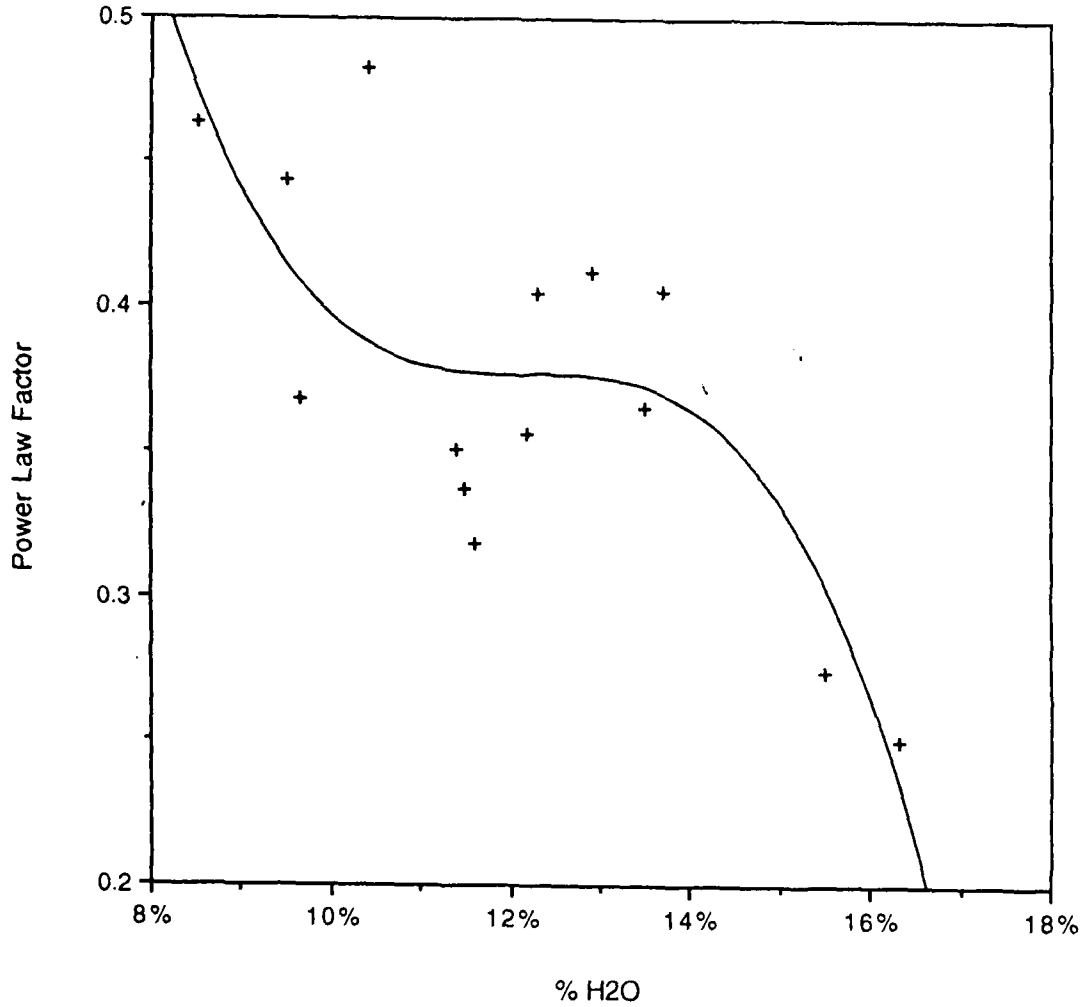

Figure 7 + Power Law Factor

Key Words and Phrases

biodegradable polymers
themoplastic starch materials
starch
poly(ethylene vinyl alcohol) (EVAL)
viscosity